



Michigan Technological University  
*Create the Future* Digital Commons @ Michigan Tech

---

Dissertations, Master's Theses and Master's  
Reports - Open

Dissertations, Master's Theses and Master's  
Reports

---

2011

## Development of a continuum mechanics model of passive skeletal muscle

Duane A. Morrow  
*Michigan Technological University*

Follow this and additional works at: <https://digitalcommons.mtu.edu/etds>



Part of the [Mechanical Engineering Commons](#)

Copyright 2011 Duane A. Morrow

---

### Recommended Citation

Morrow, Duane A., "Development of a continuum mechanics model of passive skeletal muscle",  
Dissertation, Michigan Technological University, 2011.  
<https://doi.org/10.37099/mtu.dc.etds/388>

Follow this and additional works at: <https://digitalcommons.mtu.edu/etds>



Part of the [Mechanical Engineering Commons](#)

DEVELOPMENT OF A CONTINUUM MECHANICS MODEL OF PASSIVE SKELETAL  
MUSCLE

Duane A. Morrow

A DISSERTATION

Submitted in partial fulfillment of the requirements for the degree of

Doctor of Philosophy

(Mechanical Engineering-Engineering Mechanics)

MICHIGAN TECHNOLOGICAL UNIVERSITY

2011

©2011 Duane A. Morrow

This dissertation, “Development of a Continuum Mechanics Model of Passive Skeletal Muscle,” is hereby approved in partial fulfillment of the requirements for the Degree of DOCTOR OF PHILOSOPHY IN MECHANICAL ENGINEERING-ENGINEERING MECHANICS.

Department of Mechanical Engineering-Engineering Mechanics

Signatures:

Dissertation Advisor

\_\_\_\_\_  
Tammy L. Haut Donahue

Dissertation Co-Advisor

\_\_\_\_\_  
Gregory M. Odegard

Committee Member

\_\_\_\_\_  
Kenton R. Kaufman

Committee Member

\_\_\_\_\_  
Zhanping You

Department Chair

\_\_\_\_\_  
William W. Predebon

Date

\_\_\_\_\_

# Table of Contents

<b>List of Figures .....</b>	<b>vii</b>
<b>List of Tables.....</b>	<b>x</b>
<b>Preface .....</b>	<b>xi</b>
<b>Acknowledgements .....</b>	<b>xii</b>
<b>Abstract .....</b>	<b>xiii</b>
<b>Chapter 1 - Introduction.....</b>	<b>1</b>
Introduction .....	1
Basic Skeletal Muscle Anatomy and Physiology .....	1
Generation of Muscle Tension.....	6
Passive Muscle Tension Generation.....	6
Active Muscle Tension Generation.....	7
Current Assessment of Skeletal Muscle Force .....	8
IMP as a Measure of Muscle Force .....	10
Measurement of Intramuscular Pressure .....	10
Sensor Performance in Animal Studies .....	12
Computational Models of Skeletal Muscle.....	16
Evolution of Muscle Models .....	16
Material Properties of Skeletal Muscle .....	18
Specific Aims .....	18
Specific Aim 1: Skeletal Muscle Material Property Definition .....	19
Specific Aim 2: Fitting Experimental Data to Continuum Models .....	19
Specific Aim 3: Ability to Predict IMP using Finite Element Modeling .....	19



<b>Chapter 2 - Transversely Isotropic Tensile Material Properties of Skeletal Muscle Tissue .....</b>	<b>21</b>
Abstract .....	21
Introduction .....	21
Materials and Methods .....	23
Longitudinal and Transverse Extension Tests .....	24
Longitudinal Shear Tests .....	25
Material Properties Definition .....	25
Results and Discussion .....	25
Conclusions .....	29
Conflict of Interest Statement .....	29
Acknowledgement .....	29
<b>Chapter 3 – Method for Assessing Fit of Constitutive Model to Experimental Stress/Strain .....</b>	<b>30</b>
Abstract .....	30
Introduction .....	30
Materials and Methods .....	31
Experimental Data .....	31
Constitutive Model .....	33
Curve Fitting .....	34
Data Analysis .....	34
Results .....	35
Discussion .....	36
Conclusions .....	42
Acknowledgements .....	42

**Chapter 4 – Intramuscular Pressure Predictions from a Hyperelastic  
Model of Skeletal Muscle .....43**

Abstract .....	43
Introduction .....	43
Materials and Methods.....	45
Experimental Data .....	45
Constitutive Model.....	45
Model Geometry .....	46
Finite Element Model .....	46
Results .....	47
Discussion .....	49
Model Sensitivity and Pressure Predictions .....	49
Active Stress Using Constitutive Formulation.....	52
Active Stress using Initial Stress .....	52
Active Stress using Applied Surface Stresses.....	54
Element Size Sensitivity .....	57
Number of Nodes per Element.....	58
Element Numbering .....	58
Generalized Fung Model.....	59
Transversely Isotropic Linearly Elastic Model .....	62
Isotropic Linearly Elastic Model .....	63
Conclusion.....	64

**Chapter 5 – Poroelastic Material Properties of Excised Skeletal  
Muscle in Tension using Inverse Finite Element Method.....66**

Abstract .....	66
Introduction .....	66
Materials and Methods.....	68
Load-Relaxation Tests .....	68
Material Model Determination .....	69
Finite Element Model .....	72

Material Parameter Optimization .....	74
Results .....	74
Discussion .....	76
<b>Chapter 6 – Intramuscular Pressure from a Poroelastic Model of Skeletal Muscle Tissue .....</b>	<b>79</b>
Abstract .....	79
Introduction .....	80
Materials and Methods .....	81
Load-Relaxation Tests .....	81
Finite Element Model .....	83
Results .....	84
Discussion .....	89
<b>Chapter 7 – Significance of Research .....</b>	<b>91</b>
Introduction .....	91
Skeletal Muscle Material Property Definition .....	91
Fitting Experimental Data to Continuum Models .....	93
Ability to Predict IMP using Finite Element Modeling .....	93
Future Directions .....	94
<b>References .....</b>	<b>96</b>
<b>Appendix A: Table Data.....</b>	<b>110</b>
<b>Appendix B: Copyright Permissions .....</b>	<b>124</b>

## List of Figures

Figure 1.1. Multiple scale levels of skeletal muscle tissue. ....	2
Figure 1.2. Cross-section of muscle showing three types of connective tissue sheaths. ....	3
Figure 1.3. Schematic of intermediate filaments skelemin, synemin, and desmin,.....	4
Figure 1.4. Schematic of skeletal muscle sarcomere .....	5
Figure 1.5. Diagram showing tubule systems in skeletal muscle. ....	6
Figure 1.6. Tension-length relationship of a sarcomere .....	8
Figure 1.7. Magnified image that shows a human hair compared to the pressure sensor.11	
Figure 1.8. Schematic of the microsensor's extrinsic Fabry-Perot interferometric (EFPI) measurement technique. ....	12
Figure 1.9. Relationship between relative muscle length and (A) isometric force or (B) intramuscular pressure for the rabbit tibialis anterior. ....	13
Figure 1.10. Relationship between relative change in length and (A) average isometric force or (B) average intramuscular pressure for the rabbit tibialis anterior. 14	
Figure 1.11. Intramuscular pressure and muscle stress as a function of transducer placement within a muscle. ....	15
Figure 2.1. Stages of aponeurosis dissection from an extensor digitorum longus .....	23
Figure 2.2. Test configurations .....	24
Figure 2.3. Representative stress–strain curves for longitudinal extension, transverse extension, and longitudinal shear tests .....	26
Figure 2.4. Box plots of Linear Modulus for (a) longitudinal extension, (b) transverse extension, and (c) longitudinal shear tests .....	27
Figure 3.1. Experimental stress-strain data to be modelled by material direction, including (a) LE, (b) TE and (c) LS. ....	32
Figure 3.2. Plots of the RMSE versus total number of modelled terms for (a) LE, (b) TE and (c) LS data .....	37
Figure 3.3 Plots of LE, TE and LS RMSE for all models with five total terms .....	38
Figure 3.4. Models 1–2–2 (a, c and e, left) and 2–1–2 (b, d and f, right) plotted against experimental data for (a–b) LE, (c–d) TE and (e–f) LS .....	40

Figure 4.1. 3D mesh of idealized muscle geometry. Dimensions taken from MR images of rabbit tibialis anterior. ....	46
Figure 4.2. Schematic of applied boundary conditions.....	47
Figure 4.3. Length-tension(A) and length-pressure (B) relationships for experimental and model data .....	48
Figure 4.4. Length-pressure model sensitivity to A2 (A) and D (B) parameters .....	50
Figure 4.5. Application of surface stresses equal in magnitude and opposite in direction to simulate muscle activation.....	54
Figure 4.6. Cross-section of muscle model showing pressure levels under passive (left) and combined passive and active (right) loading using equal-and-opposite stresses at each element to simulate active loading. ....	54
Figure 4.7. When elements with compressive stresses on opposing faces are arranged in series (A), the stresses on adjacent faces have the effect of cancelling each other out. As a result, the pressure in the model midsubstance is homogenous, with a net effect much smaller than intended (C).....	55
Figure 4.8. If applied surface stresses are arranged as converging on a central location (A), and central higher pressure can be created (B).....	56
Figure 4.9. Element size sensitivity reveals that elements with side lengths $\leq 1$ mm show stabilization in both reaction force and model volume when subject to a 9% strain. ....	57
Figure 4.10. Passive loading resulted in uniform pressure distribution as shown in the muscle cross-sectional slice (A). Addition of activation in initial mesh model showed non-uniform response (B). ....	59
Figure 4.11. Generalized Fung model was able to be characterized sufficiently well to replicate trends in empirical data. There is excellent agreement with the stress-strain data from (A) LE, (B) TE and (C) LS tests.....	60
Figure 4.12. Increasing shear to a magnitude that will allow convergence of the Generalized Fung model causes the LS stress prediction to be several orders of magnitude too high. ....	61
Figure 4.13. Comparison of length-pressure predictions of a transversely isotropic, hyperelastic model with a transversely isotropic, elastic model. Except for the differences in curvature associated with model linearity, the elastic model represent hyperelastic predictions well. Pressure predictions for both models are higher than empirical results. ....	63

Figure 4.14. The level of isotropy represented in the model had no appreciable impact on the pressure prediction. The pressure calculated for results of the isotropic model was nearly identical to the pressure calculated from the transversely isotropic model. ....	64
Figure 5.1. Representative plot of stress from load-relaxation tests .....	69
Figure 5.2. Relaxed stress values from LE and TE load-relaxation tests. ....	70
Figure 5.3. FE model of muscle specimen created in ABAQUS.....	73
Figure 5.4. Representative constitutive model curve-fits (blue) and experimental data (red) for the relaxation phase of load-relaxation under longitudinal (A) and transverse (B) strains .....	74
Figure 5.5. Comparison of experimental and model-predicted relaxation reaction force for a load-relaxation specimen strained to 18% .....	75
Figure 5.6. Change in reaction force with variation in Poisson's ratio .....	77
Figure 6.1. Mean (dark line) $\pm$ one standard deviation (light lines) of relaxation phase of experimental IMP (A) and model predicted pressure (B) .....	84
Figure 6.2. FEM output of specimen cross-section immediately after beginning relaxation phase of load-relaxation test (A) and 150 msec into relaxation phase (B) .....	85
Figure 6.3. Changes in the surface area available for fluid flow affects pressure relaxation time. ....	86
Figure 6.4. Pressure prediction vs empirical measurement for relaxation of muscle strained to 20% incorporating a residual pressure term .....	87
Figure 6.5. Comparison of (A) stress and (B) IMP from poroelastic model and experimental load-elongation data. ....	88

## List of Tables

Table 2.1 Skeletal muscle tensile material properties. ....	26
Table 3.1 Summary RMSE data for ALL and EACH methods by material testing direction .....	36
Table 3.2 Parameter coefficients for 1-2-2 and 2-1-2 models as determined by using ALL and EACH curve-fit methods .....	38
Table 3.3 RMSE and Linear Slope for 2-1-2 models defined using EACH and ALL methods.....	40
Table 4.1 Characteristic Model Coefficients (MPa) .....	45
Table 4.2 Comparison of the effect of number of element nodes and stabilization on model volume and predicted reaction forces.....	53
Table 4.3 Values for generalized Fung model obtained by optimization to fit experimental load-elongation data and provided by Abaqus Verification Manual .....	62
Table 5.1 Mean and variance for ln-transformed slope and intercept for relaxed modulus under longitudinal (LE) and transverse (TE) load-relaxation .....	70
Table 5.2 Regression values for test of coincidence of relaxed stress-strain .....	72
Table 5.3 Mean (SD) of specimen dimensions .....	72
Table 5.4 Optimized values (mean and standard error) for permeability, Poisson's Ratio, and Modulus for both LE and TE loading directions.. .....	75
Table 6.1 Mean (SD) of specimen dimensions. ....	82
Table A.1 Data for Table 2.1 .....	111
Table A.2 Data for Table 3.1 .....	112
Table A.3 Data for Table 5.1 .....	117
Table A.4 Data for Table 5.2.....	121
Table A.5 Data for Table 5.3.....	122
Table A.6 Data for Table 6.1.....	123

## Preface

Portions of the material contained in Chapter One was previously published in the journal *Journal of Biomechanics*. My contribution toward this article was primarily in the description of skeletal muscle anatomy and physiology used in the introduction. This is the portion of the article work was cited from for use in this dissertation.

Additional portions of the material contained in Chapter One were previously published in the journal *Annals of Biomedical Engineering*. I lead experimentation and data analysis for the performance characteristics testing of the sensor described in the article. The portion of the article text used in this chapter is limited to the description of sensor design.

The material contained in Chapter Two was previously published in the journal *Journal of the Mechanical Behavior of Biomedical Materials*. I contributed to this article as the primary author as well as being the individual who performed all experiments and data analyses.

The material contained in Chapter Three was previously published in the journal *Computer Methods in Biomechanics & Biomedical Engineering*. I was primary author of this article. In addition, I developed the method described in the article, and performed all of the data analyses that contributed to the published conclusions.



## Acknowledgements

In January 2005, I first enrolled to take an online learning course from Michigan Technological University: Advanced Engineering Biomechanics. A full seven years later finds the culmination of what began so simply, this dissertation on the development of a continuum mechanics models of skeletal muscle for the purposes of analyzing intramuscular pressure. To say that there has been much growth and learning along the way would be an understatement, and I would be remiss to not pause to thank those who have helped along the way. I offer my thanks to:

Dr. Kenton Kaufman, for giving me the support and direction to challenge myself in so many new areas well outside of my former comfort zone.

My advisors, Drs. Tammy Haut Donahue and Gregory Odegard, who handled the challenges of a full-time employed, part-time distance-learning student. Their continual input and advice helped me to reach the goals of this project and taught me more than just what is contained on the pages herein.

Dr. Savio L-Y Woo (University of Pittsburgh), and Dr. Mark H. Kempinski (Rochester Institute of Technology), for giving my younger self opportunities and first installing the base education upon which this current work was built.

The staff of the Mayo Clinic Motion Analysis and Biomechanics labs, for camaraderie and never asking, “seven years?”

My parents, Ralph and Catherine Morrow, who never wavered in their support or belief in my ability to achieve this.

My sons, Benjamin, Nathaniel, and Michael, who served as examples of the joys of discovery and learning in so many areas outside of this work.

Most importantly, my beloved wife, Missy. I couldn’t have done this without her constant support and belief in me. This success means so much more in the sharing of it with her. The love of our family is the strength and joy of my life.

## **Abstract**

Skeletal muscle force evaluation is difficult to implement in a clinical setting. Muscle force is typically assessed through either manual muscle testing, isokinetic/isometric dynamometry, or electromyography (EMG). Manual muscle testing is a subjective evaluation of a patient's ability to move voluntarily against gravity and to resist force applied by an examiner. Muscle testing using dynamometers adds accuracy by quantifying functional mechanical output of a limb. However, like manual muscle testing, dynamometry only provides estimates of the joint moment. EMG quantifies neuromuscular activation signals of individual muscles, and is used to infer muscle function. Despite the abundance of work performed to determine the degree to which EMG signals and muscle forces are related, the basic problem remains that EMG cannot provide a quantitative measurement of muscle force.

Intramuscular pressure (IMP), the pressure applied by muscle fibers on interstitial fluid, has been considered as a correlate for muscle force. Numerous studies have shown that an approximately linear relationship exists between IMP and muscle force. A microsensor has recently been developed that is accurate, biocompatible, and appropriately sized for clinical use. While muscle force and pressure have been shown to be correlates, IMP has been shown to be non-uniform within the muscle. As it would not be practicable to experimentally evaluate how IMP is distributed, computational modeling may provide the means to fully evaluate IMP generation in muscles of various shapes and operating conditions.

The work presented in this dissertation focuses on the development and validation of computational models of passive skeletal muscle and the evaluation of their performance for prediction of IMP. A transversely isotropic, hyperelastic, and nearly incompressible model will be evaluated along with a poroelastic model.

# Chapter 1 - Introduction<sup>1,2</sup>

## Introduction

Skeletal muscles are highly organized tissues that serve several functions in the human body. Muscles function by adding tension across one or more joints. This tension can be the result of either active contraction or passive elongation, and can be used to stabilize the body, create motion, or impart force to external objects. Even though each muscle functions through the same mechanisms, the particular requirements of an individual muscle cause the muscle to take on varied shapes, sizes, and orientations. Understanding the total effect of dysfunction can therefore be very complex. Clinical assessment of muscle 'strength' is often subjective, and typically involves the evaluation of a muscle group's joint moment producing capacity. Investigators have turned to computational models to determine the mechanical output of individual muscles. This chapter details the background anatomical and physiological considerations for the development of a computational model capable of predicting intramuscular pressure (IMP) in skeletal muscle. Additionally, an examination of the evolution of muscle models is presented.

## Basic Skeletal Muscle Anatomy and Physiology

On a gross level, skeletal muscle is composed of fiber-shaped fascicles that are aligned in series, as shown in Figure 1.1. The fascicles are, in turn, composed of muscle fibers, which are built from myofibrils. These muscle fibers and myofibrils are aligned along the fiber axis of the muscle tissue. Myofibrils are themselves comprised of parallel arrangements of sarcomeres in series.

---

<sup>1</sup> Portions of the material contained in this chapter are reprinted from *Journal of Biomechanics*, Vol. 130, Odegard, Haut Donahue, Morrow, and Kaufman, "Constitutive Modeling of Skeletal Muscle Tissue With an Explicit Strain-Energy Function," 061017-1:9, 2008, with permission from ASME (see Appendix B.1).

<sup>2</sup> With kind permission from Springer Science+Business Media: *Annals of Biomedical Engineering*, "Performance Characteristics of a new Generation Pressure Microsensor for Physiologic Applications," Vol. 37, 2009, pp. 1638-1645, Cottler, Karpen, Morrow, and Kaufman, Figures 1 and 2 (see Appendix B.2).

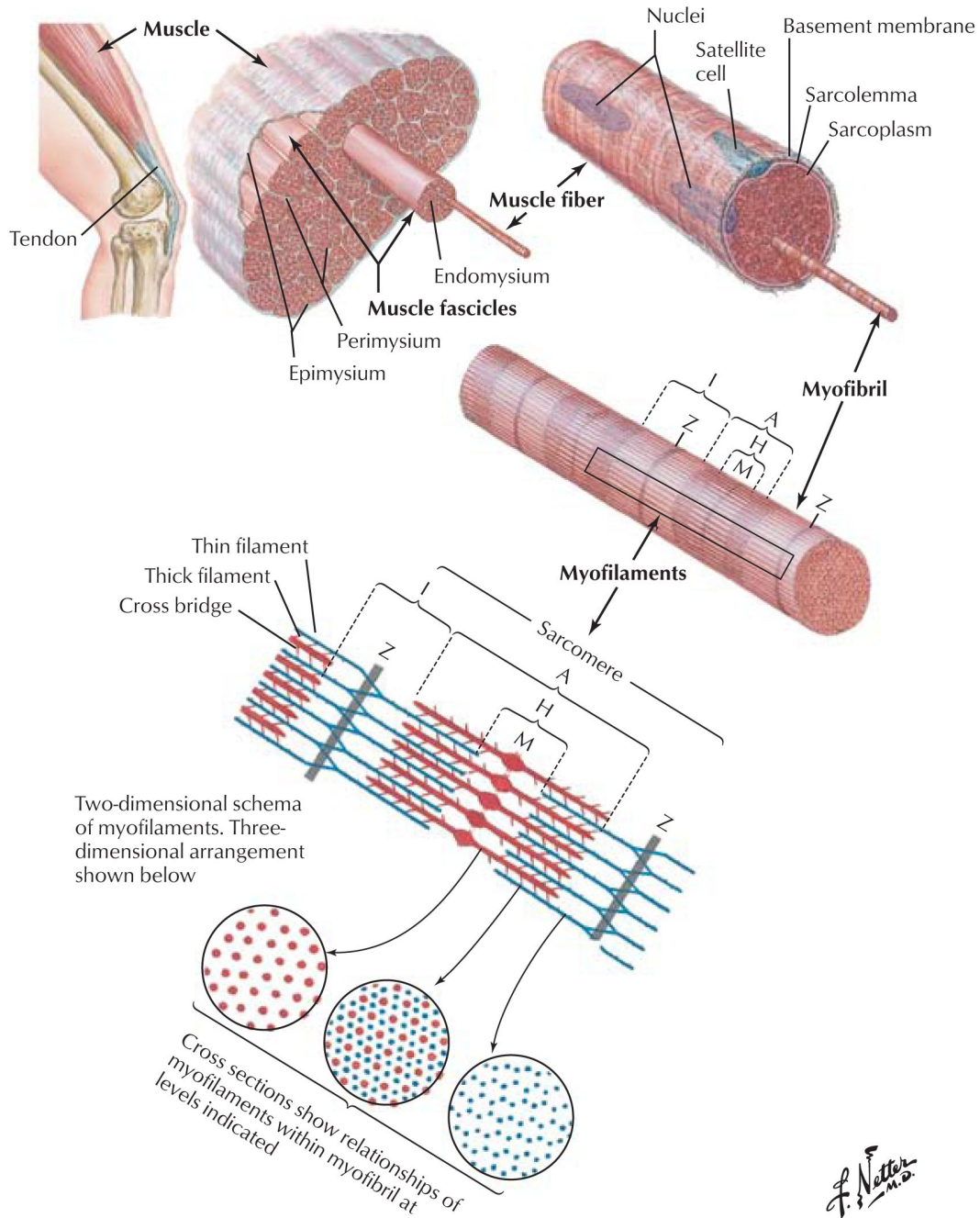


**Figure 1.1.** Multiple scale levels of skeletal muscle tissue. (Netter medical illustration used with permission of Elsevier. All rights reserved. See Appendix B.3)

This organization is further supported by three types of connective tissue sheaths (Fig. 1.2). Surrounding the muscle is the epimysium, a collagenous layer of tissue that separates the muscle from other muscles and tissues. The epimysium also makes connections to the perimysium, the second type of connective tissue sheath which separates muscle fascicles from each other. Additionally, the perimysium creates conduits that create space allowing blood vessels and nerve fibers within the muscle. The third connective tissue sheath is the endomysium which surrounds individual muscle fibers. Just as the perimysium has connections to the epimysium, the endomysium has connections with the perimysium as well.

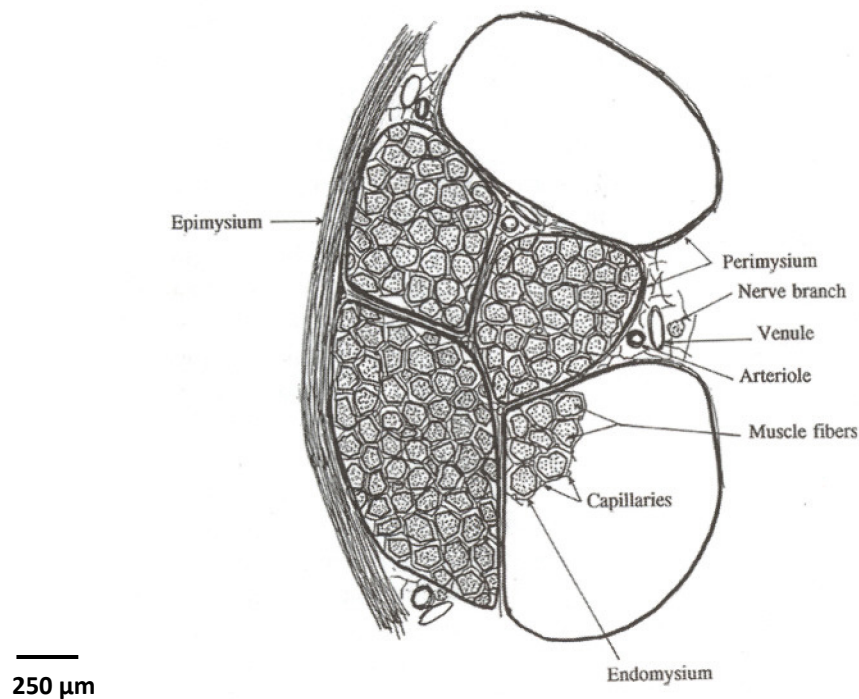


**Figure 1.2.** Cross-section of muscle showing three types of connective tissue sheaths. The 250  $\mu\text{m}$  scale is representative of the sensor diameter, indicating that the size of the sensor allows for measurement of fluid pressure between fibers, as it is sufficiently large to prevent insertion into a fiber (Reprinted, with permission, from B.R. MacIntosh, P.F. Cardiner, and A.J. McComas, 2006, *Skeletal muscle: Form and function*, 2nd edition (Champaign, IL: Human Kinetics), 8)(See Appendix B.4).

The sarcomere is the basic unit of the muscle, and much of the ability of skeletal muscle to generate tension can be understood through examination of the sarcomere. A sarcomere runs from Z-line to Z-line (Fig. 1.1). Each sarcomere contains overlapping myosin and actin filaments (sometimes referred to as thick and thin filaments, respectively). It is the alternate areas of actin and myosin interdigitation that create the striated appearance of a muscle fiber (Fig. 1.1). The dark region where actin and myosin overlap is referred to the A-band, and is centered about the M-line. There is often an H-band in the central sarcomere that consists primarily of myosin filaments and their connections to the M-line. The lightest region of the striations is referred to as the I-band, centered about the Z-line which is the area free of the thick myosin filaments. Structural stability is provided within the sarcomere by the large proteins, titin and nebulin (Fig. 1.3). Titan is a large protein, nearly 1  $\mu\text{m}$  in length, and anchors thick myosin filaments in the middle of a sarcomere when a muscle is stretched beyond its resting length; upon release of the elongating tension, this protein causes the muscle to return to its resting length. Additional reinforcement is provided to the thin actin filaments by another large reinforcing protein, nebulin. As is the case with titin reinforcement of myosin, so too does nebulin extend from the Z disk to support actin filaments.

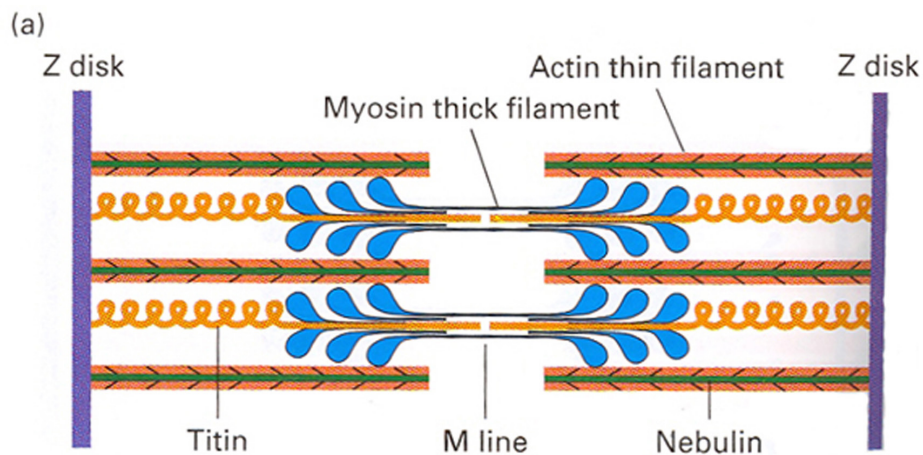


**Figure 1.3.** Schematic of intermediate filaments skelemin, synemin, and desmin, that both add structural integrity and interconnect individual sarcomeres. (Reprinted, with permission, from H. Lodish, A. Berk, S. Lawrence Zipursky, P. Matsudaira, D. Baltimore, and J. Darnell, 2000, *Molecular cell biology*, 4<sup>th</sup> ed. (New York, NY: W. H. Freeman), 19-57)(see Appendix B.5).

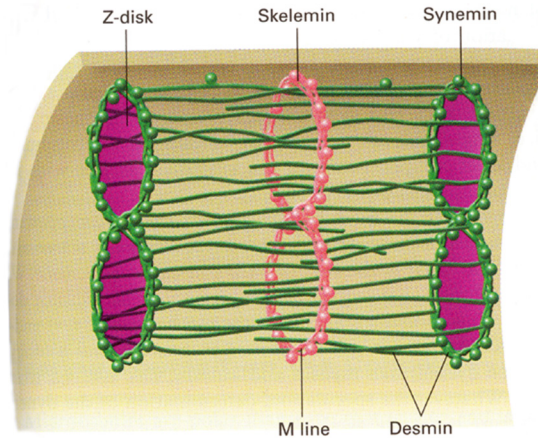


**Figure 1.4.** Schematic of skeletal muscle sarcomere showing supporting proteins titin and nebulin with respect to myosin and actin filaments. (Reprinted, with permission, from H. Lodish, A. Berk, S. Lawrence Zipursky, P. Matsudaira, D. Baltimore, and J. Darnell, 2000, *Molecular cell biology*, 4<sup>th</sup> ed. (New York, NY: W. H. Freeman), 18-30)(see Appendix B.5).

Myocellular structural support is not relegated to cytoskeletal elements within the sarcomere alone. As shown in Figure 1.4, surrounding the sarcomere are networks of intermediate filaments (so called because they are larger than thin actin filaments and smaller than thick myosin filaments). A primary intermediate filament is desmin, which forms a lattice around the sarcomere and enables the transmission of force between adjacent myofibrils.<sup>1</sup> Additional support is provided at the Z disk by synemin filaments. Another intermediate filament, skelemin, surrounds the sarcomere, and is thought to interlink this extracellular lattice by interacting with both nebulin and thick myosin elements at the M line (see Figure 1.3).

A last network of cytoskeletal elements common to cells with complex structures are the tubular systems (Fig. 1.5). Included in these tubular systems are the transverse tubules (or t-tubules) and the sarcoplasmic reticulum (SR). Although they function differently, these systems both serve to provide cellular and organelle motility as well as, to a lesser extent, structural support. The t-tubules encircle mammalian myofibrils at the dividing line of the A- and I-bands and are responsible for the transmission of excitation impulses from motor neurons to muscle fibers. The SR forms a mesh of channels that surround individual myofibrils. The SR is responsible for the transport and gating of  $\text{Ca}^{2+}$  required to trigger muscle excitation.



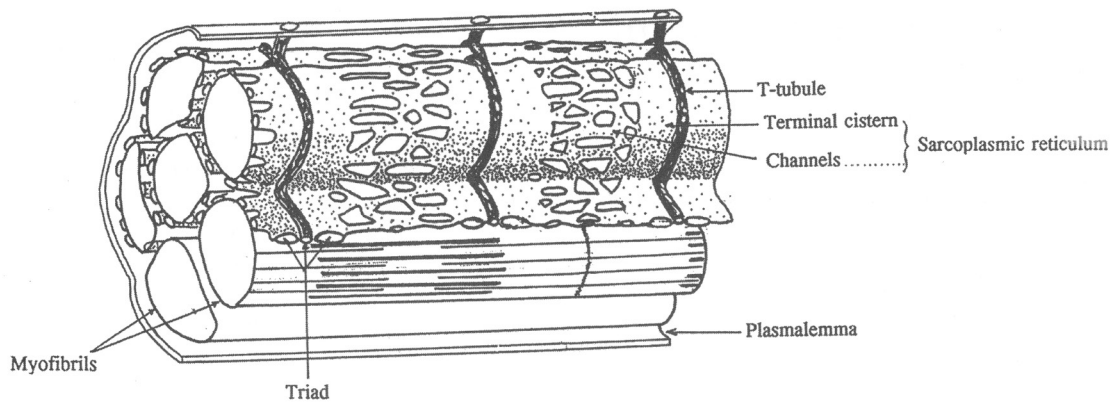


**Figure 1.5.** Diagram showing tubule systems in skeletal muscle. (Reprinted, with permission, from B.R. MacIntosh, P.F. Gardiner, and A.J. McComas, 2006, *Skeletal muscle: Form and function*, 2<sup>nd</sup> ed. (Champaign, IL: Human Kinetics), 17) (see Appendix B.4).

## Generation of Muscle Tension

Skeletal muscle is capable of generating tension under passive and active mechanisms through a series of complex interactions among its constitutive elements. These interactions are both biochemical (active tension generation) and material (active and passive tension generation) in nature. Active and passive tension work in combination to produce a total muscle tension (Fig. 1.6). The following sections will outline the generation of these tensile forces.

### *Passive Muscle Tension Generation*

Passive tension occurs when a muscle has been stretched from its resting length (Fig. 1.6) which corresponds to the plateau region where active muscle tension potential is greatest. As a muscle is lengthened beyond its resting length, the titin, desmin, and other constitutive elements of the extracellular matrix are stretched, resulting in a tensile force. This force rises exponentially with relative elongation, increasing to the point where the generative tension increases beyond the level achievable through active contraction. When released, this tension tends to restore the muscle to its resting length.



## *Active Muscle Tension Generation*

It has been known since the late 1880s that the amount of active tension a muscle could generate under isometric contraction (that is, the tensile force generated by a stimulated muscle held at a constant length) varied with muscle length at the time of contraction.<sup>2</sup> It was also known that there existed a resting length at which active muscle generation was maximal and that at shorter or longer lengths, the tension a muscle could generate diminished (Fig. 1.6). In 1954, two landmark papers were published, by two unrelated Huxleys, that were the basis for understanding that the relative overlap of actin and myosin filaments determines the active force generation potential of a sarcomere.<sup>3,4</sup> This phenomenon has come to be known as the sliding filament theory.

H. E. Huxley, in 1969,<sup>5</sup> proposed that the biochemical interactions of actin and myosin filaments cause muscle contraction and are the mechanism responsible for active muscle tension production. This theory, known as the cross-bridge theory, holds that when an activation signal is received by the muscle and transmitted via the T-tubes,  $\text{Ca}^{2+}$  is released in the SR which triggers heads of the myosin thick filament (Fig. 1.3) to interact with actin thin filaments. This interaction induces sarcomeric contraction and is the source of active tension in skeletal muscle. When the stimulating muscle activation impulse ends, the release of  $\text{Ca}^{2+}$  also ceases, as does the actin-myosin interaction, and the tension generated is released.

The cross-bridge theory helps to explain functionally why the amount of overlap of actin and myosin filaments accounts for changing tension-generating capacity as postulated by the sliding-filament theory. There are three phenomenological areas of consideration in the development of active tension:

- 1) Plateau Region: this is the portion of the length-tension curve (Fig. 1.6) where the active tension generation is maximal. At sarcomere lengths in this region, the amount of overlap is accordingly maximal.
- 2) Ascending Region: the region of sarcomeric shortening (to the left of the plateau region). As the sarcomere shortens, the actin filaments overlap not only with myosin, but also with opposing actin filaments (Fig. 1.6). When sarcomeres are shortened to these lengths, this double-overlap decreases the potential for

myosin heads to interact with actin, resulting in decreased active tension production. This tension continues to decrease with continued shortening until further sarcomeric contraction is not possible and the active tension potential is reduced to zero.

- 3) Descending Region: the region where sarcomeric lengthening beyond the plateau region results in decreasing active tension production. In this region, the amount of overlap between actin and myosin is reduced, thereby reducing the number of myosin heads able to interact with actin filaments (Fig. 1.6). As the sarcomeric lengthening continues, a point will be reached where there is no longer any actin-myosin overlap, and active tension potential is eliminated.

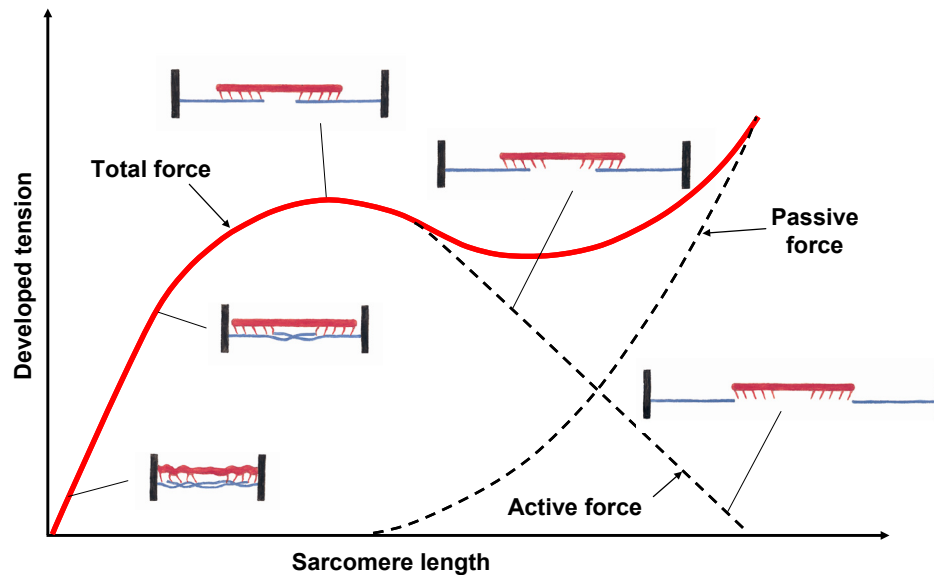


**Figure 1.6.** Tension-length relationship of a sarcomere. (Netter medical illustration used with permission of Elsevier. All rights reserved.)(see Appendices B.1 and B.3).

In practice, the active tension generated in the descending region cannot be measured independently. Rather, it is in this region that the measured tension is a result of active and passive tension.

## Current Assessment of Skeletal Muscle Force

While objective quantification of skeletal muscle force production is clinically desirable, it has remained difficult to implement. Muscle force, as it is currently assessed in clinical

settings, is achieved through 1) manual muscle tests, 2) isokinetic/isometric dynamometry, or 3) electromyography.

Manual muscle testing assesses the ability of a subject to move voluntarily against gravity and to resist a force applied by an examiner. While it is the most common non-instrumented method for measuring patient muscle force production,<sup>6-9</sup> manual muscle grading is only a subjective estimate of joint moment capacity.

Instrumented strength testing is a more accurate indication of actual strength status and is needed to define true capability. Instrumented methods include hand-held dynamometers,<sup>10-12</sup> load cells,<sup>13</sup> hand-grip dynamometers,<sup>14</sup> and isokinetic dynamometers.<sup>15,16</sup> Instrumented measurement has been shown to be more sensitive to differences in muscles strength than non-instrumented manual measurement.<sup>17-20</sup> While instrumented methods are better than non-instrumented methods for providing information about joint muscular moments, these methods fail to provide detailed information about individual muscles.

Direct muscle force is difficult to measure *in vivo*. A tendon buckle transducer was proposed by Salmons<sup>21</sup> to measure force from a single muscle or from a muscle group with a common tendon. This technique is limited to muscles with relatively long tendons that can be exposed surgically and has been used most extensively in animal,<sup>22-28</sup> and to a much lesser extent, in humans.<sup>23,29-32</sup> These experiments are, by their very nature, extremely invasive. Accordingly, there is a paucity of direct muscle tension data available.

Another method that has been used previously to obtain a direct measurement of muscle tension *in vivo* involves the use of a fiber-optic cable that is passed through the distal tendon of the muscle of interest.<sup>33</sup> As tension increases in the tendon, the light that passes through the optic fiber is modulated. While this transducer is less invasive than the buckle-type transducer, and has been used in humans in studies of the lower extremity,<sup>34-36</sup> the applications of this sensor are limited. First, the sensor requires a 19 gauge needle to pass through a tendon, necessitating two breaks in the skin for each sensor. Additionally, the light passing through the fiber is subject to additional modulation from potential fiber deformation during movement of the tendon relative to

the skin. Lastly, the need to pass through the tendon further limits the number of muscle where this sensor can be used: passing through the tendons of deep skeletal muscles would not be clinically viable.

Electromyography (EMG) is often used to quantify neural input to a muscle and infer a muscle's mechanical output insofar as it is related to muscle activation. EMG is a measure of the electrical activity occurring in conjunction with muscle contraction. Substantial effort has gone into the quantification of electromyographic activity<sup>37-44</sup> and the determination of the extent to which EMG can be said to relate to muscle mechanical output.<sup>44-54</sup> However, EMG is limited in that it is only a measure of muscle activation, and does not address tension developed during passive muscle extension. Additionally, cases of electromechanical coupling disorders can result in partial or total dissociation of EMG from muscle force. The limitations of these previous muscle measurements can be overcome with the measurement of IMP. IMP is the interstitial fluid pressure that develops as a muscle undergoes active or passive perturbation. IMP has been considered as a direct correlate of muscle force.

## **IMP as a Measure of Muscle Force**

Hill<sup>55</sup> noted that contracting muscle fibers apply pressure on the interstitial fluid volume and cause mechanical pressure to develop. This observation led to the measurement of IMP as a direct measure of muscle force. Through animal studies<sup>55-61</sup> and human studies,<sup>62-74</sup> investigators have shown an approximate linear relationship exists between IMP and muscle force.

## **Measurement of Intramuscular Pressure**

As mentioned previously, IMP may be used as a surrogate measure for muscle force, capable of capturing force generated through passive and active mechanisms. Until recently, most commercially-available IMP sensors have been comprised of fluid-filled catheters. These systems require infusion to maintain accuracy<sup>75-77</sup> and are sensitive to hydrostatic artifacts. In contrast, a fiber optic system does not require careful positioning during measurement as it is insensitive to hydrostatic artifact.<sup>78,79</sup> Additionally, the speed of response of fiber optic transducers provide adequate dynamic responses sufficient to measure changes in IMP.<sup>79</sup> Baumann et al.<sup>80</sup> suggested that the IMP is related to the active and passive components of muscle tension. A fiber optic

system is also preferable from a patient-safety standpoint, as the measurement device requires no electrical connection to the patient.<sup>81</sup> The large size of the fiber optic catheter proved to be too large for comfort, and rendered falsely low pressure during relaxation following exercise.<sup>82</sup> Recently developed microsensor fiber optic technology<sup>83</sup> has been used to construct transducers with a diameter of  $\sim 250\ \mu\text{m}$ , sufficiently small (Fig. 1.7) to insert using a 25-gauge needle, comparable in size to needles used during standard fine-wire EMG studies. These transducers have also been shown to be biocompatible,<sup>84</sup> accurate to  $< 2\%$  full-scale output (FSO), repeatable to  $< 0.5\%$  FSO, with a hysteresis of  $< 1\%$  FSO.<sup>83,85</sup>

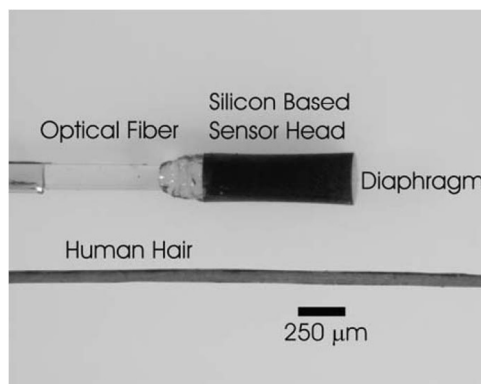


**Figure 1.7.** Magnified image that shows a human hair compared to the pressure sensor mounted at the end of a  $135\ \mu\text{m}$  diameter single-mode optical fiber. (Figure and legend with kind permission from Springer Science+Business Media: *Annals of Biomedical Engineering*, “Performance Characteristics of a New Generation Pressure Microsensor for Physiologic Applications”, Vol. 37, 2009, 1641, Cottler,

These diaphragm-based pressure microsensors function with the formation of a low-finesse Fabry–Perot cavity between the polished end-face of a fiber and a reflective surface that deflects with pressure (Fig. 1.8). Light emitted from a broadband source is passed through a single fiber, where a portion of the light is reflected off the fiber/air interface ( $R_1$ ). The remaining light propagates through the air gap between the fiber and the diaphragm and is reflected back into the fiber ( $R_2$ ).  $R_1$  is the reference (fixed) reflection while  $R_2$  is the sensing (variable) reflection. These two light waves interfere constructively or destructively based on the path length difference between the sensing reflection and the reference reflection. The resulting interferogram travels back through

the optical fiber to the demodulation unit.<sup>85</sup> Absolute gap information is contained in the frequency content of the returned signal (Fig. 1.8).<sup>86</sup> Therefore, as the diaphragm deflects due to pressure changes, the interference pattern of the returned light can be demodulated to calculate the path length difference, which is then correlated with an observed pressure level.

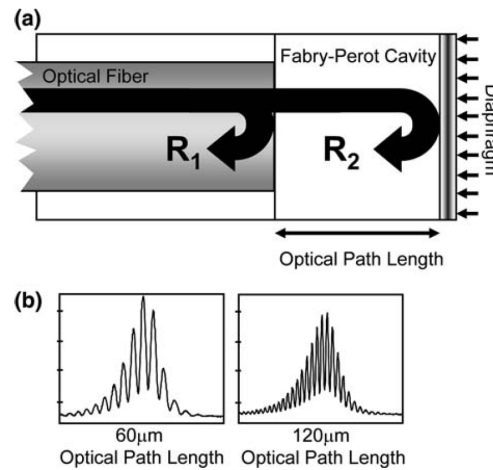


**Figure 1.8.** Schematic of the microsensor’s extrinsic Fabry-Perot interferometric (EFPI) measurement technique. (a) Light propagates through an optical fiber, a portion of the light is reflected by the polished end face of the fiber (R<sub>1</sub>) and the remaining light travels through the Fabry–Perot cavity and is reflected back by a diaphragm (R<sub>2</sub>). The optical path length changes as pressure deflects the diaphragm and can be determined through interferometric measurements of R<sub>1</sub> and R<sub>2</sub>. (b) Resultant interferogram based on the reflections of R<sub>1</sub> and R<sub>2</sub> show the characteristic fringe pattern, with a unique frequency component that increases as the optical path length increases. Figure and caption with kind permission from Springer Science+Business Media: *Annals of Biomedical Engineering*, “Performance Characteristics of a New Generation Pressure Microsensor for Physiologic Applications”, Vol. 37, 2009, 1641, Cottler, Karpen, Morrow, and Kaufman, Figure 2)(see Appendix B.2).

### *Sensor Performance in Animal Studies*

In addition to the documented characterizations of these sensors in pressure chambers instrumented with NIST-traceable sensors, animal studies have been performed to ensure that force-length and pressure-length relations were well-correlated with these sensors. The IMP sensors showed strong length-tension and length-pressure correlation for active and passive perturbations in the tibialis anterior (TA) muscle of New Zealand White rabbits (NZW). In 2003, Davis et al.<sup>59</sup> demonstrated strong correlation over a large range of strains for both active and passive perturbations in an isolated NZW TA (Fig. 1.9). Subsequently, Winters et al.<sup>61</sup> examined the length-tension-pressure

relationship of the NZW TA when perturbed in an intact myofascial compartment. While the observed levels of IMP were higher in the TA in an intact compartment, the correlation remained strong (Fig. 1.10).

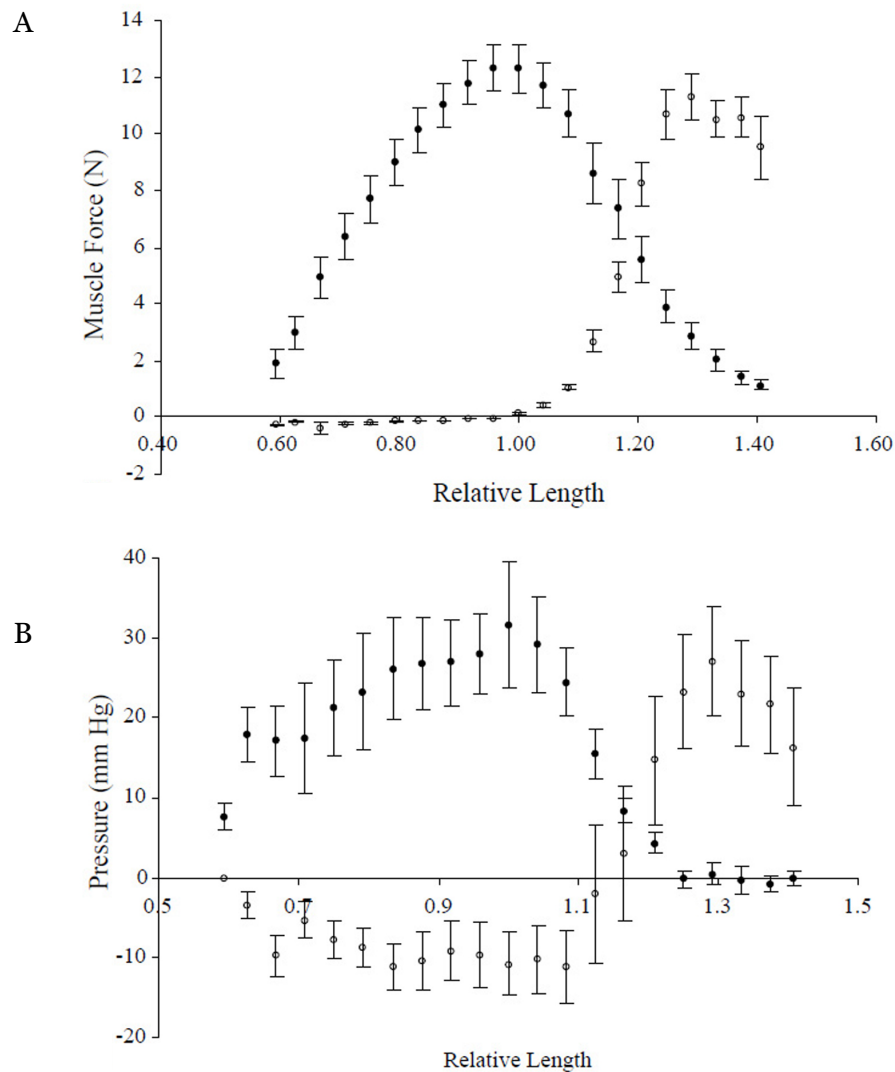


**Figure 1.9.** Relationship between relative muscle length and (A) isometric force or (B) intramuscular pressure for the rabbit tibialis anterior. Filled symbols represent measurements from activated muscles while open symbols represent measurement from passive muscles. Force and pressure were better correlated at long lengths, independent of activation state. Data are plotted as mean  $\pm$  SEM. (Figure and legend reprinted from J Biomech, Vol. 36/Iss. 4, Davis J, Kaufman KR, Lieber RL, Correlation between active and passive isometric force and intramuscular pressure in the isolated rabbit tibialis anterior muscle, Pages 505-512, Copyright (2003), with permission from Elsevier)(see Appendix B.6).

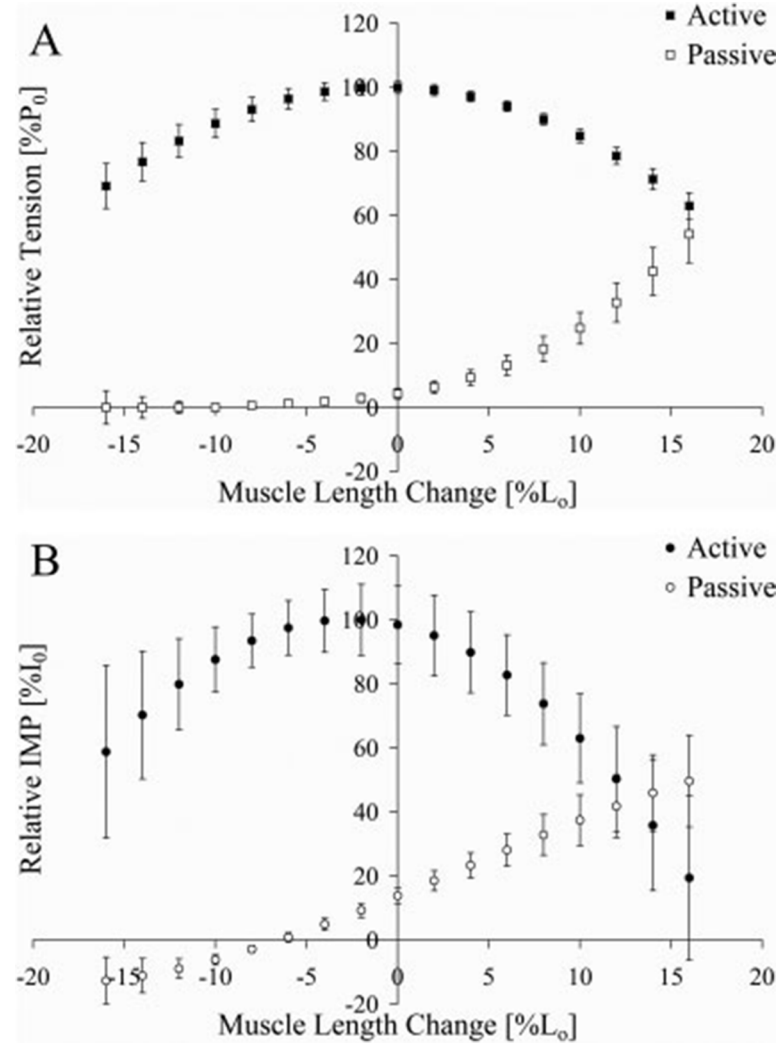


**Figure 1.10.** Relationship between relative change in length and (A) average isometric force or (B) average intramuscular pressure for the rabbit tibialis anterior. Filled symbols represent measurements from activated muscles; open symbols represent measurements from passive muscles. Force and pressure correlations did not differ between limbs, and passive stretch generally maintained higher correlations. Data are plotted as mean  $\pm$  SEM. (Figure and legend reprinted from Muscle & Nerve, Vol. 40/Iss. 1, Winters TM, Sepulveda GS, Cottler PS, Kaufman KR, Lieber RL, Ward SR, Correlation between isometric force and intramuscular pressure in rabbit tibialis anterior muscle with an intact anterior compartment, Pages 79-85, Copyright (2009), with permission from Wiley)(see Appendix B.7).



Care must be taken in sensor placement, however, as considerable regional pressure heterogeneity has been observed within a muscle. Pressure measurements obtained at multiple locations in a NZW TA muscle were compared to a single force measured at the distal end of the muscle (Fig. 1.11). These data demonstrate that IMP varies within the muscle, but are consistent at the proximal medial and, to a lesser extent, mid-belly of a muscle.<sup>87</sup>

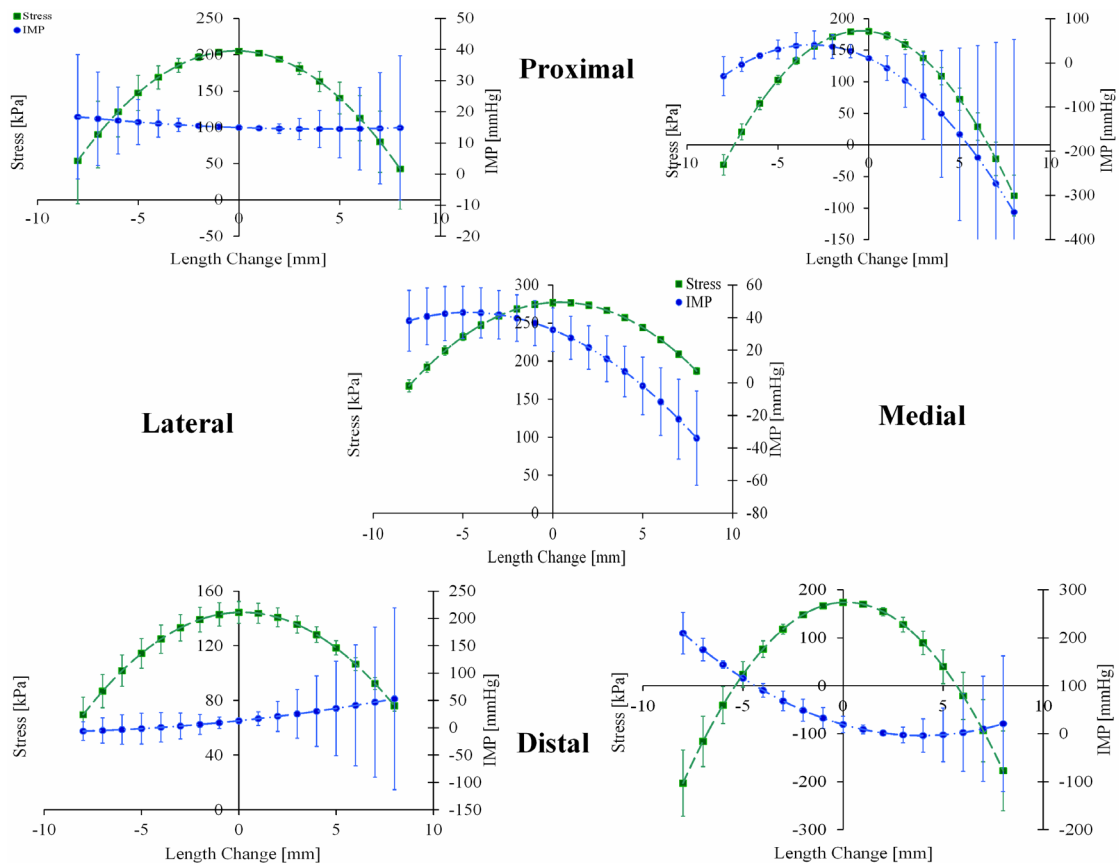


**Figure 1.11.** Intramuscular pressure and muscle stress as a function of transducer placement within a muscle. Top graphs represent the proximal medial and lateral regions, middle graph represents the middle region and bottom graphs represent the distal medial and lateral regions of the rabbit TA muscle. Note that the proximal medial and middle regions of the muscle have the best relationships between IMP and muscle stress.<sup>87</sup>

The presence of this regional pressure heterogeneity is hypothesized to be attributable to the non-uniform nature of the muscle's anatomy. Not only are skeletal muscles non-uniform in geometry and cross-section, the regions where the much stiffer aponeuroses attach to connect muscle to tendons vary between proximal and distal ends. These non-uniformities only increase with comparisons between muscles. The presence of inhomogeneity in IMP within a muscle has been supported by the findings of other investigators.<sup>88,89</sup> Moreover, there are reports that the absolute IMP depends on the depth of the recording catheter within the muscle, the shape of the muscle,<sup>71,90</sup> and the compliance of the surrounding tissue.<sup>91</sup>

To be able to use the IMP sensor as a clinical tool, this heterogeneity must be understood. While it is impracticable to conduct sufficient animal experiments to determine how muscle pressure varies with muscle geometry, an analytical model of muscle pressure could be helpful in answering this questions. Furthermore, the model could be used to provide a mechanism to understand the practical application of IMP as a clinical measurement tool. It is hypothesized that a validated 3D continuum mechanics model using finite element analysis can be used to model the pressure distribution in skeletal muscles.

## **Computational Models of Skeletal Muscle**

It has been reported that skeletal muscle tissue exhibits the same mechanical behavior on both the muscle fiber- and sarcomere-associated length scales.<sup>92</sup> Therefore, for the modeling of mechanical behavior, skeletal muscle tissue can be modeled as a continuous and homogeneous effective continuum with mathematically defined properties and symmetry on multiple length-scale levels. It has been further suggested that muscle tissue is incompressible<sup>93,94</sup> and exhibits transversely isotropic symmetry.<sup>92,95</sup> Therefore, it is assumed that at all functional length-scale levels, muscle tissue has an identical, incompressible, and transversely isotropic response.

### *Evolution of Muscle Models*

As discussed previously, currently available methods for clinical examination or instrumented strength testing only provide information regarding muscle groups. In the absence of direct measurement of individual muscle function, investigators have used

computational models to try and fill gaps in knowledge. Mathematical models of muscle have evolved over the past century. Blix<sup>96</sup> observed that muscle force varies with sarcomere length. Hill created a mathematical model that described the velocity-force characteristics of muscle force generation.<sup>97</sup> Numerous investigators have used Hill-type muscle models to predict individual muscle forces.<sup>92,98-100</sup>

While this type of model has been used to characterize the active and passive material properties, only recently has this model been expanded to examine how model components scale with muscle level (e.g., from fiber to bundle, from bundle to muscle).<sup>101</sup> This was achieved through both serial and parallel combinations of the elements of a typical linear solid model. However, these models do not account for mechanical equilibrium in the muscle<sup>102</sup> or curvature of muscle during contraction.

In an effort to address these deficiencies and incorporate the effects of musculoskeletal anatomy and physiology, investigators began to create models based on continuum mechanics.<sup>95,103-106</sup> A continuum modeling approach allows for the prediction of stresses in the three-dimensional space occupied by the muscle and can be used in conjunction with the finite element method to accurately predict muscle forces under a variety of conditions.

A number of models have been developed that use a continuum description of muscle fibers. Combinations of fibers were arranged to create two- or three-dimensional models of muscle.<sup>102,105-109</sup> While the approaches taken by these models for solving active and passive muscle fiber force contribution varied (e.g., using a distributed moment model of contraction;<sup>107</sup> treating the muscle as a linked fiber matrix mesh<sup>106</sup>) these models all treated muscle fibers as isotropic and hyperelastic, with effects of the assumed transverse isotropy resulting from the arrangement of the fibers. More recently, 3D anisotropic models have been proposed, based in part on the work of Humphrey, Weiss, and Criscione,<sup>110-112</sup> and have been developed for muscle under compression<sup>113,114</sup> as well as tension.<sup>103,115</sup>

While each of the proposed continuum models predict the stress associated with skeletal muscle for given levels of deformation and activation, a constitutive model has not yet been developed that explicitly states the strain energy associated with the active response

for skeletal muscle tissue. Current models have strain-energy density formulations that are defined as derivatives with respect to imposed strains. Such a formulation requires that the strain energy be recalculated for any variations of the deformations to be studied. Having an explicit strain-energy density formulation is required for establishing a dynamical framework that can be used to directly calculate the strain energy and internal stresses of muscle tissue, and ultimately describe muscle behavior under a wide range of conditions.

### *Material Properties of Skeletal Muscle*

Regardless of the level of complexity, the inherent validity of a model is tied to the material properties used to determine model parameters. Given this, it is surprising to note the relative lack of studies examining the material properties of skeletal muscle tissue. Following the assertion that skeletal muscle may be thought of as being transversely isotropic, it may be fully characterized by testing the tissue under longitudinal extension (LE), transverse extension (TE), and longitudinal shear (LS). Of the investigators who have looked to characterize muscle in the fiber direction,<sup>59,113,116-125</sup> many have used the load and displacement seen across the entire musculotendinous unit to derive stress and strain,<sup>59,117,119,121-125</sup> making it difficult to isolate the properties of the muscle tissue itself. That these studies used different muscles from several different species increases the difficulty of generalization. Further, the only studies that have reported experimentally-determined transverse material properties have been under compression.<sup>95,113,126,127</sup> In the very few studies known to report shear properties, the study by Gao et al was limited to an examination of epimysium,<sup>128</sup> and the studies by Van Loocke examined muscle samples under a compression applied 45° from the fiber direction.<sup>113,114</sup> Thus, there is a clear need to collect a comprehensive set of data for 3D characterization of skeletal muscle tissue.

### **Specific Aims**

Previous 3D computational models of skeletal muscle have been developed to model force production<sup>95,104,106,129</sup> and strain distribution.<sup>103,115,130,131</sup> To our knowledge, no models have been created capable of the study of the development of IMP in 3D. The goal of this study is to develop a model of skeletal muscle tissue that can be used to build a model of intact muscle, which will provide a mechanism to understand the practical application of IMP as a clinical measurement. A detailed outline of the history of the

evolution of computational models of skeletal muscle, along with a delineation of the anatomical and physiological considerations incorporated in the development of the proposed models follows in Chapter 2. The current efforts in pursuit of this goal are organized into the following three specific aims:

### *Specific Aim 1: Skeletal Muscle Material Property Definition*

The inherent validity of any computational model is tied to the material properties used to determine model parameters. Given this, it is surprising to note the relative lack of studies examining the material properties of skeletal muscle tissue. Therefore, this investigation aims to evaluate the three-dimensional material properties of skeletal muscle tissue as a single-phase solid continuum material (*Specific Aim 1a* – Chapter 2) and as a poroelastic continuum material (*Specific Aim 1b* - Chapter 5).

### *Specific Aim 2: Fitting Experimental Data to Continuum Models*

The accuracy of a constitutive model is tied directly to the ability of that model to be well characterized with experimental data. When characterizing a model for mechanical response, consideration must be given to the method for handling several data sets. This is especially important for biological materials in which the constitutive equations can be relatively complex and the amount of observed variability between samples can be substantial.

The goal of this aim is to examine the differences in methods that can be used to determine the coefficients of a material model and provide a framework for a practical method to determine if a proposed model adequately characterizes the data it is to represent (Chapter 3).

### *Specific Aim 3: Ability to Predict IMP using Finite Element Modeling*

Specific Aim 3 examines the ability to predict the development of IMP in a single-phase continuum model (*Specific Aim 3a* – Chapter 4) and in a poroelastic continuum model (*Specific Aim 3b* – Chapter 6). This Aim uses the models developed in Specific Aims 1 and 2 and compares the pressure developed in these theoretical models with experimental IMP measurements.

A conclusion of this work is presented in Chapter 7. This chapter includes a summarization of the findings to date. Additionally, commentary is provided on the ultimate development of a model of an intact muscle that may be used in the parametric analysis of IMP in individual muscles with variations in muscle geometry, anatomy, and bounding constraints seen in vivo.

## **Chapter 2 - Transversely Isotropic Tensile Material Properties of Skeletal Muscle Tissue<sup>3</sup>**

### **Abstract**

Of the plethora of work performed analyzing skeletal muscle tissue, relatively little has been done in the examination of its passive material properties. Previous studies of the passive properties of skeletal muscle have been primarily performed along the longitudinal material direction. In order to ensure the accuracy of the predictions of computational models of skeletal muscles, a better understanding of the tensile three-dimensional material properties of muscle tissue is necessary. To that end, the purpose of this study was to collect a comprehensive set of tensile stress-strain data from skeletal muscle tissue. Load-deformation data was collected from eighteen extensor digitorum longus muscles, dissected free of aponeuroses, from nine New Zealand White rabbits tested under longitudinal extension (LE), transverse extension (TE), or longitudinal shear (LS). The linear modulus, ultimate stress, and failure strain were calculated from stress-strain results. Results indicate that the linear modulus under LE is significantly higher than the modulus of either TE or LS. Additionally, the ultimate stress of muscle was seen to be significantly higher under LE than TE. Conversely, the failure strain was significantly higher under TE than under LE.

### **Introduction**

Measurement of individual muscle performance could allow for the monitoring of disease progression, evaluation of therapeutic intervention efficacy, and improvement in

---

<sup>3</sup> Reprinted from Journal of the Mechanical behavior of Biomedical Materials, Vol. 3 (1), Morrow, Haut Donahue, Odegard, Kaufman, Transversely Isotropic Tensile Material Properties of Skeletal Muscle Tissue, 124-129, 2010, with permission from Elsevier (see Appendix B.8).

the understanding of how various conditions affect muscle function. In the absence of direct measurement of individual muscle function, investigators have used computational models to try and fill gaps in knowledge. Models of skeletal muscle have advanced from the unidirectional Hill-type muscle model introduced in 1938<sup>97</sup> to three-dimensional continuum-based muscle models that have been developed more recently.<sup>103,105-109,132</sup> Regardless of the level of complexity, the inherent validity of a model is tied to the material properties used to determine model parameters. Given this, it is surprising to note the relative lack of studies examining the material properties of skeletal muscle tissue.

From the arrangement of skeletal muscle architecture (i.e., the parallel bundling of serially-arranged muscle fibers), it has been hypothesized that skeletal muscle can be considered transversely isotropic<sup>115</sup> with the fiber (longitudinal) axis defining the plane of symmetry. A transversely isotropic material may be fully characterized by testing the tissue under longitudinal extension (LE), transverse extension (TE), and longitudinal shear (LS). Of the investigators who have looked to characterize muscle in the fiber direction,<sup>59,116-119,121-125</sup> many have used the load and displacement seen across the entire musculotendinous unit to derive stress and strain,<sup>59,117,119,121-125</sup> making it difficult to isolate the properties of the muscle tissue itself. That these studies used different muscles from several different species increases the difficulty of generalization. Further, the only studies that have reported experimentally-determined transverse material properties have been under compression.<sup>95,113,126,127</sup>

In the very few studies known to report shear properties, the study by Gao et al. was limited to an examination of epimysium,<sup>128</sup> and the studies by Van Loocke examined muscle samples under a compression applied 45° from the fiber direction.<sup>113,114</sup>

The aim of the current study was to collect a set of data that will allow the characterization of skeletal muscle as a three-dimensional transversely isotropic material. Stress-strain relations are derived from uniaxial tension tests of muscle under LE, TE, and LS and can be used to build computational models of muscles of varying geometries.



## Materials and Methods

Nine New Zealand White rabbits were obtained with institutional approval (IACUC A17308). Hind limbs were amputated mid- femur and stored in a freezer within one hour of sacrifice. From the 18 available fresh-frozen hind limbs, 6 limbs each were used for LE, TE, and LS tests. Tests were performed on extensor digitorum longus (EDL) muscles, chosen for its regular cross-section and low pennation angle.<sup>133</sup> To ensure that only muscle tissue was tested, aponeuroses were carefully dissected away (Fig. 2.1) using a blade breaker (Fine Science Tools, Foster City, CA). Unless otherwise indicated, specimen length, width, and thickness were measured before clamping using a micrometer. As the compliance of the muscle tissue was such that trimming samples for TE testing resulted in irregular cross-sections, samples for these tests were trimmed to the length of the clamps after mounting them in the test fixtures. All material tests were performed at a strain rate of  $0.05\% \text{ s}^{-1}$  to minimize viscoelastic effects.<sup>113</sup> Saline was applied to the specimens to maintain tissue moisture throughout testing.

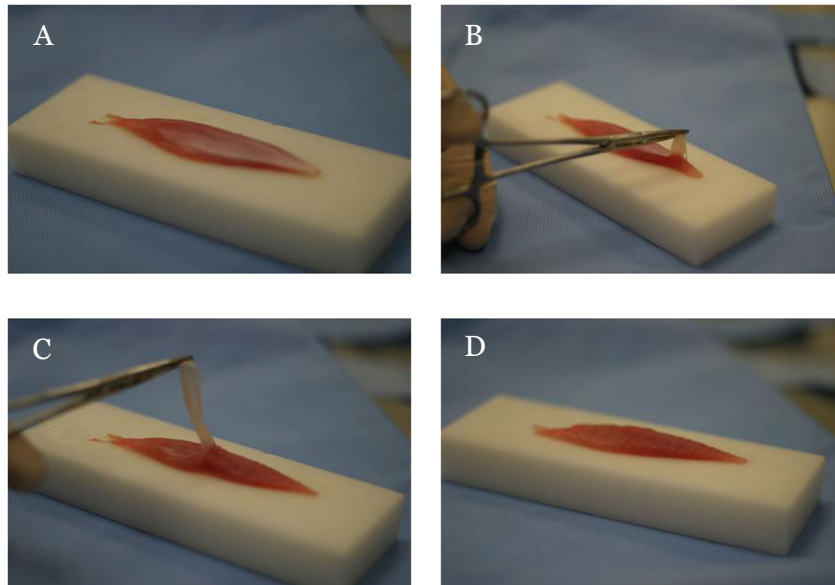


**Figure 2.1.** Stages of aponeurosis dissection from an extensor digitorum longus: starting with (A) an intact muscle, (B) a small portion of aponeurosis is separated from the muscle near the transition to full tendon, (C) a blade breaker is used to progressively separate the aponeurosis from the muscle belly, until (D) the connective tissue is entirely separated from the muscle.

## Longitudinal and Transverse Extension Tests

Material testing under the LE and TE conditions was performed on an MTS 312 material test device (MTS, Eden Prairie, MN). Specimens were mounted to the test device using sinusoidally-grooved clamps. LE specimens were gripped to provide deformation along muscle fiber direction (Fig. 2.2(A)); TE specimens were gripped in the clamp jaws such that applied extension would occur perpendicular to the fiber direction (Fig. 2.2(B)). To ensure that the load passed through the entire cross-section of the TE test specimens, muscle lengths were cut to the width of the clamps (25.4 mm). Force measurements were sampled at 20 Hz using a 111.2-N load cell (Lebow, Columbus, OH), and the second Piola-Kirchoff stress was calculated as the force divided by the initial cross-sectional area. Material elongation was determined using crosshead displacement. Since the muscle was deformed beyond the small strain range, Green strain was used as a deformation measure and calculated as:

$$e = \frac{1}{2}(\lambda^2 - 1) \quad (2.1)$$

where  $\lambda$  is the stretch ratio,

$$\lambda = \frac{l_i}{l_o} \quad (2.2)$$

where  $l_o$  is the original crosshead displacement and  $l_i$  is the current crosshead displacement. Extension samples were strained at  $0.05\% \text{ s}^{-1}$  until either failure or the stroke length limit of 50 mm was reached.

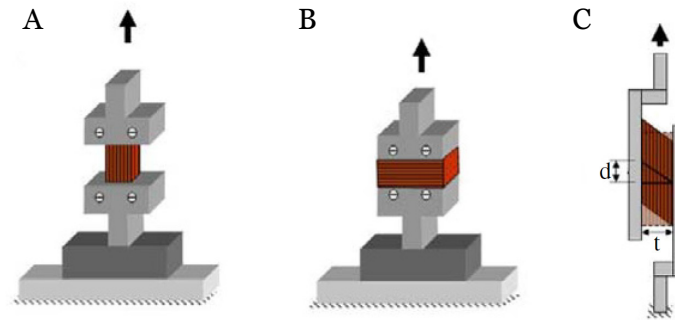


**Figure 2.2.** Test configurations for (A) longitudinal extension, (B) transverse extension, and (C) longitudinal shear tests.

### *Longitudinal Shear Tests*

Longitudinal shear tests were performed on an ElectroForce 3200 test device (Bose Corporation, Eden Prairie, MN). Cyanoacrylate was used to glue the superficial and deep faces of the muscles to plexiglas platens which were, in turn, screwed to shear test fixture uprights. Fixture uprights were offset, ensuring that the measured force passed through the specimen midsection (Fig. 2.2(C)). Force measurements were sampled at 20 Hz using a 45-N load cell (Sensotec, Columbus, OH); the second Piola-Kirchoff stress was calculated as the applied force divided by the initial cross-sectional area. As with the elongation tests, deformation measurements were obtained using crosshead displacement and Green shear strain was used and calculated as:

$$\gamma = \tan\left(\frac{d}{t}\right) \quad (2.3)$$

where  $d$  is the longitudinal displacement of the material, and  $t$  is the thickness of the test specimen. Samples were strained at  $0.05\% \text{ s}^{-1}$  until either failure or the stroke length limit was reached.

### *Material Properties Definition*

Linear modulus, ultimate stress, and failure strain under LE, TE, and LS were determined from their respective stress-strain plots from individual trials. Material properties for the linear region of the stress-strain curve were determined using the method described by Haut Donahue et al.<sup>134</sup> Summary statistics were calculated using a one-way ANOVA, with significance set at  $p < 0.05$ .

## **Results and Discussion**

Typical stress-strain results for LE, TE, and LS tests are shown in Figure 2.3. The linear modulus of the EDL under LE is significantly higher than under either TE or LS (Table 2.1); no significant difference was found between the modulus for TE and LS.

As the displacement of 10 mm did not cause material failure of the EDL under LS, failure properties are reported for LE and TE only. Failure under LE or TE was observed as a separation of muscle fibers within the muscle tissue (as opposed to a complete midsubstance failure of the tissue). It is important to note that muscle fiber separation was not observed until after the maximum load in the TE specimens was reached (Fig.

**Table 2.1**  
Skeletal muscle tensile material properties (see Appendix A.1).

	Linear Modulus (kPa)		Ultimate Stress (kPa)		Failure Strain	
	Mean $\pm$ SD	CV	Mean $\pm$ SD	CV	Mean $\pm$ SD	CV
Longitudinal Extension	447 $\pm$ 97.7	0.218	163 $\pm$ 75.7	0.464	0.505 $\pm$ 0.222	0.440
Transverse Extension	22.4 $\pm$ 14.7*	0.656	27.5 $\pm$ 9.9*	0.360	1.82 $\pm$ 0.924*	0.508
Longitudinal Shear	3.87 $\pm$ 3.39*	0.876	NA	NA	NA	NA

2.3). Therefore, the material microstructure was continuous up to the maximum load. The ultimate stress was significantly higher under LE; conversely, the failure strain was significantly higher for specimens under TE (Table 1.1). Results had a statistical power of  $>0.90$ . Additionally, while material failure did not occur during LS testing, the technique of cementing the specimens to the platens was very efficacious. Visual inspection of the post-test samples revealed that the tissue of the cemented region remained affixed to the platens, and that the cement did not penetrate beyond the surface.

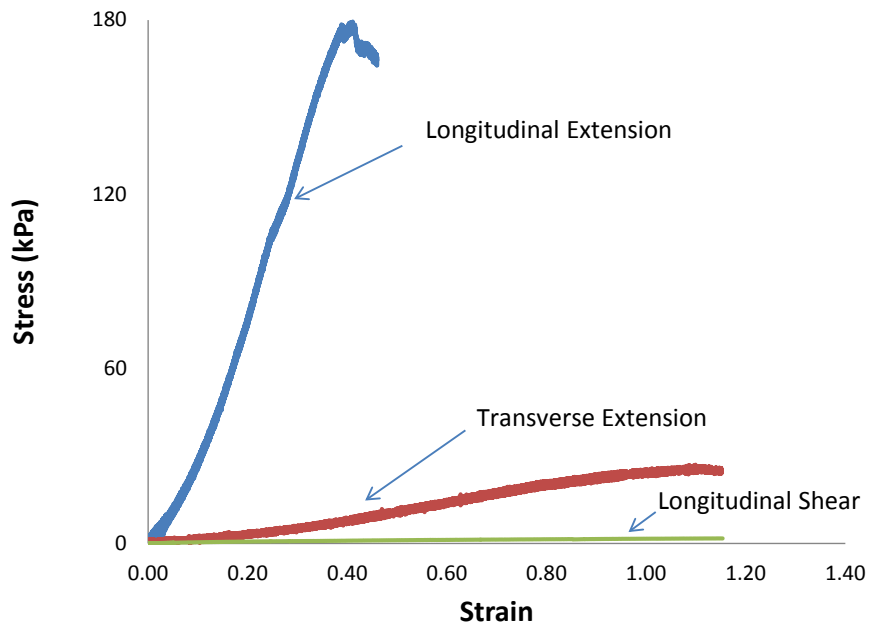


**Figure 2.3.** Representative stress–strain curves for longitudinal extension, transverse extension, and longitudinal shear tests.

The amount of variability in biological experimental data should always be accounted for when assessing experimental data. As the coefficient of variation (Table 1.1) was less than 1, the data can be considered low-variance. Additionally, the linear modulus values for each test direction lie within the 10th and 90th percentile of the sample distribution (Fig. 2.4). Results of this study indicate a higher linear modulus in LE, than in either the TE or LS. Given the large disparity between the linear moduli found in this study, the larger modulus for LE (447 kPa) compares favorably with the 100.700 kPa range Mathur et al.<sup>127</sup> described during low-magnitude indentations of murine skeletal muscle cells. Likewise, the order of magnitude reduction seen in the transverse modulus of 22 kPa from the current study correlates with the reported value of 75 kPa reported by Linder-Ganz and Gefen.<sup>122</sup>

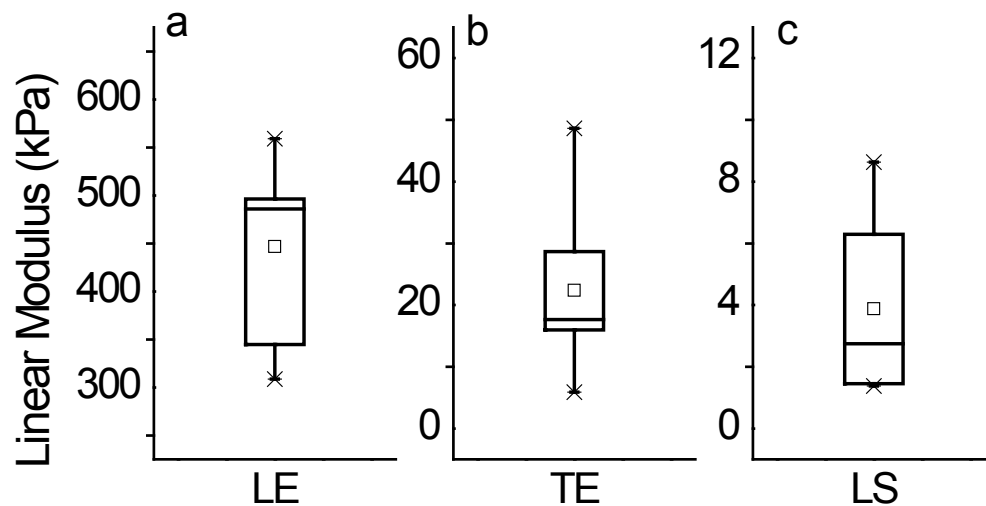


**Figure 2.4.** Box plots of Linear Modulus for (a) longitudinal extension, (b) transverse extension, and (c) longitudinal shear tests. Minimum and maximum values are represented by Xs; whiskers connect values between the 10th and 90th percentile.

The effect of aponeurosis on the linear modulus under LE and TE can be seen through comparison with work performed previously.<sup>135</sup> In the previous study uniaxial tensile elongation tests were performed on medial gastrocnemius muscles from New Zealand White rabbits using the same protocol as this study. The resulting linear moduli from LE and TE tests (767 kPa and 81 kPa, respectively) are significantly higher than the moduli reported in the current study ( $p < 0.01$  and  $p < 0.02$ , respectively). This is not an unexpected result, with the mechanical response of the muscle reinforced by the

collagenous aponeurosis. Additionally, since the longitudinal and transverse moduli properties of tendon have been reported as being 2700 kPa and 50 kPa, respectively,<sup>103</sup> it was not surprising that the contribution of the aponeurosis was comparatively larger in the longitudinal direction. These results suggest that the presence of aponeurosis would strongly influence how the tissue may be represented and may nullify the assumption of transverse isotropic material symmetry. However, because the aponeuroses were dissected from test samples, transverse isotropy can still be assumed in the tissue corresponding to the muscle fiber axis.

Results of the current study indicate that the ultimate stress in muscle under LE is significantly higher than under TE; the converse is true for the failure strain. Van Ee et al.<sup>136</sup> performed a study in which rabbit tibialis anterior muscles were loaded to failure in the longitudinal direction, reporting an ultimate stress of 460 kPa and a failure strain of 0.31. The larger ultimate stress and the lower failure strain may, at least in part, be attributable to the presence of aponeurosis in Van Ee test specimens. The additional strength provided by the tendinous aponeurosis, giving the higher ultimate stress, also constrains the deformation of the softer muscle material at failure.

Comparisons with studies of skeletal muscle under compression<sup>113,114</sup> suggest that skeletal muscle tissue is a bimodular material. Contrary to the findings of the current study, under the same strain rate, Van Looke et al. found the cross-fiber modulus to be higher than the fiber-direction modulus. Additionally, the moduli found were substantively lower than those of the current study; the longitudinal and transverse modulus of fresh porcine muscle, calculated for a strain of 0.3, were found to be 2.04 and 4.56 kPa, respectively.

One limitation of this study is that testing was performed on fresh-frozen samples. Previous studies have examined the effects of freezing and/or rigor on skeletal muscle tissue material.<sup>113,136</sup> However, a comparison of the linear modulus of specimens tested under longitudinal extension one-hour post-mortem with specimens tested one hour after thawing from a pre-rigor freeze<sup>136</sup> revealed no apparent difference; this suggests that the results of the current study offer a good estimation of skeletal muscle material properties. However, further testing may need to be performed on samples within 4 hours of sacrifice before material properties can be considered suitable for modeling in

vivo musculature. Additionally, the quasi-static rate of extension used in this study is likely to be well below the rates seen under physiological conditions. This data may be augmented by subsequent studies performed at strain rates typical experienced in vivo. Lastly, at a testing length:width ratio of approximately 1:5, the aspect ratio of the TE specimens was less than the optimal ratio of 5:1 preferred to ensure that all clamping effects are eliminated in elongation tests in accordance with St. Venant's principle.<sup>137</sup> Testing was performed on specimens with this geometry due to difficulties that would be encountered in cutting out specimen geometries to the small dimensions that would be required to achieve this aspect ratio in a rabbit skeletal muscle.

## **Conclusions**

This study marks the first time a set of 3D passive tensile material properties has been collected. These results show that even with the aponeurosis dissected away, skeletal muscle still has a significantly higher elastic modulus in the fiber direction than in the cross-fiber direction. The order of magnitude decrease between the elastic modulus of skeletal muscle under LE and TE is likewise demonstrated by an additional order of magnitude decrease in the elastic modulus of LS. Further, the data provided by this study are sufficient to characterize continuum models that represent skeletal muscle as transversely isotropic and hyperelastic.

## **Conflict of Interest Statement**

The authors affirm that they have no financial affiliation or involvement with any commercial organization that has direct financial interest in any matter included in this manuscript.

## **Acknowledgement**

Funding for this study was gratefully provided by NIH grant number HD31476 from the National Institute of Child Health and Human Development.

## **Chapter 3 – Method for Assessing Fit of Constitutive Model to Experimental Stress/Strain<sup>4</sup>**

### **Abstract**

Higher-order polynomial functions can be used as a constitutive model to represent the mechanical behaviour of biological materials. The goal of this study was to present a method for assessing the fit of a given constitutive three-dimensional material model. Goodness of fit was assessed using multiple parameters including the root mean square error and Hotelling's  $T^2$ -test. Specifically, a polynomial model was used to characterise the stress strain data, varying the number of model terms used (45 combinations of between 3 and 11 terms) and the manner of optimisation used to establish model coefficients (i.e. determining coefficients either by parameterisation of all data simultaneously or averaging coefficients obtained by parameterising individual data trials). This framework for model fitting helps to ensure that a given constitutive formulation provides the best characterisation of biological material mechanics.

### **Introduction**

The accuracy of a constitutive model is tied directly to the ability of that model to be well characterised with experimental data. When characterising a model for mechanical response, consideration must be given to the method for handling several data sets. This is especially important for biological materials in which the constitutive equations can be relatively complex and the amount of observed variability between samples can be substantial.

Several transversely isotropic, hyperelastic, three-dimensional formulations have been developed recently for modelling biological soft tissues such as tendon and skeletal muscle.<sup>105,108,110,112,113,132</sup> Although many functional forms of constitutive equations are

---

<sup>4</sup> The material contained in this chapter was previously published in the journal *Computer Methods in Biomechanics and Biomedical Engineering* (see Appendix B.9).



generally used for these materials, a polynomial strain energy density function could be used with varying polynomial orders to represent the toe regions typical at low strains. Increases in polynomial order does not always result in a more accurate representation of the data being modelled, as oscillations not observed in the experimental data can appear in curves of models with unnecessarily high order.

Characterisation of constitutive models is often achieved using stress – strain curves from multiple uniaxial load-deformation tests for all manner of biological soft tissues including, but not limited to tendon,<sup>138,139</sup> ligament,<sup>140,141</sup> meniscus,<sup>142,143</sup> and muscle tissue.<sup>113,114</sup> Constitutive model parameters can be determined through optimisation-based curve-fitting techniques, either simultaneously fitting all available stress – strain data from multiple samples or fitting data curves from individual samples and averaging resultant model parameters. It remains unclear, however, which method, if any, is preferable for this class of materials.

The goal of this study was to examine the differences in methods that can be used to determine the coefficients of a material model and provide a framework for a practical method to determine if a proposed model adequately characterises the data it is to represent. This was explored through the analysis of a model of a transversely isotropic and hyperelastic material using the two techniques described above. The characterised data were previously reported stress–strain data from skeletal muscle tissue under longitudinal extension (LE), transverse extension (TE) and longitudinal shear (LS; Morrow et al. 2008). Characterisation methods have been evaluated using the root mean square error (RMSE) between the resultant model and each dataset. The determined constitutive functions have been assessed through an analysis of the residuals and variances between the models and experimental data.

## **Materials and Methods**

### *Experimental Data*

Twelve fresh-frozen extensor digitorum longus muscles from skeletally mature New Zealand white rabbits underwent uniaxial material tests, with the institutional approval (IACUC A17308), experiencing deformations under either LE (n ¼ 4), TE (n ¼ 4) or LS (n ¼ 4). Full details on the experimental set-up are available in Morrow et al. (2009).

In brief, the tissue was strained under position control at 0.05% s<sup>-1</sup>, to minimise viscoelastic effects, and sampled at 20 Hz. The second Piola–Kirchhoff stress was calculated as the measured force divided by the initial cross-sectional area. Lagrange strain was calculated from the applied displacement and initial specimen length (for LE and TE) or thickness (for LS). Results of these tests are shown in the stress–strain plots of Figure 3.1.

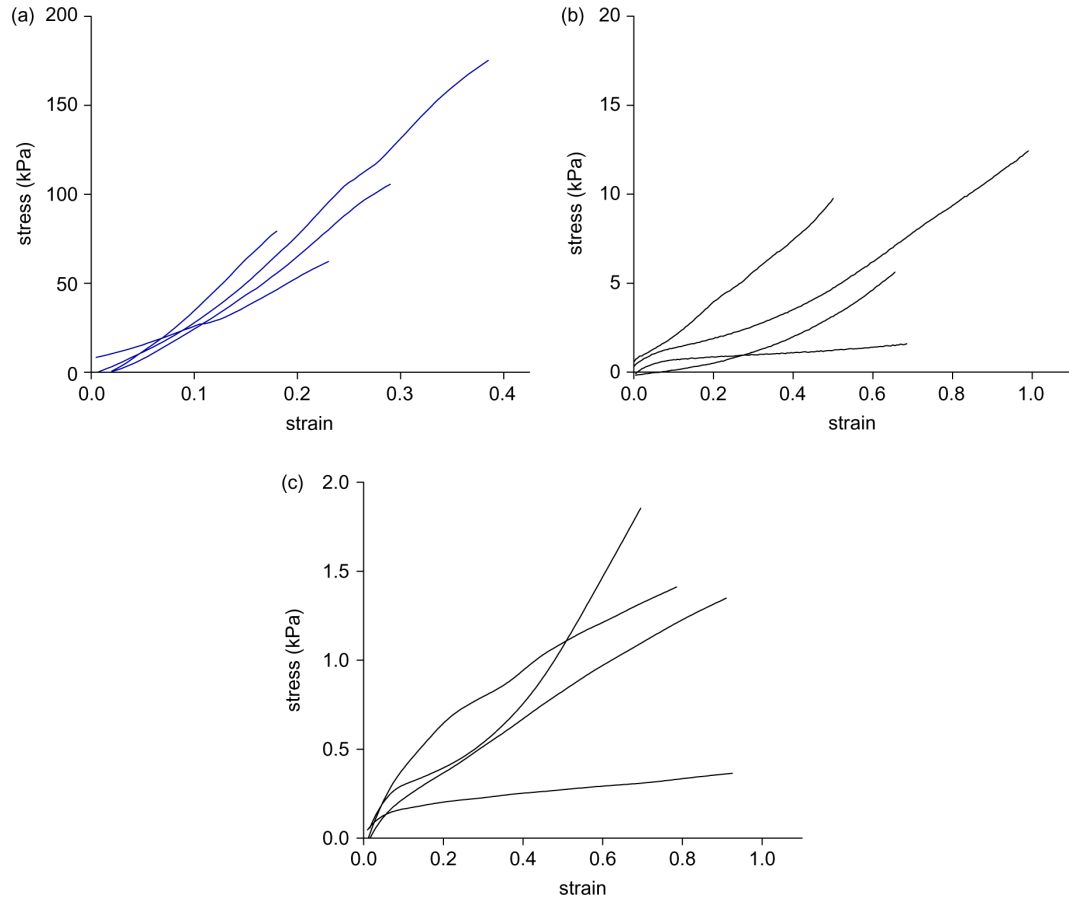


**Figure 3.1.** Experimental stress-strain data to be modelled by material direction, including (a) LE, (b) TE and (c) LS.

### Constitutive Model

The skeletal muscle tissue was modelled as an incompressible,<sup>96</sup> transversely isotropic, hyperelastic material. Because of the incompressible transverse isotropy, only the terms associated with the Green deformation tensor invariants  $I_1$ ,  $I_2$  and  $I_4$  were included.<sup>144</sup> A polynomial expansion of these invariants was used for the strain energy function.<sup>145</sup>

$$W = \sum_{i=1}^3 a_i (I_1 - 3)^i + \sum_{j=1}^3 b_j (I_2 - 3)^j + \sum_{k=2}^6 c_k (I_4 - 3)^k \quad (3.1)$$

In order to fit this model to the experimentally derived stress–strain data, the second Piola–Kirchoff stress function was calculated as

$$\mathbf{S} = 2 \left( \frac{\partial W}{\partial I_1} \frac{\partial I_1}{\partial \mathbf{C}} + \frac{\partial W}{\partial I_2} \frac{\partial I_2}{\partial \mathbf{C}} + \frac{\partial W}{\partial I_4} \frac{\partial I_4}{\partial \mathbf{C}} \right) \quad (3.2)$$

where  $\mathbf{C}$  is the Green deformation tensor. Substitution of Equation (3.2) into Equation (3.1) yields

$$\mathbf{S} = 2 \left[ \left( \sum_{i=1}^3 i a_i (I_1 - 3)^{i-1} \right) \mathbf{I} + \left( \sum_{j=1}^3 j b_j (I_2 - 3)^{j-1} \right) (\mathbf{I}_1 \mathbf{I} - \mathbf{C}) + \left( \sum_{k=2}^6 k c_k (I_4 - 3)^{k-1} \right) \mathbf{M} \right] \quad (3.3)$$

where  $\mathbf{I}$  is the identity matrix and  $\mathbf{M}$  is the structural tensor which defines material symmetry, itself defined as

$$\mathbf{M} = m_0 \otimes m_0 \quad (3.4)$$

For this case, the axis of transverse isotropic symmetry was defined as  $m_0 = \frac{1}{\sqrt{2}} [1 \ 0 \ 0]$ . The stress function can then be solved for each of the three applied deformations (i.e. LE, TE and LS) through appropriate selection of the Green deformation matrix  $\mathbf{C}$ .

### *Curve Fitting*

Unconstrained nonlinear optimisation was performed to obtain the model parameter coefficients using the FMINUNC function of the MATLAB Optimization Toolbox (Mathworks Inc., Natick, MA, USA). In order to obtain the model parameters for this three-dimensional material, stress–strain data from each test direction needed to be considered simultaneously. Best-fit model parameters were found using two different methods of curve fitting: data was curve-fitted using all data as a single data set (ALL method); obtaining model parameters iteratively using one trial from each of the test directions (LE, TE and LS) and averaging the four sets of model coefficients (EACH method).

In order to evaluate the effect of level of the polynomial order, these methods by fitting the model using the EACH and ALL methods for all permutations of the polynomial function. Best-fit parameters were determined for the 45 combinations of the constitutive model, varying between one and three I1 terms, one and three I2 terms and one and five I4 terms. Where model formulations are specified, a three-digit name is used, where the digits denote the included number of I1, I2 and I4 terms, respectively (i.e. models are referred to as a-b-c, where a is the number of I1 terms, b is the number of I2 terms and c is the number of I4 terms).

### *Data Analysis*

Curve-fits were assessed using the RMSE to compare the derived models against each of their experimental stress-strain curves using

$$RMSE = \sqrt{\frac{\sum_{i=1}^n (\sigma_{e,i} - \hat{\sigma}_{m,i})^2}{n - (q + 1)}} \quad (3.5)$$

where  $n$  is the number of points in each data set,  $\sigma_{m,i}$  and  $\sigma_{e,i}$  are the model-predicted and experimentally measured stresses for the  $i$ th strain, respectively and  $q$  is the number of terms in the model. The RMSE was determined for each modelling method and polynomial formulation combination. A two-tailed, pairwise Student's t-test was used to

determine if there is any difference in the RMSE between the ALL and EACH methods for each material test direction.

The goodness-of-fit of the optimised models was further evaluated using the standardised variance ( $s_{var}$ ). The models for the computed EACH and ALL models for each polynomial formulation were individually compared against experimental stress–strain data using

$$\bar{s}_{res} = \frac{(\sigma_{e,i} - \hat{\sigma}_{m,i})}{RMSE} \quad (3.6)$$

For a good curve-fit, the variance between a model and experimental for each direction should have an overall mean value of zero. Since LE, TE and LS data are modelled simultaneously; the multivariate Hotelling’s T<sup>2</sup>-test was used to evaluate the null hypothesis

$$H_0 : \bar{\mathbf{s}}_{res} = \mathbf{0} \quad (3.7)$$

For all statistical tests, significance was set at  $p < 0.05$ .

## Results

The mean and standard deviations for each curve-fitting method in each test direction are reported in Table 3.1. The mean RMSEs for models characterised using the ALL method were found to be significantly lower than those characterised using the EACH method ( $p, 0.001$ ). Additionally, the coefficients of variance indicate that the variability in the RMSE for the ALL LE and TE is much smaller (by a factor of two) than the corresponding EACH values.

Hotelling’s T<sup>2</sup>-test revealed that the standardized variance was not significantly different from zero for any polynomial formulations derived by the ALL method, and for most of those resulting from use of the EACH method. The only combinations whose variance was significantly different from 0 were 1–1–1, 1–1–2, 1–1 4, 1–1–5 and 2–2–1.

**Table 3.1**  
Summary RMSE data for ALL and EACH methods by material testing direction (see Appendix A.2)

	ALL			EACH		
	Mean (kPa)	SD (kPa)	CV	Mean (kPa)	SD (kPa)	CV
LE	8.57 <sup>a</sup>	1.66	0.19	12.50 <sup>a</sup>	5.01	0.40
TE	2.22 <sup>a</sup>	0.46	0.21	2.60 <sup>a</sup>	1.11	0.43
LS	0.48	0.24	0.50	0.49	0.21	0.42

<sup>a</sup> Significant difference ( $p < 0.05$ ) between mean RMSE for ALL and EACH.

## Discussion

While results indicate that the ALL method provides a better fit, the effect of polynomial terms is unknown. Since the ultimate goal is to use this material model in a finite element formulation, having fewer terms, thereby reducing the computational cost of the model, would be beneficial. Figure 3.2 shows plots of the RMSE for the LE, TE and LS against the total number of terms in the various ALL models. These plots reveal the presence of two or three striations, or mean levels, of RMSE for the available combination of terms. Observing the patterns of the LE and TS RMSE (Fig. 3.2(a) and (c)) indicate that the lower RMSEs for those directions can be attained using four variables. Examination of the TE RMSE (Fig. 3.2(b)), however, reveals that five variables need to be used to minimize RMSE.

Even though the RMSE for curve fits are the largest for testing in the LE direction (Fig. 3.3), it should be noted that the higher magnitudes of the stresses in that direction result in a lower coefficient of variance than either TE or LS (Table 3.1). This is encouraging since extension in the longitudinal direction is considered the most clinically relevant loading condition. Further, the magnitudes of the changes in RMSE indicate a substantially better fit when all data are considered in fitting a model; the mean RMSE for EACH method curve fits is greater than that of ALL method fits by 45 and 17% for LE and TE, respectively.

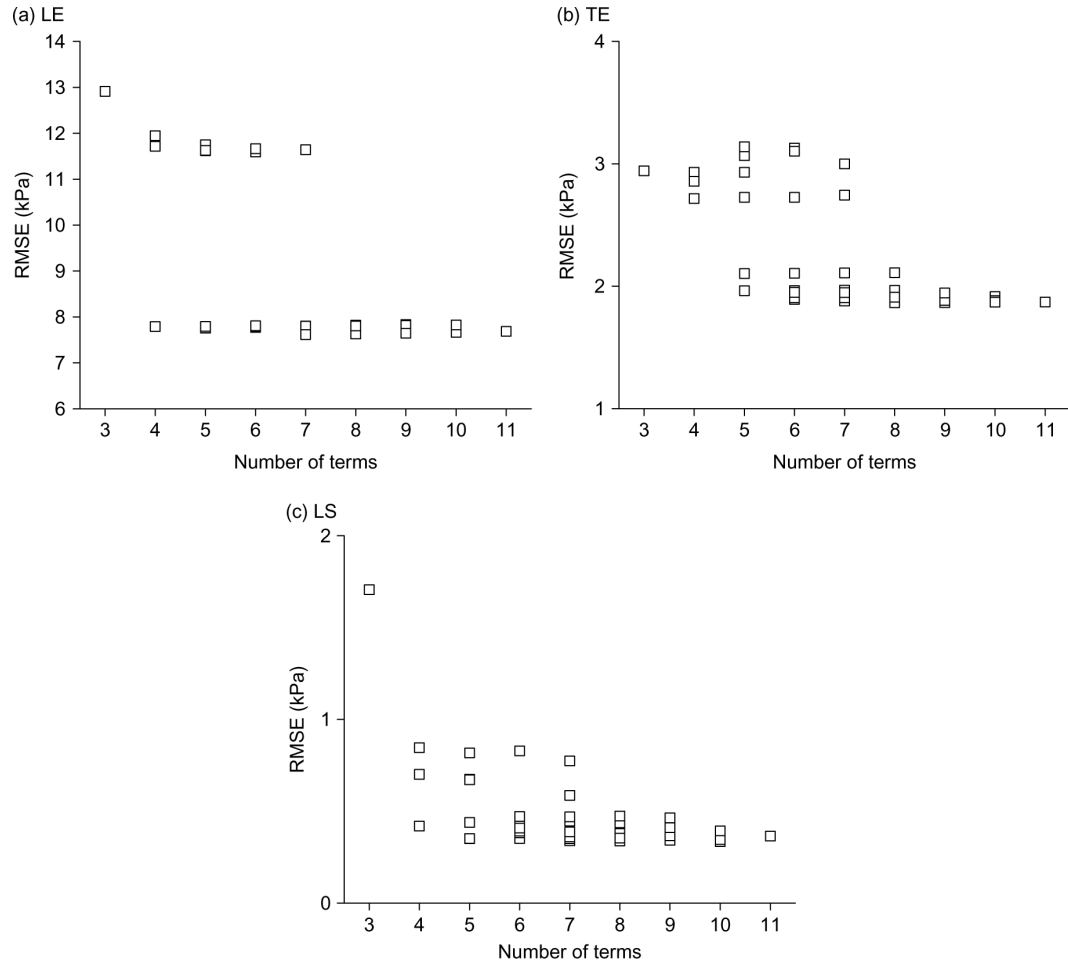


**Figure 3.2.** Plots of the RMSE versus total number of modelled terms for (a) LE, (b) TE and (c) LS data. As indicated by the LE and LS, four or more terms must be used to minimise RMSE. Consideration of TE urges the use of five or more terms to minimise RMSE for this model.

To find which combination of five terms gave the closest fit to the experimental data, the RMSE for each direction was plotted for each five-term model (Fig. 3.3). It is clear from the figure that the 1–2–2 and 2–1–2 models have the smallest overall RMSEs when considering all the three directions of testing. The characteristic variables found for these models are shown in Table 3.2. Further, with p-values from the Hotelling's  $T^2$ -test of 0.771 and 0.562, respectively, the standardised residuals of these curve-fits are both indistinguishable from zero.

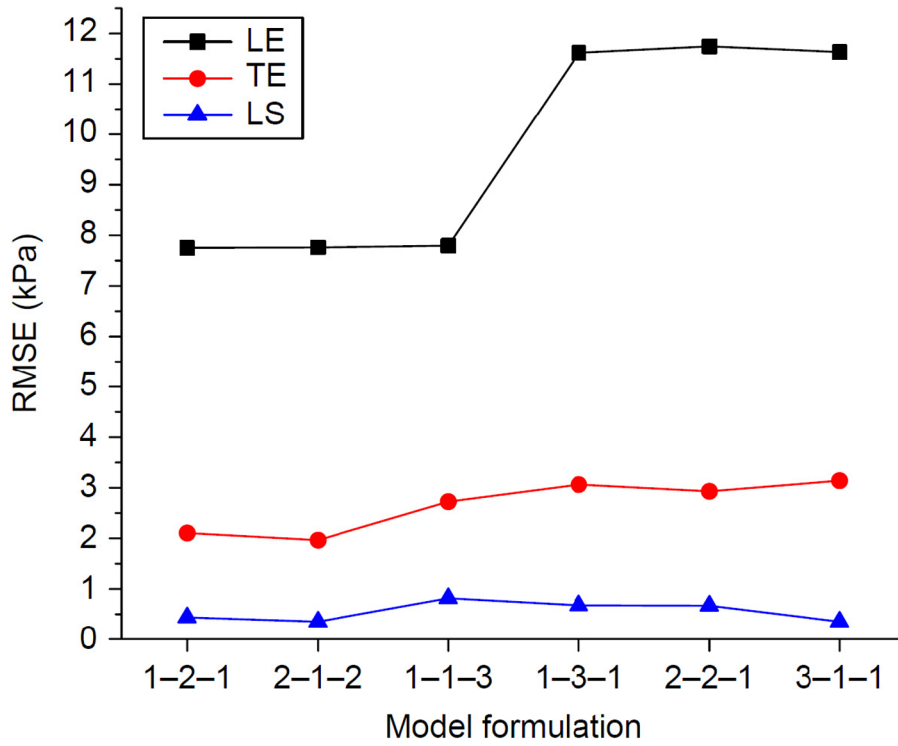


**Figure 3.3** Plots of LE, TE and LS RMSE for all models with five total terms. The two model formulations on the far left (1-2-2 and 2-1-2) clearly have the lowest RMSEs for all the three directions.

**Table 3.2**  
Parameter coefficients for 1-2-2 and 2-1-2 models as determined by using ALL and EACH curve-fit methods

Method	Model terms numbers			$I_1$ term coefficients		$I_2$ term coefficients		$I_4$ term coefficients	
	# $I_1$ terms	# $I_2$ terms	# $I_4$ terms	$a_1$	$a_2$	$b_1$	$b_2$	$c_2$	$c_3$
ALL	1	2	2	3.46	–	–1.82	1.62	25.00	28.79
	2	1	2	1.65	2.01	–0.77	–	24.84	29.16
EACH	1	2	2	3.53	–	–1.92	1.81	27.13	28.80
	2	1	2	1.76	2.46	–0.91	–	26.67	29.86

Note: kPa values.



In order to further determine whether one model is superior, plots of the model against the experimental data are examined (Fig. 3.4). While the 1–2–2 and 2–1–2 models both appear to fit the general trend of the experimental data well, it is clear by visual inspection that the 1–2–2 LS model (Fig. 3.4(a)) is not a good fit. At the same time, the fit of LE, TE and LS data for the 2–1–2 model all follow the general tenor of their respective experimental data, making it a good fit from RMSE, variance and visual inspection standpoints.

While the RMSE values for ALL method curve fits are significantly lower for EACH models, this does not automatically translate into differences that are biologically and/or clinically significant. As a measure of relative goodness-of-fit, RMSE can be used to discriminate between given models. This discrimination does not, however, give an indication of how the differences in these fits translate into the material properties described by a given model. Also, given the nature of the complex polynomial selected for this constitutive model, a direct comparison of the individual coefficients cannot be used to discern downstream differences in the tissue description.

In order to establish a sense of the magnitude of the biological relevance of the differences in the models found using the EACH and ALL methods, we have chosen to examine the linear elastic portions of the stress–strain curves that the models describe. This was done on the model that was ultimately deemed to best represent the example data, the 2–1–2 model (i.e. two  $I_1$  terms, one  $I_2$  term and two  $I_4$  terms). The linear moduli for the EACH and ALL 2–1–2 models were found for all the three material directions, using the method described by Haut Donahue et al.<sup>134</sup> These moduli, along with the RMSE values for these two models have now been included in the manuscript as Table 3.3.

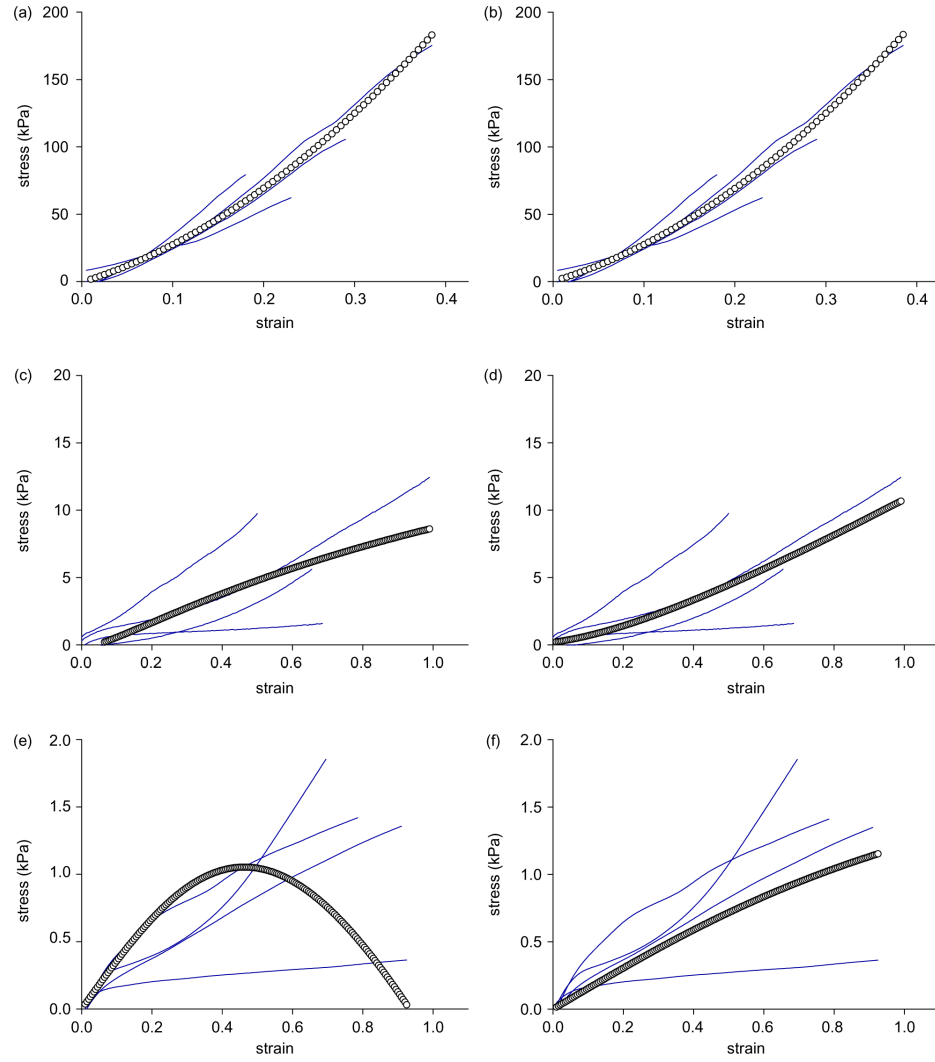


**Figure 3.4.** Models 1–2–2 (a, c and e, left) and 2–1–2 (b, d and f, right) plotted against experimental data for (a–b) LE, (c–d) TE and (e–f) LS. While both models report similar RMSEs for all directions, the 1–2–2 LS plot's shape clearly departs from the shape of the typical experimental data plot.

**Table 3.3**  
RMSE and Linear Slope for 2-1-2 models defined using EACH and ALL methods.

	RMSE			Linear slope		
	EACH (kPa)	ALL (kPa)	Difference (%)	EACH (kPa)	ALL (kPa)	Difference (%)
LE	8.5E+0	7.8E+0	9	4.7E+2	5.3E+2	12
TE	2.1E+0	2.0E+0	6	1.3E+1	1.2E+1	9
LS	3.6E−1	3.5E−1	3	1.5E+0	1.4E+0	14

While these results show that there is roughly a 10% change in the moduli across all directions between the ALL and EACH methods, this would not be enough to put the change into context. As such, we have gone to the literature to look for what would constitute significant changes in linear modulus of passive skeletal muscle.

Examination of the data in Table 3.3 shows that there are differences in the linear moduli of 60, 1 and 0.1 kPa for the LE, TE and LS directions, respectively. While there has been little in the way of examining passive skeletal muscle tissues (in comparison to the prolific volume of work done on active muscle properties), there has been even less to show differences in transverse material properties in particular. However, in the data on passive longitudinal properties, Bensamoun et al.<sup>146</sup> showed that a difference of 3.41 kPa in stiffness could be attributed to improvement in muscle function in patients undergoing treatment to hyperthyroidism, and Van Ee et al.<sup>136</sup> found that stiffness would increase by over 40 kPa as a skeletal muscle progressed from immediate post-mortem to post-mortem hour 10. Given these supporting data, we feel that the differences that are found between modeling methods are biologically and clinically significant. Additionally, it may be noted that, while assessments concerning inter-specimen variability could be addressed through testing a single specimen under each test condition, the destructive nature of these experiments (e.g. straining samples beyond 15%) precluded the use of specimens for more than one trial.

The fitting of multi-dimensional data to a multivariate model is complex, and often requires a multifaceted approach to find the solution that best realises the goal of the modeller. The RMSE is very useful as one gauge of the goodness-of-fit between a model and the data it represents. By the nature of its mean normalisation, the coefficient of variance can help to further elucidate relative differences in samples. While the Hotelling's  $T^2$ -test did not eliminate many of the models under consideration from contention, it is still necessary to make sure that the overall variance between data and representative model is zero overall. In general terms, this indicates that the model effectively splits the data, with data equally spread above and below the model. Lastly, as was obvious in the final criteria for making a distinction between the 1-2-2 and 2-1-2 models, a computational model should never be accepted entirely based on overall statistical measures; qualitative inputs, such as visual inspection, can provide invaluable assistance in the selection between the otherwise indistinguishable models.

With a lower RMSE between experimental data and characterised models than that of the EACH method for every evaluated case, the use of the ALL method fits data better for every combination of terms in this polynomial formulation. In turn, this formulation, having up to three I1 terms, three I2 terms and five I4 terms, is highly flexible, making it capable of replicating other isotropic or transversely isotropic constitutive functions used in the mechanical analysis of biological tissues. While a particular case may exist for which the EACH method would be suitable, the RMSE findings and general flexibility of the model suggest that the ALL method will be the best at characterising 3D stress–strain data.

## **Conclusions**

When fitting a material model to experimental data from multiple trials, a better fit is obtained by fitting all data simultaneously. While RMSE can be used to find which combination of terms in a polynomial constitutive formulation most closely characterises experimental data, visual inspection should still be performed to ensure that the resulting model has an appropriate general shape and inflection points.

## **Acknowledgements**

Funding for this study was gratefully provided by the NIH Grant No. HD31476 from the National Institute of Child Health and Human Development. The authors affirm that they have no financial affiliation or involvement with any commercial organization that has direct financial interest in any matter included in this manuscript.

## **Chapter 4 – Intramuscular Pressure Predictions from a Hyperelastic Model of Skeletal Muscle**

### **Abstract**

Intramuscular pressure (IMP) has been shown to be a mechanical correlate for muscle force. As microsensors capable of providing clinical measurements of IMP are developed, the need increases for the ability to appropriately interpret these pressure values. While several 3D mathematical models have been created to aid in the analysis of skeletal muscle force and deformation, none have been developed that have been shown to be able to aid in the understanding of IMP. This work examines the pressure values predicted using a finite element model implementation of a single-phase continuum mechanics-based transversely isotropic and hyperelastic model under passive elongation. These values are compared against empirical results of passive load-elongation tests. Model predicted pressure values overestimated experimental data by an order of magnitude. Permutations of the model were evaluated, analyzing, in turn, the effects of hyperelasticity and anisotropy on pressure predictions. Neither of these factors contributed to the error in the calculated pressure levels. Additionally, methods of adding active muscle contraction by either adding terms to the hyperelastic constitutive equation or by imposing stresses on muscle elements are examined. Results of these investigations reveal that incorporation of active muscle contraction will likely require use of a user-defined material model.

### **Introduction**

Recent advances in the development of a microsensor<sup>83,85</sup> for measuring intramuscular pressure (IMP) have made minimally invasive quantification of mechanical muscle output a clinical possibility. IMP has been shown to be an effective surrogate measure for muscle tension.<sup>55-58,62-72</sup> However, as IMP has been shown to be sensitive to sensor placement,<sup>56,66,71,90,147</sup> the shape of the muscle,<sup>71,90</sup> and the compliance of the surrounding tissue,<sup>91</sup> a thorough understanding of the magnitude of the measured output is necessary. An empirical assessment of all of these issues would be onerous. Computational modeling of biomechanical tissues allows for investigation of their

loading response when experimental methods are impracticable. A 3D finite element analysis (FEA) of a continuum-based model could be used to model skeletal muscles of varying shape and surroundings. Such a model could then be interrogated to analyze the variance in IMP throughout the muscle. The quality of the FEA is dependent upon the accuracy of the constitutive model used and its suitability to predict the pressure recordings. Several continuum-based models of skeletal muscle exist. These models assume skeletal muscle is transversely isotropic, hyperelastic, and incompressible.<sup>103,105,106,132,148</sup> However, these models have typically been used to examine strain<sup>103,132</sup> or force,<sup>106</sup> and the only published model to examine IMP was in 2D.<sup>105</sup>

Additionally, no models that are currently available have been characterized using experimental data sufficient to fully describe a hyperelastic, transversely isotropic material. A new model was developed recently<sup>148</sup> using a transversely isotropic, hyperelastic, and nearly incompressible material model for implementation in the ANSYS FEA platform (ANSYS, Inc., Canonsburg, PA). This model was characterized using load-elongation data collected from New Zealand White rabbit (NZW) extension digitorum longus muscles.<sup>149</sup> This model has been shown to be able to accurately predict the passive force-length relationship of skeletal muscle.<sup>150,151</sup> The initial goal of this study was to evaluate the use of an FEA implementation of the transversely isotropic, hyperelastic, and nearly incompressible material model to be able to predict IMP as well as muscle tension. An ANSYS model was developed of an isolated NZW tibialis anterior (TA) muscle. Pressures predicted by the model were compared to previously published experimental length-pressure and length-tension data from an isolated NZW TA.<sup>59</sup> Following the hyperelastic modeling attempt, sensitivity of pressure predictions, active stress implementation, model meshing variables, and constitutive model selection were investigated to account for the hyperelastic model failure. Multiple ways of implementing active stress were explored including alterations to the constitutive formulation, addition of an initial uniform stress, and applied surface stresses. Analyses were performed on element size, number of element nodes and element numbering to determine optimized values for each of these variables. The final investigation considered the constitutive model used to characterize the skeletal muscle. A Generalized Fung model and a transversely, isotropic elastic model were attempted to better represent experimental results. While many of the methods investigated in this chapter have been examined towards understanding the length-tension relationship of

skeletal muscle, the investigation here focuses also on the ability to characterize the length-pressure relationship. Understanding if a single-phase solid model can predict pressure is crucial to the goal of understanding how IMP is manifest in skeletal muscle.

## Materials and Methods

### *Experimental Data*

The length-tension-IMP characteristics of the tibialis anterior (TA) of NZW rabbits were collected experimentally. In brief, the TA was isolated and dissected free up to the proximal tendon. The femur was secured with pins and the distal tendon was clamped and attached to a force transducer to collect resultant forces from imposed displacements. IMP was collected by insertion of a microsensor (Luna Innovations, Inc., Roanoke, VA) into the mid-belly of the TA. As the IMP sensor measured relative pressure, the pressures used for this study were zeroed at  $L_0$ . Strains were imposed at 3% intervals between 0% and 23% strain. Full details of the experimental data collection can be found in Davis, et al.<sup>59</sup>

### *Constitutive Model*

A polynomial strain energy density formulation was used to represent the skeletal muscle tissue as transversely isotropic, hyperelastic, and isovolumetric:

$$W = \sum_{i=1}^2 a_i (I_1 - 3)^i + b(I_2 - 3) + \sum_{k=2}^3 c_k (I_4 - 1)^k + \frac{1}{d} (J - 1)^2 \quad (4.1)$$

where  $a_i$ ,  $b_j$ ,  $c_k$ , and  $d$  are material parameters;  $J$  is the Jacobian, and  $I_1$ ,  $I_2$ , and  $I_4$  are the first, second, and fourth invariants of the deformation tensor, respectively. The material parameters were determined by simultaneously fitting stress-strain data from material tests of NZW rabbit skeletal muscle under longitudinal extension, transverse extension, and longitudinal shear.<sup>149</sup> The best fit of the material data was obtained when using 2  $a$ -terms, 1  $b$ -term, and 2  $c$ -terms.<sup>148</sup> Values used are given in Table 4.1.

**Table 4.1**  
Characteristic Model Coefficients (MPa)

$a_1$	$a_2$	$b_1$	$c_1$	$c_2$	$d$
0.0016	0.0020	-0.0008	0.0248	0.0292	0.001

### *Model Geometry*

The FEA geometry was created from Magnetic Resonance images of a NZW rabbit hindlimb. The scans were manually segmented in Analyze (Mayo Clinic, Rochester MN) to record aspects of muscle geometry, including length, thickness, and location of tendinous attachments and were used to create a representative muscle geometry (Fig. 4.1). Since the scanned muscle was shorter than the reported average length of the experimental muscles, the geometry of the segmented muscle was scaled to match the experimental tests.

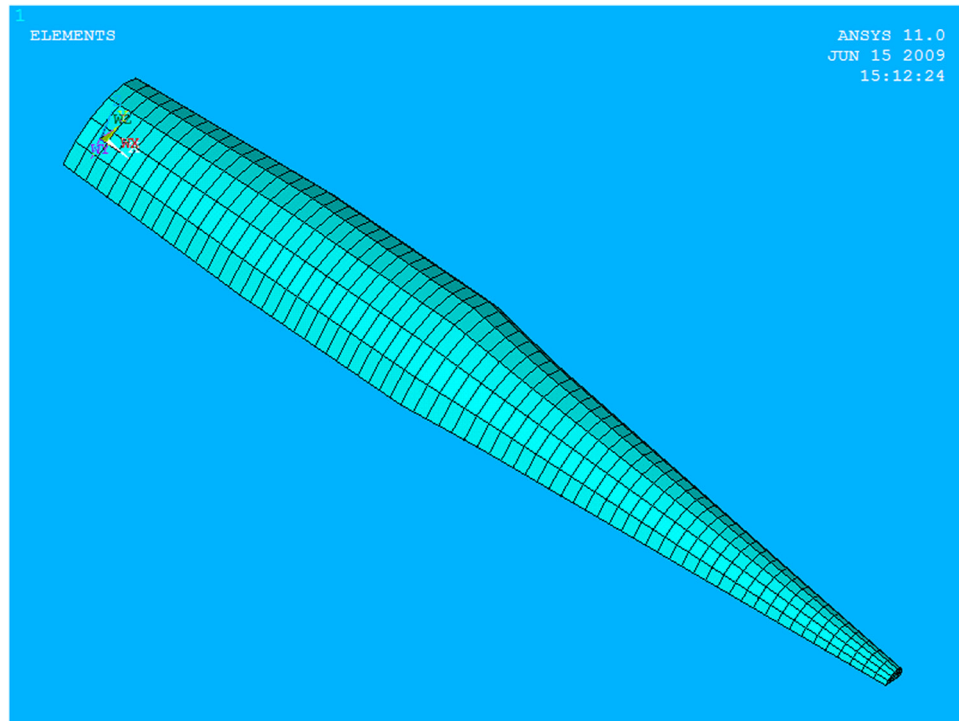


**Figure 4.1.** 3D mesh of idealized muscle geometry. Dimensions taken from MR images of rabbit tibialis anterior.

### *Finite Element Model*

The defined muscle geometry was meshed in using 852 8-noded brick elements with a mixed u-p formulation to simulate incompressibility. Displacement boundary conditions were used to simulate experimental trials (strained from 0 to 24%). All nodes



in the area of proximal tendon attachment were pinned (i.e., all displacements were set to zero). Nodes in the area of the distal tendon, on the deep surface of the TA, were set equivalent to the imposed displacement for each experiment (Fig. 4.2). For each displacement, resultant forces for proximal tendon area nodes were summed vectorially and plotted to create the length-tension comparison. IMP was modeled as the calculated hydrostatic pressure, taken from a node in the deep muscle belly representative of the location of the IMP microsensor in the experimental trials.

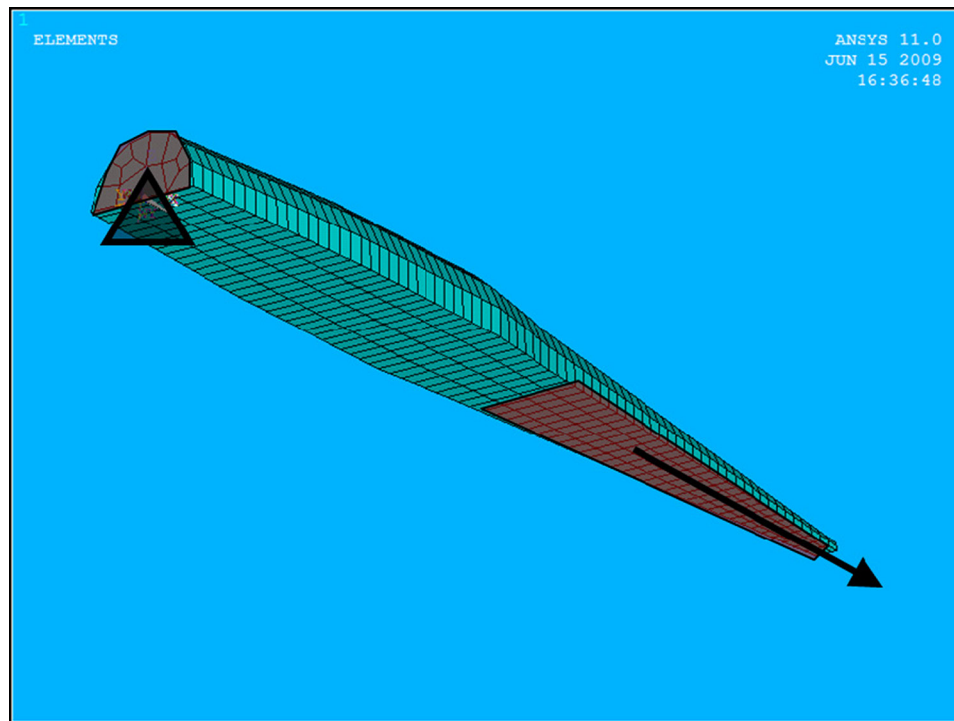


**Figure 4.2.** Schematic of applied boundary conditions. The nodes representing the proximal tendon attachment site (upper left) had encastre boundary conditions applied while nodes corresponding to the distal aponeurosis attachments (lower right) had a uniform displacement applied corresponding to the displacement simulated.

## Results

The experimental results of the length-tension relationship were successfully predicted by the computational model. As shown in Figure 4.3A, all model predicted tensions fell within one standard deviation of the experimental means. The model was not predictive

of the experimental length-pressure relationship, however, as it over predicted experimental values for all strains above 2% (Fig. 4.3B).

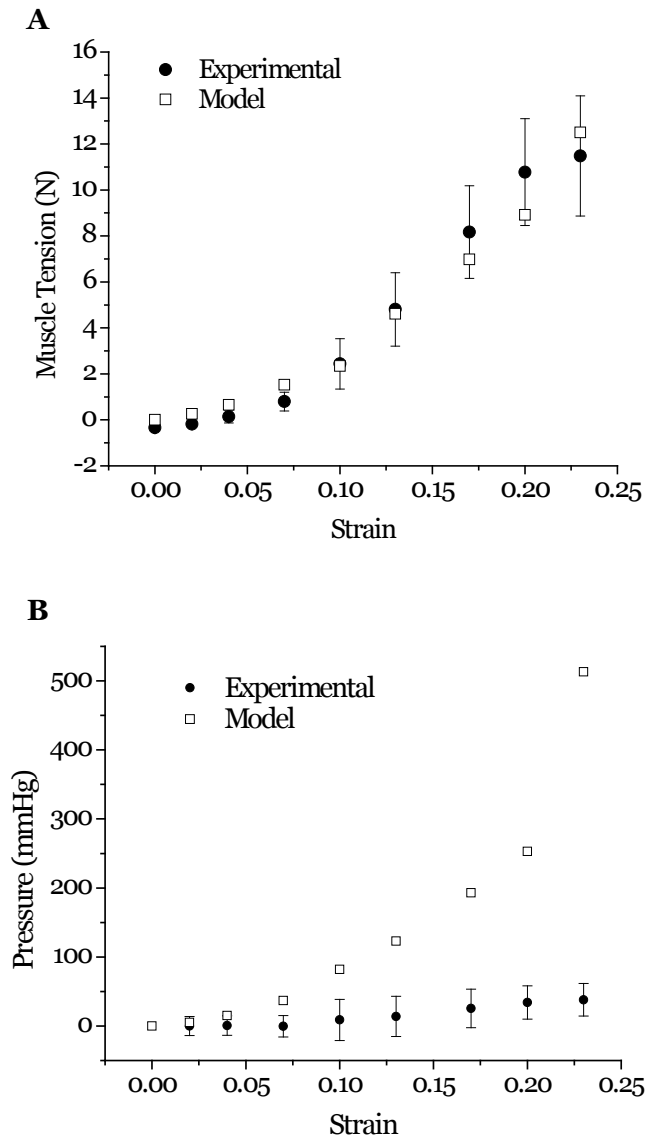


**Figure 4.3.** Length-tension(A) and length-pressure (B) relationships for experimental and model data. Model tension predictions all fall within one standard deviation of the mean of the experimental results. Pressure predictions exceed experimental results by an order of magnitude.

## Discussion

Like other published continuum-based models, the current model has shown the ability to accurately predict the length-tension relationship of skeletal muscle.<sup>103,105,106,132</sup> The model predicted tensions falling within one standard deviation of the mean over a large range of strains indicating a high level of robustness. That the model was characterized with one data set<sup>149</sup> and characterized against a completely different set of experimental results<sup>59</sup> is further confirmation of the robustness of the solution.

The ability of the constitutive model to predict the length-tension response did not directly lead to an accurate prediction of the length-pressure relationship of skeletal muscle. Predicted values were an order of magnitude higher than the experimental results.<sup>59</sup> The values reported in the experiment used in the current study had subsequently been validated in a separate set of experiments reported by Winters, et al.<sup>61</sup> Winters reported pressures of ~50 mmHg at 16% strain. This is nearly twice the pressure reported by Davis at a similar strain (25 mmHg at 17% strain). The difference in the results may be accounted for by the difference in experimental methods. In the Davis paper, tension and pressure were measured in an isolated TA; in the Winters study, the muscle remained in an intact myofascial compartment. The constraints of the native environment may be responsible for these higher pressures. Still, the observed increases were only a factor of two, well below the order of magnitude predicted by the model.

### *Model Sensitivity and Pressure Predictions*

To investigate the sensitivity of the pressure predictions to the model parameters, pressure was calculated for varied model input parameters. Of the six parameters in the constitutive formulation (Eq. 4.1), only the A2 and D terms appeared to have a substantive effect on the predicted pressures (Fig. 4.4). While altering the values for each of these terms did affect the pressure predictions, neither reduced the pressure to the levels observed experimentally.

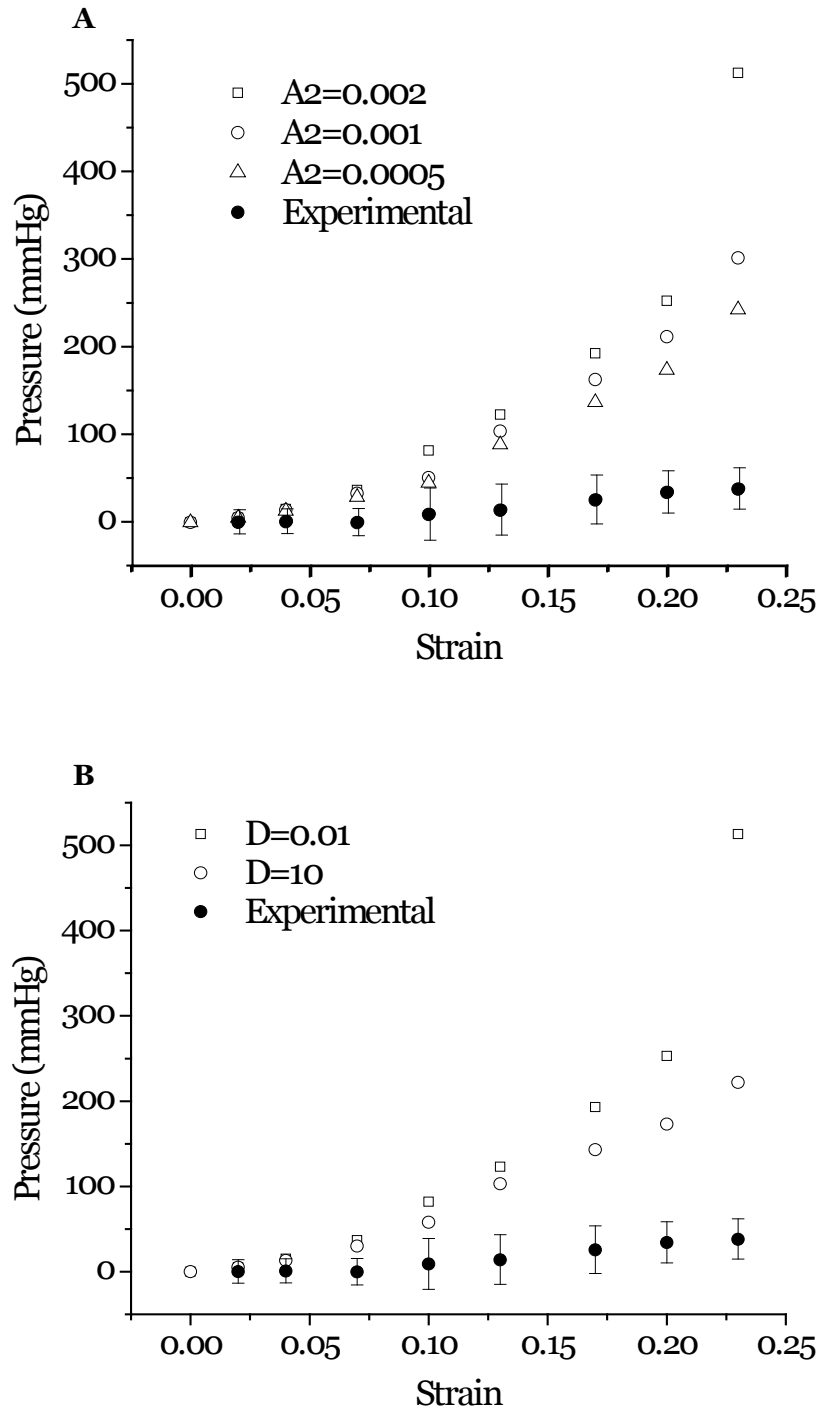


**Figure 4.4.** Length-pressure model sensitivity to  $A_2$  (A) and  $D$  (B) parameters. While variation in each parameter yielded changes in pressure, predicted pressure values remained substantially higher than experimental values.

Taken together, these conclusions lead to questions regarding the ability of this constitutive model to represent intramuscular pressure. One consideration would be the nature of the output measure available to represent IMP. With an ANSYS hyperelastic model, material pressure is represented by HPRES, or hydrostatic pressure. This pressure is given as

$$HPRES = -\frac{1}{3}\sigma_{ii} \quad (4.2)$$

where  $\sigma_{ii}$  represents the principle stresses in the solid. This is sometimes referred to as the spherical stress. While the spherical stress provides an indication of the pressure within a volume of material, this isochoric stress is not truly reflective of what is measured by the IMP microsensor. Recall that IMP is measured as the pressure of the interstitial fluid surrounding the skeletal muscle fibers. The lumped-parameter approach appears to be sufficient for characterizing the stress-strain behavior of muscle, but a material description that considers the solid and fluid components of fluid separately may be more appropriate for pressure characterization.

Additionally, the characterization of skeletal muscle as incompressible may need to be re-evaluated. This has recently been examined in an imaging-based study investigating muscle volume on the single-fiber and fiber-bundle levels.<sup>152</sup> This study found that, while individual fibers could be described as isovolumic, examination of the bundle volume showed a decrease in volume of up to 40% with a 130% strain. A change in volume with strain would be indicative that incompressibility should not be enforced in the constitutive material model. The results of the D-term sensitivity shown in Figure 4.5B would seem to support this as being desirable from a pressure output standpoint as well. The D-term operates as a kind of Lagrangian multiplier enforcing the volumetric portion of the strain energy density function (Eq. 4.1). An increase in the D-term value indicates a relaxation of the isovolumic restriction. This increase corresponds with a decrease in the model-predicted pressure. While the decrease in pressure does not reduce to the level of the experimentally-observed pressure, the change supports that further investigation of the isovolumic assumption is warranted.

### *Active Stress Using Constitutive Formulation*

Current methods used for adding active muscle tension typically involve the addition of a separate component to the energy density function. Usually, implementation of a solution of this type requires the use of a user-defined material. Use of a user-defined material can also involve installation of additional software and programming libraries to run. Thus this type of solution becomes less universal and more difficult to share with other investigators. Part of this investigation focused on alternative methods to incorporate muscle activation into a finite element formulation using built-in functions to facilitate collaborations with others.

The most easily implemented solution would be the addition of another term of the constitutive formula. Recall that the 2<sup>nd</sup> Piola-Kirchoff stress,  $\mathbf{S}$ , can be derived from the strain energy density equation using:

$$\mathbf{S} = 2 \sum_{a=1}^5 \frac{\partial \Psi}{\partial I_a} \frac{\partial I_a}{\partial \mathbf{C}} \quad (4.3)$$

where  $I_a$  are invariants of the deformation tensor and  $\mathbf{C}$  is the right Cauchy-Green deformation tensor. Combining Equations 4.3 and 4.1 yields

$$\mathbf{S} = 2 \left[ \left( \sum_{i=1}^3 i a_i (I_1 - 3)^{i-1} \right) \mathbf{I} + \left( \sum_{j=1}^3 j b_j (I_2 - 3)^{j-1} \right) (I_1 \mathbf{I} - \mathbf{C}) + \left( \sum_{k=2}^6 k c_k (I_4 - 1)^{k-1} \right) \mathbf{M} \right] \quad (4.4)$$

A cursory examination of this equation reveals that, for any set of variable characterizations, the formulation requires zero stress at zero strain. Muscle is defined in constitutive models as being at optimal length at the point of zero strain. This also happens to be the point at which active muscle tension is maximal. Since this is clearly at odds with the zero stress/zero strain criteria, any combination of model terms using this formulation will not be able to represent active muscle tension.

### *Active Stress using Initial Stress*

Current models that implement active stress do not differentiate the magnitude of the active stress within the muscle by location. Accordingly, another consideration for imposing an active muscle stress state involved use of a uniform stress, applied in the

longitudinal direction of each muscle element. This addition of one additional stress factor would have the same effect as having a separate strain energy density term. This was implemented in ANSYS using the INISTATE command. Conceptually, a muscle experiencing activation and passive elongation would be modeled in a two-step process: an initial stress would be applied (representing muscle activation); then, a deformation would be applied (representing passive elongation). A uniform pre-stress was successfully applied to the model. Unfortunately, the model would not converge when a subsequent deformation was applied. This seems to have been the results of the material model. Hyperelastic materials, especially at the level of biomechanical materials, have very low stiffness initially and become stiffer with deformation. A low initial stiffness will result in very large deformations for even a very small force. The best method to solve this type of loading would be to apply a very small load initially, gradually increasing it as the stiffness is updated based on the resulting deformation. Unfortunately, INISTATE applies the full load in the first load step, when the stiffness is very small, which I believe caused the model to be divergent.

Convergence could be achieved through use of the STABILIZE command. However, use of STABILIZE had the effect of dissipation of the stresses in the body, hence negating the calculated reaction forces. A comparison of the reaction forces with stabilization on or off for various strains reveals that the reaction forces are dissipated when the stabilize command is implemented (Table 4.2).

**Table 4.2**

Comparison of the effect of number of element nodes and stabilization on model volume and predicted reaction forces. Asterisks indicate models with reaction forces that compare favorably to empirical data (all simulations with STABILIZE off).

<b>ET (nodes)</b>	<b><math>\lambda</math></b>	<b>STABILIZE</b>	<b>Model Volume (mm<sup>3</sup>)</b>	<b>Reaction Forces (N)</b>
20*	1.02	off	2375.45	0.25
20	1.02	on	2375.45	-3.0E-4
20*	1.18	off	2375.45	8.9
20	1.18	on	2375.45	1.8E-3
8*	1.02	off	2315.29	0.26
8	1.02	on	2321.29	6.8E-11
8*	1.18	off	2329.16	8.8
8	1.18	on	2504.29	2.9E-9

### *Active Stress using Applied Surface Stresses*

The next attempt at adding active muscle tension was inspired by the sarcomeric contraction that occurs during muscle activation. Accordingly, equal and opposite stresses were applied to create compression on each element in the longitudinal (i.e., fiber) direction (Fig. 4.5). The magnitude of the applied stress was selected to be one-half of the anticipated stress based on values from literature.<sup>59</sup>

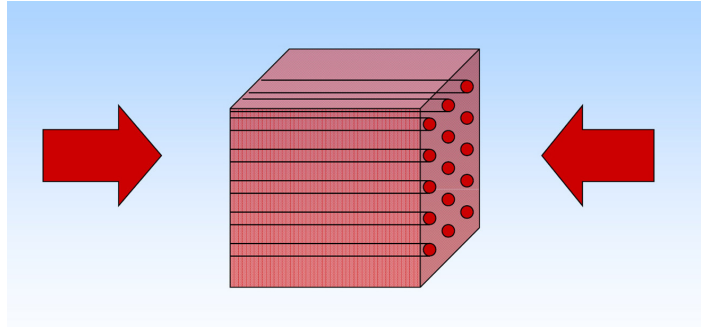


**Figure 4.5.** Application of surface stresses equal in magnitude and opposite in direction to simulate muscle activation.

This method of simulating muscle activation successfully increased the observed stresses in an individual muscle element. When this was incorporated into a whole-muscle model, however, there was no observable difference between a passive muscle and an activated muscle for any given strain level (Fig. 4.6).

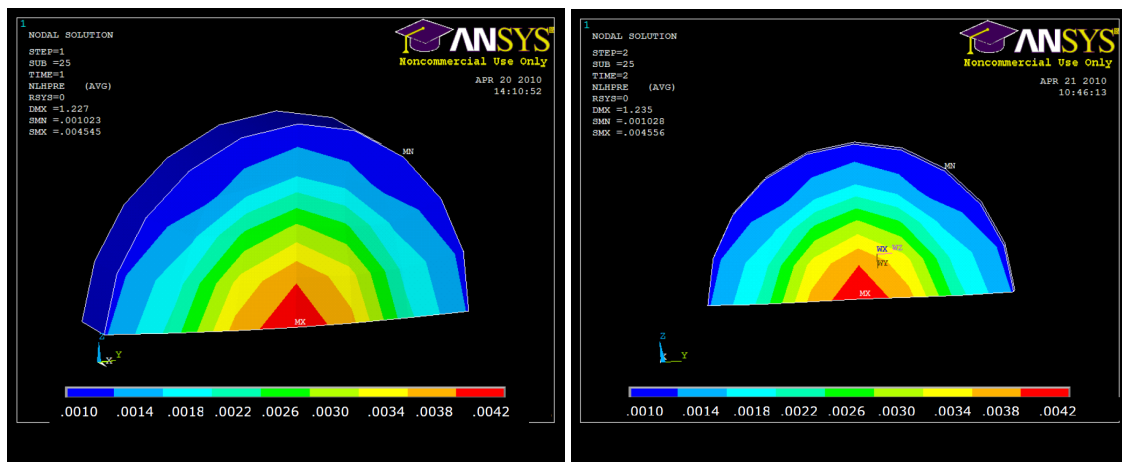


**Figure 4.6.** Cross-section of muscle model showing pressure levels under passive (left) and combined passive and active (right) loading using equal-and-opposite stresses at each element to simulate active loading. There are no differences in the pressure due to this loading.



The lack of this method to manifest itself in higher pressure readings in the muscle midsubstance was examined. It was shown that, for elements in series, the opposing stresses at adjacent faces canceled each other's effects as demonstrated in Figure 4.7.

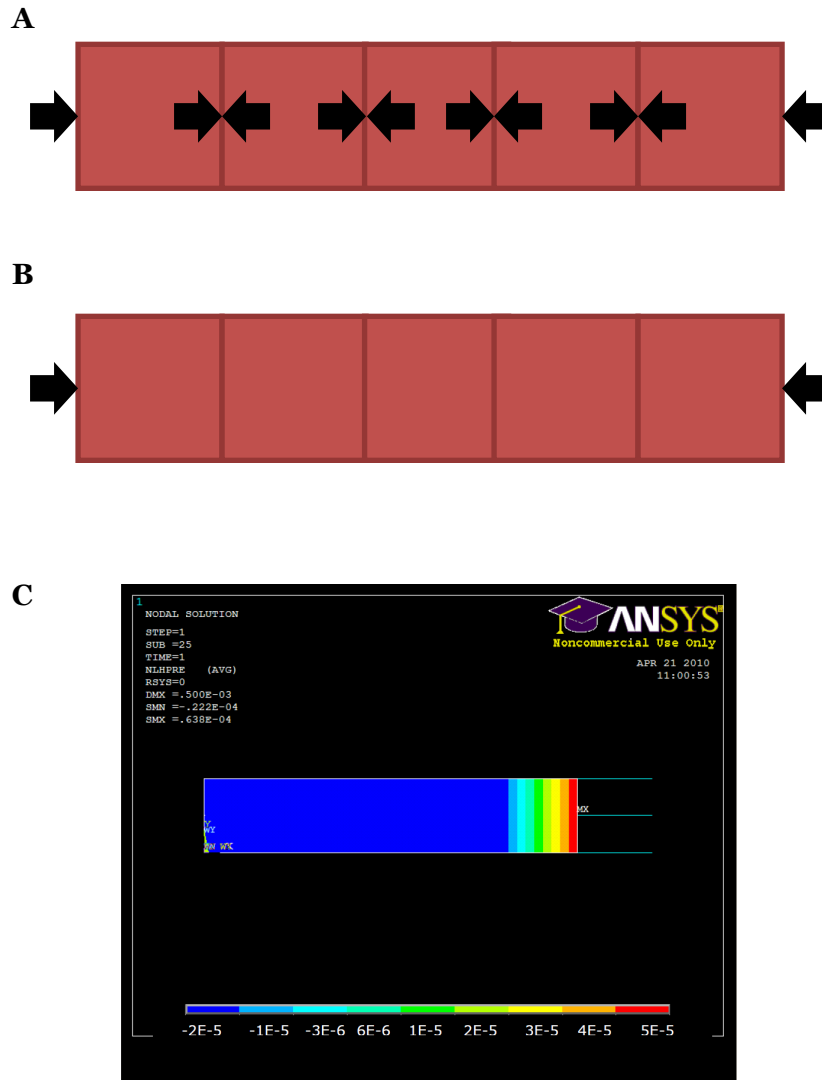


**Figure 4.7.** When elements with compressive stresses on opposing faces are arranged in series (A), the stresses on adjacent faces have the effect of cancelling each other out. As a result, the pressure in the model midsubstance is homogenous, with a net effect much smaller than intended (C). The pressure gradient at the far-right portion of the model in (C) is caused by the passive loading applied through stiff spring elements (representing tendons). It should be noted that there were no observed differences in results from loading directly onto the muscle material or loading via stiff springs as shown above.

A higher pressure could be affected by aligning all compressive surface pressures to align to a user-selected central point (Fig. 4.8). The method, however, is not rooted in empirical science and is arbitrary in its implementation. As such, it was considered an unsatisfactory solution.

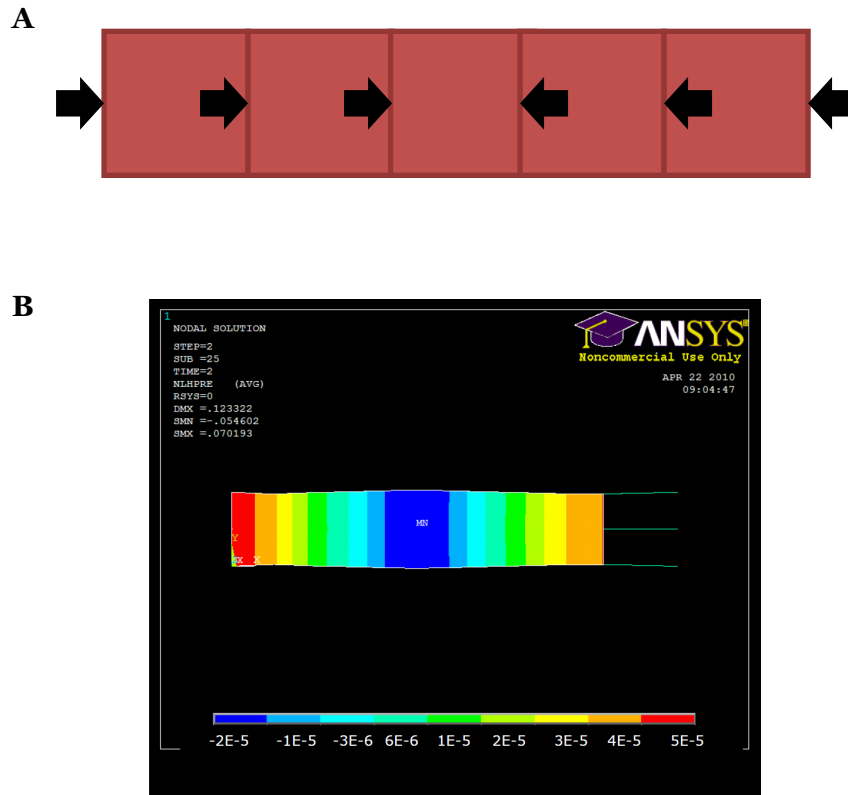


**Figure 4.8.** If applied surface stresses are arranged as converging on a central location (A), and central higher pressure can be created (B). This has a net effect that compares favorably against 4.7(C) above, but is artificially induced.

In summary, investigations have shown that a separate stress term cannot be added to the AHYPER formulation to represent muscle activation. Attempts at using an initial stress state to apply a pre-stress representing active muscle stress were also unsuccessful. In this case, the high magnitude of active muscle stresses needed at low deformation levels cause convergence issues with finite element model software. While model stabilization could be performed, allowing model convergence, stabilization had the unfortunate side effect of eliminating the applied pre-stress. Other methods of applying stresses directly to individual elements were also investigated. Applying

compressive stresses to opposing element faces successfully increased the stress in an individual element. When elements were arranged in series, however, stresses on adjacent faces have the net effect of cancelling each other out. Lastly, a selective assignment of compressive force application could be implemented, effecting an increase in IMP (as in Figure 4.8). Unfortunately, there are no available biological reasons for the application of stresses in this manner, making this approach arbitrary and artificial. The conclusion drawn from these activities is that a full model of skeletal muscle, capable of predicting IMP from active and passive sources, will require use of a user-defined material model. This will allow combinations of constitutive formulae to be implemented, and will not require that stresses be applied to elements in ways not consistent with biological function.

### *Element Size Sensitivity*

Element size was evaluated using a sensitivity analysis. The 3D muscle mesh generated for this study (Fig. 4.1) was populated by hexahedral elements ranging in size from 0.5 to 5 mm on a side. The effect of element size on reaction force and model volume for an imposed 9% strain is shown in Figure 4.9. There is a 10% drop in volume when elements are larger than 1.5 mm compared with a mesh of smaller elements. Similarly, the reaction force drops with elements that have side lengths of more than 1 mm. Based on this sensitivity analysis performed at 9% strain, it is recommended to use elements with a length of 1 mm per side to maintain both reaction force and model volume while maximizing element size.

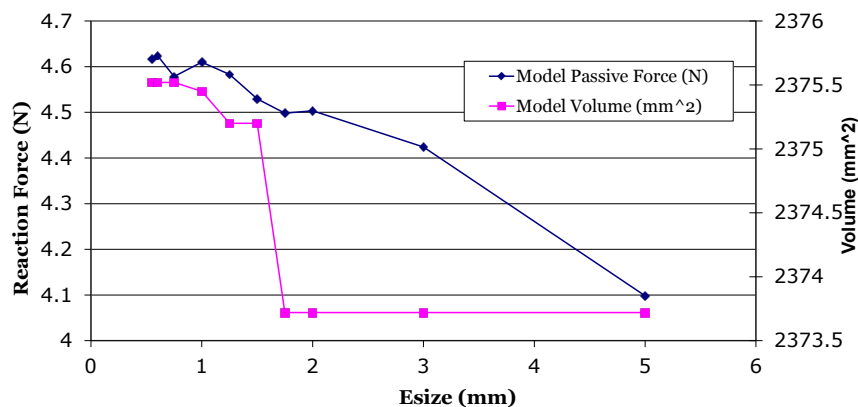


**Figure 4.9.** Element size sensitivity reveals that elements with side lengths  $\leq 1$  mm show stabilization in both reaction force and model volume when subject to a 9% strain.

### *Number of Nodes per Element*

An additional mesh consideration involves the number of nodes that should be used in an element to obtain a satisfactory solution. The number of nodes in hexahedral elements was evaluated in an ANSYS model under strains of 2% and 9% (see Table 4.2). It is clear from this sensitivity analysis that 20-noded elements maintained their volume much more consistently than the similarly strained 8-noded elements. Volumes for the model populated by 20-noded elements did not change at all. The 8-noded-element model only experienced volume changes under 2% and the resulting reaction forces calculated compared favorably with empirical data. Thus, the use of either 8 or 20 noded elements does not affect the resulting model reaction forces appreciably.

### *Element Numbering*

Creation of the mesh shown in Figures 4.1 and 4.2 was achieved through interactions with ANSYS customer service. Initial attempts at mesh creation began with standard creation of semi-circular cross-sectional areas using keypoints. Keypoints were subsequently connected to form surfaces and, from there, a volume. This volume, even when used with a relatively simple isotropic and linearly elastic material model, would not converge. A customer service representative eventually suggested creation of the mesh by creating a sagittal cross-sectional area and using the volume sweep command in ANSYS. This created a model that converged rapidly under passive deformation (Fig. 4.10). As shown in Figure 4.10(B), the response of active loading, as implemented using applied surface pressures, did not yield a symmetrical response. Given that the geometry, boundary conditions, and activation loading were similarly symmetrical, the response should have been as well.

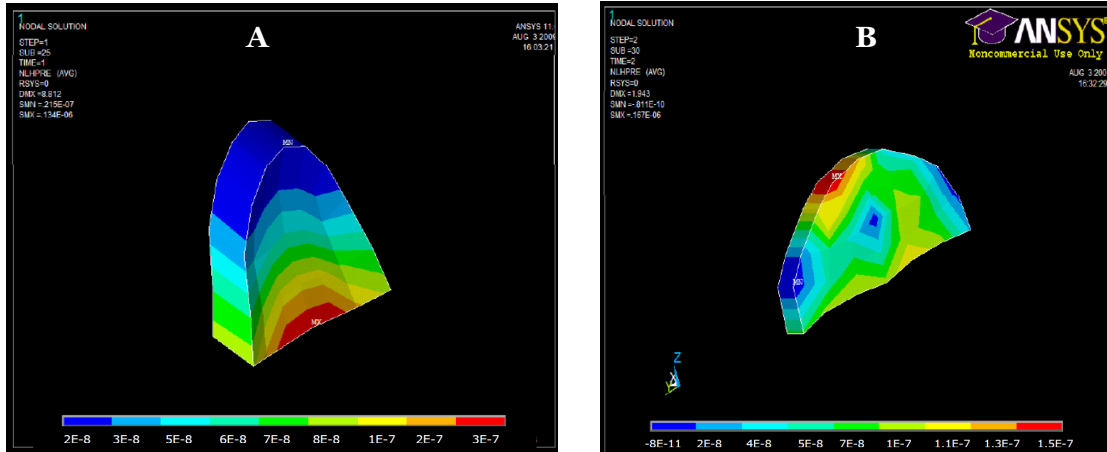


**Figure 4.10.** Passive loading resulted in uniform pressure distribution as shown in the muscle cross-sectional slice (A). Addition of activation in initial mesh model showed non-uniform response (B).

Subsequent analysis of the mesh revealed the non-symmetrical response to be the result of the node numbering system applied during the volume sweep meshing routine on ANSYS. Reassigning element outward facing normals needed to be performed to achieve the symmetrical response. The problem of how to appropriately apply an active stress still remained unanswered, so continued investigation was required.

### *Generalized Fung Model*

A number of efforts were undertaken in the consideration of which constitutive formulation should be used to characterize skeletal muscle in the finite element formulation. Recall that creation of a skeletal muscle model began by assuming that skeletal muscle should be modeled as transversely isotropic, hyperelastic, and nearly incompressible. FE implementation began using ANSYS, which had the built-in AHYPER formula, the only anisotropic hyperelastic model in ANSYS. When it was determined that the AHYPER model that was built into ANSYS would not be capable of characterizing activated muscle, and when the pressure response to deformation greatly overpredicted experimental results (Fig. 4.4), available anisotropic hyperelastic models using Abaqus (Simulia, Warwick RI) were considered. Abaqus contained two built-in anisotropic hyperelastic models, a generalized Fung<sup>153</sup> form and a Holzapfel-Gasser-Ogden<sup>154</sup> form. The Holzapfel-Gasser-Ogden form was developed to accommodate

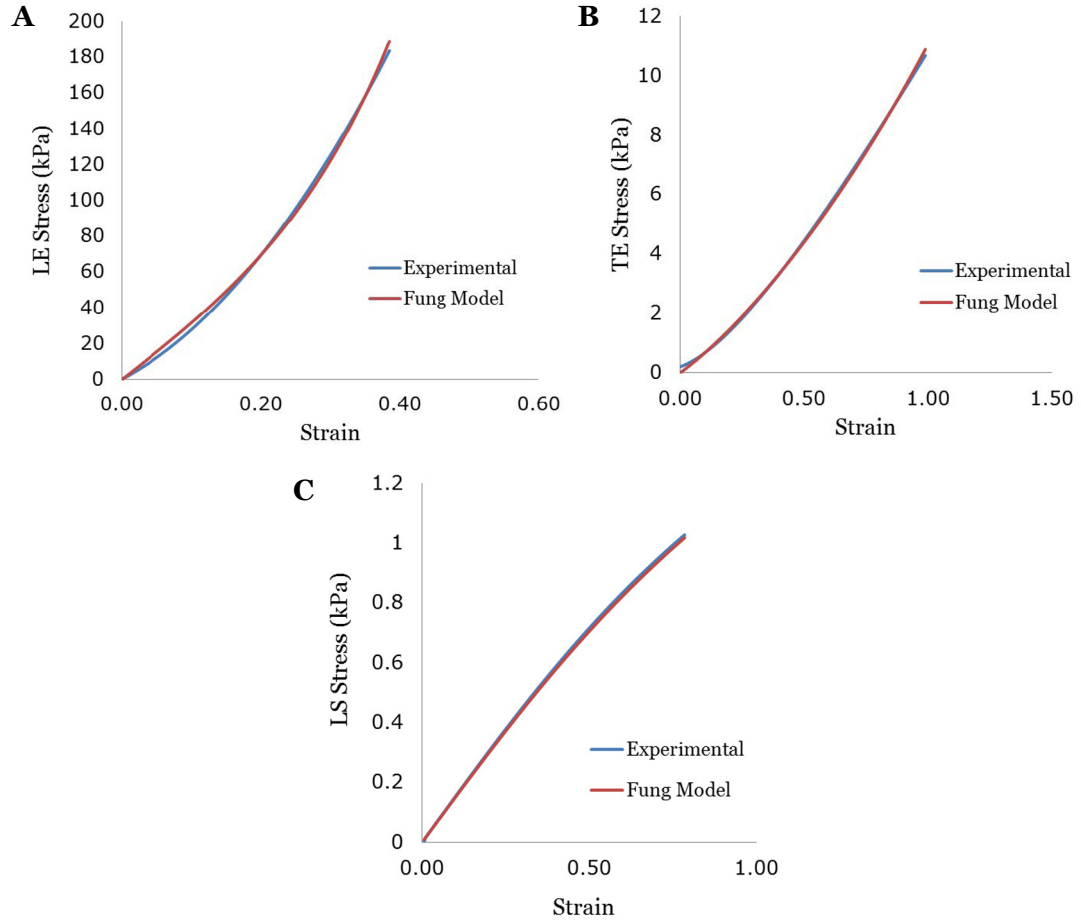


**Figure 4.11.** Generalized Fung model was able to be characterized sufficiently well to replicate trends in empirical data. There is excellent agreement with the stress-strain data from (A) LE, (B) TE and (C) LS tests.

multiple planes of isotropy. Since a transversely isotropic formulation only requires one family of fibers, this model was deemed more complex than required and was not considered. To account for the transverse isotropy without the additional complexity, Generalized Fung model was chosen. A least-squares optimization was created in MATLAB for the Generalized Fung form and characteristic values were obtained that created reasonably good agreement with empirical data (Fig. 4.11).

Unfortunately, this model would not converge when run in Abaqus. The characteristic parameters obtained using optimization of experimental results were compared with the parameters given in the example problem from the Abaqus Validation Manual (see Table 4.3). The largest discrepancy found in parameters that affected model performance (the  $b$  parameters) was in the shear term, which was three orders of magnitude larger in the

validation example than in the curve-fit for the muscle data. (As an aside, the C term also varies by orders of magnitude. This value, however, scales the entire response and was not found to be the source of non-convergence.) The validation model shear value was subsequently substituted for the value determined from fitting the Fung model to experimental data. Using the validation shear term allowed the FE model to converge. However, use of this term also causes the LS stress values to increase several orders of magnitude as well (Fig. 4.12). Several  $b_4$  values were used in a manual search to find a suitable solution (i.e., a model that would converge and match empirical shear stress – shear strain results). No values were found which produced reasonable matches to shear stress data as well as a convergent model. There are a few particular traits of the generalized Fung model that make this a not entirely unexpected result. Part of the convergence issues could be a result of the fact that the generalized Fung model is not polyconvex.<sup>155</sup> Additionally, it has been noted that the Fung model may exhibit decreasing shear stress with increasing shear under moderate loading, a behavior that may cause problems when attempting to model biological tissues.<sup>156</sup>

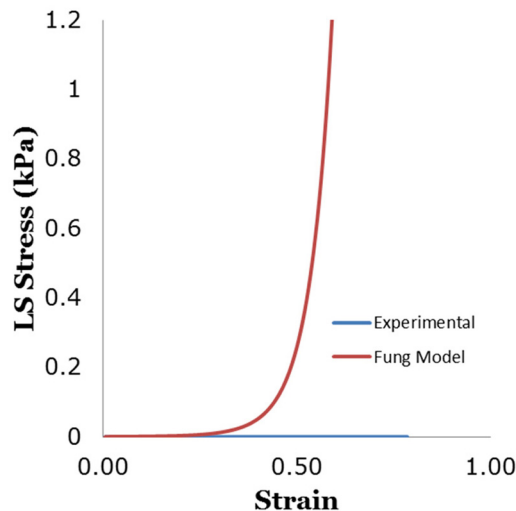


**Figure 4.12.** Increasing shear to a magnitude that will allow convergence of the Generalized Fung model causes the LS stress prediction to be several orders of magnitude too high.

**Table 4.3**

Values for generalized Fung model obtained by optimization to fit experimental load-elongation data<sup>149</sup> and provided by Abaqus Verification Manual.<sup>157</sup>

	C (MPa)	b1	b2	b3	b4
Optimization	0.575	0.8597	0.034	0.025	0.001
Validation	2.7E+04	0.9925	0.418	0.009	5

### *Transversely Isotropic Linearly Elastic Model*

One additional check was evaluated to determine if the high estimate of hydrostatic pressure as predicted by the transversely isotropic, hyperelastic, and nearly incompressible (TIHI) model implemented in ANSYS was a problem with the material definition. A transversely isotropic, linearly elastic (TIE) model was created in Abaqus. The model was defined using the linear portion of the stress-strain results from published experiments.<sup>149</sup> TIE simulations were run to stretch ratios of 1.2. A rectangular brick mesh was created for testing, to eliminate any confounding influence of geometry. The brick was representative of the size of the modeled muscles, with a length of 25 mm, a width of 6 mm, and a thickness of 5 mm. As guided by previous sensitivity analyses, elements were 1 mm long per side. As shown in Figure 4.13, the results of the TIE model were similar in magnitude to the predictions of the TIHI model for both length-pressure and length-tension. The TIE model did not match the TIHI model, in that the response of the TIE model was predictably more linear than the TIHI model prediction. Still, we are able to ascertain that a TIE model would offer a close prediction to the empirical length-tension data, as the TIHI did. Similarly, the length-pressure predictions are significantly higher than published experimental results. This indicates that the inability to accurately predict pressure was not an idiosyncrasy in how pressure was calculated in ANSYS. Nor is the excessive pressure a result of the hyperelastic formulation, as both TIE and TIHI models drastically over-predict pressure.



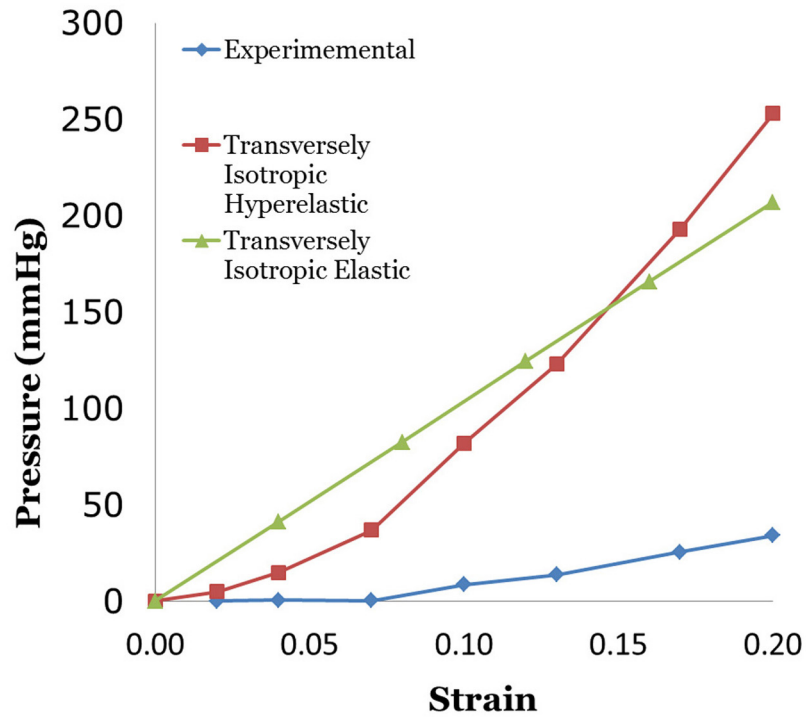


**Figure 4.13.** Comparison of length-pressure predictions of a transversely isotropic, hyperelastic model with a transversely isotropic, elastic model. Except for the differences in curvature associated with model linearity, the elastic model represent hyperelastic predictions well. Pressure predictions for both models are higher than empirical results.

### *Isotropic Linearly Elastic Model*

Further reduction of the model complexity was achieved by creating a model that was isotropic and linearly elastic. In this case, the only modulus used was that of the LE also used for the transversely isotropic linearly elastic model. Again, to avoid any potential confounding influence of muscle geometry, a rectangular mesh was loaded to 20% strain. Pressure was taken from an element in the central portion of the model. As indicated by the results of Figure 4.14, the level of isotropy (i.e., full isotropy or transverse isotropy) had no appreciable impact on the pressure predicted by the model.

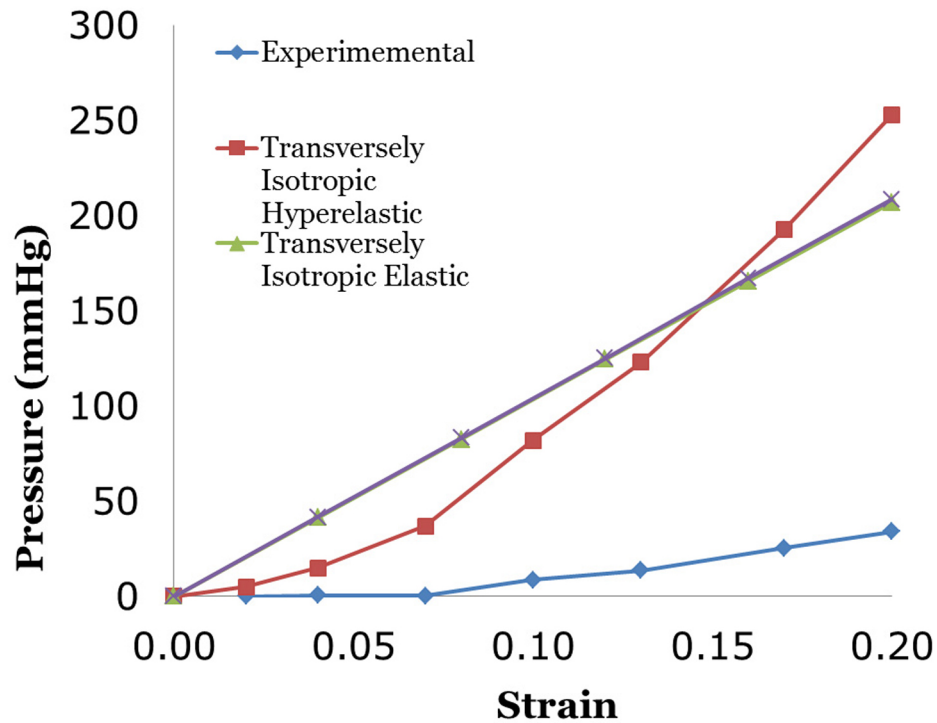


**Figure 4.14.** The level of isotropy represented in the model had no appreciable impact on the pressure prediction. The pressure calculated for results of the isotropic model was nearly identical to the pressure calculated from the transversely isotropic model.

## Conclusion

The application of active stress using a single-phase constitutive formulation was evaluated. It was shown that a separate stress term cannot be added to the AHYPER formulation to represent muscle activation. Attempts were also made to add stresses representing muscle activation using either an initial stress on the whole model or the compressive stresses at each element. Neither of these methods was successful and representative of muscle stress activation using scientifically sound criteria. Modeling of activation stress will likely require use of a user-defined material model. Additional studies were conducted to show sensitivity of element size on predicted reaction force and muscle volume, revealing that, for this scale of muscle, elements should have a side length of no more than 1 mm.

This investigation has supported that a continuum mechanics based, single-phase material model can be used to describe the length-tension relationship of skeletal

muscle. This was demonstrated using a transversely isotropic, hyperelastic, nearly incompressible model, which was characterized with one set of experimental data<sup>149</sup> and validated against an independent set.<sup>59</sup> It was revealed, however, that prediction of IMP, extracted as the hydrostatic pressure, dramatically over-predicted empirical pressure values. While pressure did show some degree of sensitivity to some of the terms of the ANSYS AHYPER model formulation, the magnitude of the sensitivity was not sufficient to bring the pressure to within an order of magnitude above experimental data.

An additional anisotropic hyperelastic model was considered. The generalized Fung model in Abaqus was evaluated. This constitutive model could be well characterized using experimental stress-strain data from load-elongation studies of rabbit skeletal muscle. The parameters that characterized experimental results would not allow for a convergent finite element model. This was found to be due to characteristics associated with the term used to characterize the shear response. It is asserted, therefore, that this formulation is not well-suited to model the characteristic behavior of skeletal muscle.

The inability to predict pressure with a single-phase material model was further assessed using a transversely isotropic, linearly elastic model. While there were obvious differences in the shape of the response, these were associated with the comparison of a linear model with a hyperelastic model. The magnitudes of the pressure were, however, similar for each model type and, consequently, greatly exceeded empirical results. Reducing the complexity of the model by one more layer, the pressures predicted by an isotropic linearly elastic model were compared to those predicted by the transversely isotropic linearly elastic model. This model showed only insignificant changes in calculated pressures. It is therefore concluded that, although single-phase solid models are able to predict the length-tension relationship, a different type of constitutive model is required to predict the length-pressure response in skeletal muscle.

## **Chapter 5 – Poroelastic Material Properties of Excised Skeletal Muscle in Tension using Inverse Finite Element Method**

### **Abstract**

Simulation of the time-dependent behavior of skeletal muscle can be achieved using a poroelastic material model. Characterization of such a model through direct evaluation of material properties, such as permeability and Poisson's ratio, can be difficult for biological soft tissues. An inverse finite element optimization method can be used to determine material properties by comparison of more easily obtained experimental results with model output. In this study, the reaction forces of excised samples of rabbit tibialis anterior muscles under longitudinal and transverse load relaxation are used to solve for permeability, Poisson's ratio, and the drained modulus of skeletal muscle. Results of this analysis indicate that the permeability does not differ under longitudinal or transverse load-relaxation. The longitudinal and transverse drained moduli of skeletal muscle are also not different; this suggests that the observed transverse isotropy usually associated with muscle is due more to a fluid-tissue interaction than the behavior of the solid components of muscle alone. Additionally, the derived Poisson's ratios of the excised samples were both found to be negative. This finding stands in contrast with previous assertions of the isovolumic nature of skeletal muscle. It is hypothesized that the negative Poisson's ratio may be a consequence of testing excised samples of muscle tissue that do not have all of the connective tissue constraints of an intact muscle. Further work is warranted to determine the full impact of these additional constraints on muscle performance and how these impact the behavior witnessed by excised muscle belly tissue.

### **Introduction**

Computational models have been used to examine loads and strains experienced in skeletal muscle since the introduction of the Hill-type muscle model.<sup>97</sup> Models have advanced from this early one-dimensional model to represent the behavior of complex 3-D geometries using various continuum mechanics-based approaches.<sup>103,105-109,132,148</sup> Many of these models have been created based on the assumptions that skeletal muscle is

hyperelastic, transversely isotropic,<sup>115,148,149</sup> and isovolumic.<sup>5,158</sup> These assumptions can all be incorporated into a single-phase solid mechanics model. However, muscle has also been observed to have time-dependent behaviors.<sup>97</sup> The non-linear creep and load-relaxation behaviors can be accounted for using a time-dependent model.

The time-dependent behavior of skeletal muscle has previously been attributed to the inherent viscoelasticity of the tissue. Studies have been conducted on muscle at multiple length scales, ranging from single fiber<sup>159-161</sup> to tissue-level.<sup>95,114,119,120,162-164</sup> Tsaturyan et al. suggested that the observed time-dependent behavior may not be from the inherent viscoelasticity of muscle material, but may arise from extracellular fluid filtration within the tissue.<sup>165</sup> Yang and Taber (1991), expanding on the work of Tsaturyan, confirmed that poroelastic effects could explain many of the apparent viscoelastic behaviors exhibited by cardiac muscle.<sup>161</sup> This is supported by the fact that muscle consists of 77% fluid,<sup>166</sup> approximately 12% of which is extracellular,<sup>167</sup> and this extracellular fluid is known to shift and redistribute with exercise and changes in posture.<sup>167-169</sup> The exact mechanisms responsible for this redistribution are, however, not completely understood at this time. While a viscoelastic model may be able to predict time-dependent responses of skeletal muscle, viscoelastic theory does not offer much insight to the underlying causative tissue behaviors.<sup>161</sup>

Inverse finite element analysis can be used to characterize skeletal muscle as a poroelastic material. An inverse finite element analysis begins by assigning initial value estimates of material properties for the continuum model. A finite element analysis is then performed, and model predicted outputs are compared with known empirical values. An optimization routine can then be employed to adjust the material parameter model inputs until simulation results most closely match experimental data. This method has been used effectively in previous studies of meniscus<sup>170</sup> and cartilage,<sup>171</sup> but not in skeletal muscle. Therefore, the aim of the study was to determine the poroelastic material properties of skeletal muscle from longitudinal and transverse load-relaxation tests of skeletal muscle tissue. It was anticipated that the transverse isotropy previously observed in skeletal muscle would still be apparent in a poroelastic analysis.

## Materials and Methods

### *Load-Relaxation Tests*

Twenty tibialis anterior (TA) muscles from New Zealand White rabbits were obtained with institutional approval (IACUC A17308). Hind limbs were amputated mid- femur and TAs were dissected free of surrounding tissue, including all fascia. Testing was completed within two hours of sacrifice to prevent confounding effects of rigor mortis.<sup>136</sup> Ten muscles each were used for load-relaxation tests in either longitudinal or transverse loading. The TA muscle was chosen for its low pennation angle.<sup>133</sup> Specimen samples were cut from the muscle midbelly using a razor tissue-punch. As the relaxed stress in muscles under load-relaxation loading has been shown to be strain-rate insensitive,<sup>159</sup> all material tests were performed at a uniform rate of displacement. Tissues were elongated at a rate of 3.8 mm/sec, corresponding to 0.1 fiber-lengths/sec.<sup>133</sup>

Load-relaxation tests were performed on an MTS 858 material test device (MTS, Eden Prairie, MN). Specimens were mounted to the test device using thin film clamps (Imada, Northbrook, IL). Longitudinally aligned (LE) specimens were gripped and mounted to provide deformation along muscle fiber direction; transversely aligned (TE) specimens were gripped in the clamp jaws such that applied extension occurred perpendicular to the fiber direction. Gage dimensions were taken under a pre-stress corresponding to 1% of the ultimate stress of the muscle by direction.<sup>149</sup> Material elongation was determined using crosshead displacement. Strain was reported using Green strain, the mechanical correlate to second Piola-Kirchoff stress, and calculated as:

$$e = \frac{1}{2}(\lambda^2 - 1) \quad (5.1)$$

where  $\lambda$  is the stretch ratio,

$$\lambda = \frac{l_i}{l_o} \quad (5.2)$$

where  $l_o$  is the original crosshead displacement and  $l_i$  is the current crosshead displacement. Samples underwent 5 cycles of load-relaxation in increments of approximately 3% strain and 300-second relaxation periods. Operating in this range ensured that tissue would not be strained to the point of creating damage or plastic deformation.<sup>172</sup> Force measurements were sampled at 20 Hz using a 1000-gf load cell

(Transducer Techniques, Temecula, CA), and the second Piola-Kirchoff stress was calculated as the force divided by the initial cross-sectional area.

### *Material Model Determination*

The relaxation stresses, defined as the stress at the end of each relaxation (Fig. 5.1), were used to form an initial estimate of the solid matrix model.

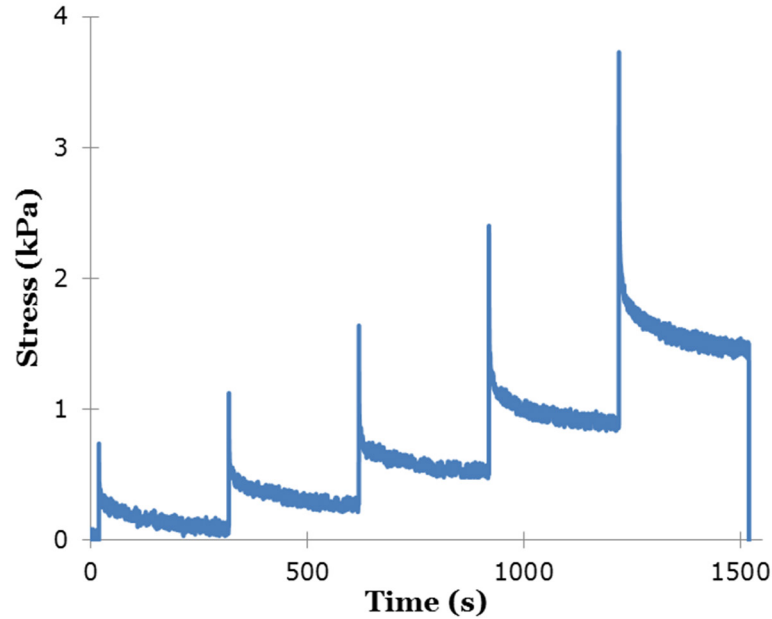


**Figure 5.1.** Representative plot of stress from load-relaxation tests. Relaxed moduli were calculated using stress from the end of each relaxation step.

Relaxation stresses from all load-relaxation cycles for LE and TE trials were collected (Fig. 5.2). By visual inspection, it would appear that there is no difference in the slopes. To evaluate this, because no appropriate tests exist to test the parallelism of non-linear curves, a natural log transformation was applied to stress values to create a linear stress-strain relationship.

Parallelism was assessed using a large-sample Z test with a null hypothesis that the slopes are equal (with significance set at  $p \leq 0.05$ ).<sup>173</sup> The Z statistic for a large-sample (i.e., greater than 25 samples in each group) is given by:

$$Z = \frac{\beta_{LE} - \beta_{TE}}{\sqrt{S_{\beta_{LE}}^2 + S_{\beta_{TE}}^2}} \quad (5.3)$$

where

$S_{\beta_{LE}}^2$  estimates the variance of the estimated slope  $\beta_{LE}$  for the relaxed modulus of skeletal muscle under longitudinal extension, and

$S_{\beta_{TE}}^2$  estimates the variance of the estimated slope  $\beta_{TE}$  for the relaxed modulus of skeletal muscle under transverse extension

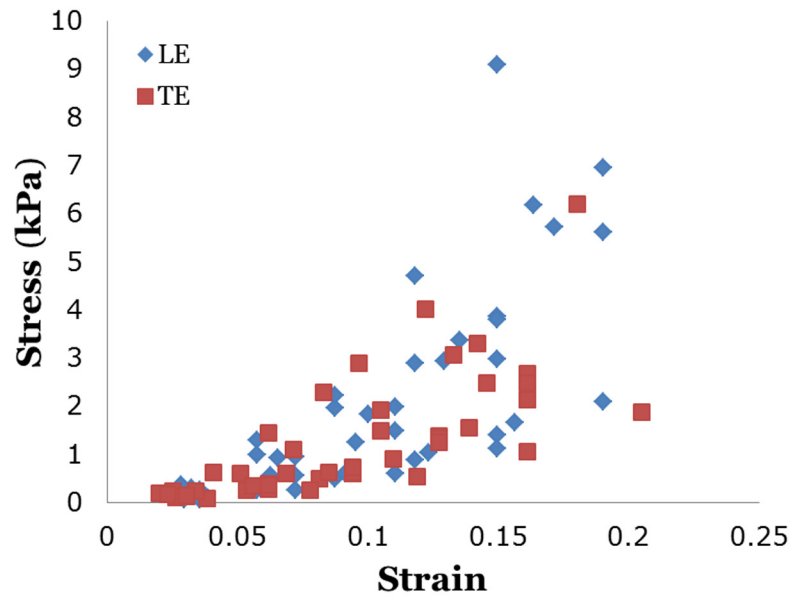


**Figure 5.2.** Relaxed stress values from LE and TE load-relaxation tests.

**Table 5.1**

Mean and variance for ln-transformed slope and intercept for relaxed modulus under longitudinal (LE) and transverse (TE) load-relaxation (see Appendix A.3).

		LE	TE
Slope ( <i>ln</i> MPa)	mean	18.83	19.41
	variance	129.02	178.30
intercept	mean	-8.78	-8.94
	variance	1.97	1.81



Comparison of the slopes (see Table 5.1) results in  $Z = -0.033$ , corresponding to  $p = 0.48$ . This fails to reject the null hypothesis, indicating that the slopes are not different. Using the same procedure to evaluate the intercept yields  $Z = 0.082$ , likewise indicating the intercepts are not different ( $p = 0.47$ ). While performing these tests would seem to be sufficient to indicate that the regression lines are coincident (i.e., same slope and intercept), it may be noted that there are two separate tests being used to evaluate this one hypothesis, which reflects on the power of the test. A conservative method to circumvent this problem would be to use  $\alpha/2$  to test for statistical significance at an actual level of  $\alpha$  (i.e., test using  $\alpha = 0.025$  to determine significance at  $\alpha = 0.05$ ). This may be too conservative and make it too difficult to reject coincidence.<sup>173</sup> While it is true that a rejection of either null hypothesis would be enough to reject a hypothesis of coincidence, the way to assure coincidence is through multiple regression testing using dummy variables.<sup>173</sup> Use of a dummy variable increases the number of comparisons that can be made for a given data set by assigning finite values to nominal variables. Additionally, this test is able to maintain the desired  $\alpha$ -level. In this instance, we are comparing LE and TE slopes, so a regression is performed with an added directionality variable (LE = 0, TE = 1). A partial F statistic is calculated using:

$$F = \frac{[SS \cdot Model(X, Z, XZ) - SS \cdot Model(X)]/2}{MS \cdot Error(X, Z, XZ)} \quad (5.4)$$

Where  $SS \cdot Model(X)$  is the sum of squares of the model with strain as the predictor of stress,  $SS \cdot Model(X, Z, XZ)$  is the sum of squares for the model with strain, dummy term, and an interaction term as possible predictors of stress, and  $MS \cdot Error(X, Z, XZ)$  is the Mean Square Error in the model with strain and dummy terms incorporated as well (values obtained from the regression equations are listed in Table 5.2). Subsequent analysis yields  $F = 0.319$  which, with  $df_1 = 2$  and  $df_2 = 94$ , corresponds to  $p = 0.73$ , indicating that the lines cannot be said to be different. Since the drained moduli and intercepts for both LE and TE are not different, the solid matrix of the muscle can be modeled as isotropic.

<b>Table 5.2</b> Regression values for test of coincidence of relaxed stress-strain			
<b>Source</b>	<b>df</b>	<b>SS</b>	<b>MS</b>
Model (X)	1	107.00	107.00
Error (X)	96	40.06	0.42
Model (X,Y,Z)	3	107.28	35.76
Error (X,Y,Z)	94	39.78	0.42

### *Finite Element Model*

A finite element (FE) model was created in ABAQUS (Simulia Corp., Providence, RI) for each experimental muscle specimen using the gage measurements obtained during material testing (Table 5.3). A two-sided, two-sample t-test of the specimen geometries revealed that the LE specimens were longer than the TE specimens ( $p < 0.05$ ), but the width, thickness, and cross-sectional areas were not significantly different (again with significance set at  $p \leq 0.05$ ). The discrepancy in the specimen lengths was a result of constraints in the available material in the transverse direction of a rabbit TA. A rectangular mesh with 1350 nodes (Fig. 5.3) was populated by 8-noded elements with linear displacements and pore pressure degrees of freedom (C3D8P). Pressure was assumed to be zero at the nodes on the unclamped surfaces. Likewise, there were no flow restrictions placed on these nodes. Clamped surface nodes were restricted to have zero fluid flow. Displacement boundary conditions were defined as encastre at the stationary cross-head and  $u_x = u_y = 0$ ,  $u_z = d$  at the moving cross-head, where  $u_x$ ,  $u_y$ ,  $u_z$  represent displacement in the  $x$ ,  $y$ , and  $z$  directions, respectively, and  $d$  represents the imposed displacement.

**Table 5.3**  
Mean (SD) of specimen dimensions. All measurements in mm (see Appendix A.4).

	length	width	thickness
LE	22.0 (4.1)	5.4 (1.0)	3.6 (0.4)
TE	11.3 (2.1)	11.3 (2.1)	5.6 (1.2)



## Material Parameter Optimization

Material parameters were found using a previously validated,<sup>171</sup> non-linear least-squares optimization approach using the “lsqnonlin” routine in MATLAB (The Mathworks, Inc., Natick, MA). Parameters were estimated from the response of the first load-relaxation step response. Optimization was achieved through comparison of the experimental reaction force with the sum of the reaction forces from the corresponding nodes in the modeled specimen. Arbitrary initial parameter values were written to an ABAQUS input file which was run iteratively until the model converged to a minimal error value. Two-tailed t-tests were performed to test if the LE permeability, Poisson’s ratio, and modulus as determined by optimization were different from those found for TE. Significance for all tests was set at  $p \leq 0.05$ .

## Results

A representative optimization for both LE and TE trials are shown in Figure 5.4. Neither the permeability ( $p=0.43$ ) nor the relaxed modulus ( $p=0.45$ ) showed significant difference between LE and TE loading (see Table 5.4). Poisson’s ratio did vary significantly between directions ( $p=0.006$ ). While the Poisson’s ratios were different, the common factor was that both values were negative (LE: -0.56; TE: -0.35).

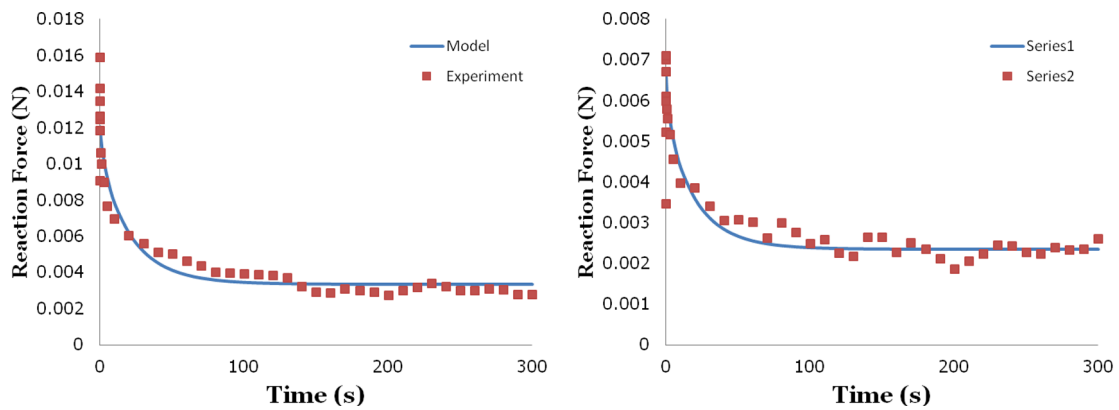


**Figure 5.4.** Representative constitutive model curve-fits (blue) and experimental data (red) for the relaxation phase of load-relaxation under longitudinal (A) and transverse (B) strains.

**Table 5.4**

Optimized values (mean and standard error) for permeability, Poisson's Ratio, and Modulus for both LE and TE loading directions. Only Poisson's ratio demonstrated significant differences ( $p=0.006$ ) (see Appendix A.5).

	Permeability (mm/s)	Poisson's Ratio	Modulus (kPa)
LE	9.84E-5 (5.95E-6)	*-0.56 (0.0096)	8.00 (0.41)
TE	1.38E-4 (1.57E-5)	*-0.35 (0.020)	6.62 (0.42)

\* indicates significant difference between LE and TE

The validity of the solution obtained by optimization using only the first load-relaxation cycle, strained only to ~3%, was assessed for a large-strain deformation. Reaction forces were recorded for an additional specimen that was subjected to a single longitudinal load-relaxation at 18% strain. A FEM simulation of the experiment was run using poroelastic material model parameters from the LE model of Table 5.3. Model results agree qualitatively well when graphically compared with experimental results (Fig. 5.5).

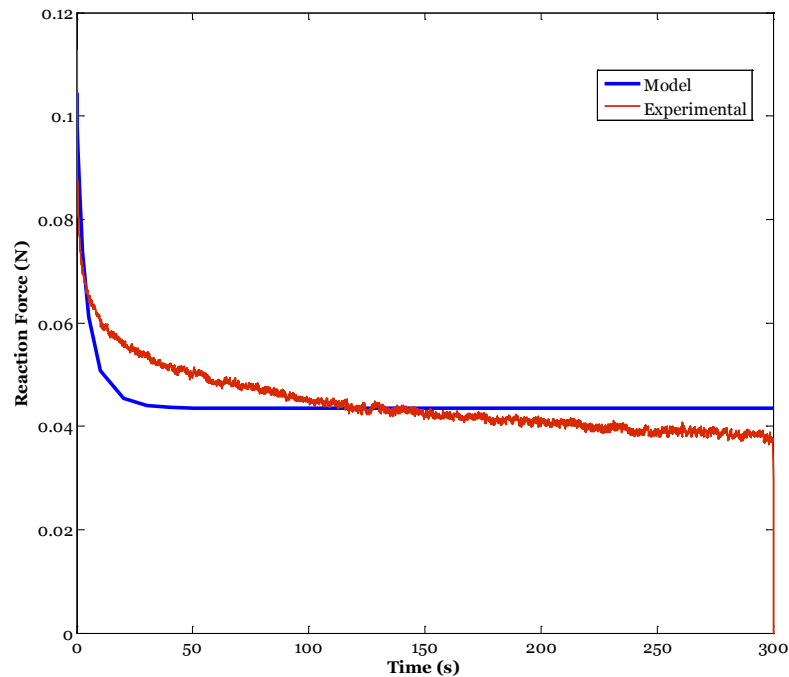


**Figure 5.5.** Comparison of experimental and model-predicted relaxation reaction force for a load-relaxation specimen strained to 18%. The model, characterized using load-relaxation results at strains <4%, offers good qualitative agreement with large strain experimental results.

## Discussion

An inverse finite element method coupled with optimization has been used to characterize a poroelastic model of skeletal muscle under tension. While the model was characterized from tissue strained less than 4%, the model is able to predict the response of tissue strained to 18%, showing the robustness of the solution.

It is notable that the LE and TE relaxed moduli did not differ significantly. Skeletal muscle has previously been shown to have an instantaneous modulus under LE that is significantly higher than under TE.<sup>149</sup> This disparity in the relationship between relaxed and instantaneous modulus may support the previous suppositions that the time-dependent behavior of skeletal muscle may be due to the interaction of the fluid and the solid matrix.<sup>161,165</sup> Titin<sup>174-176</sup> and desmin<sup>116,117,177</sup> have garnered much attention for their role in providing passive resistance to muscle elongation. With the drained moduli being not significantly different, it would appear that the components that contribute to the transverse structural stability of skeletal muscle (e.g., skelemin, synemin) appear to provide just as much strength as their longitudinal counterparts in the absence of interstitial fluid flow.

It was surprising that the values for Poisson's ratio were found to be negative. The converged values for Poisson's ratio were reached regardless of the initial values used in the optimization so the solution is not just a local minimum. Additionally, a recent study by Meyer, et al (2011) examined the changes in volume of a skeletal fiber with increasing strain and compared that with the volume change seen in a bundle of fibers.<sup>152</sup> This study reported an observed increase in volume for some muscle fibers at strain levels between 0 and 50%. While the study did not report an increase in volume in the measured bundles, it should be noted that there were no strain values reported between 0 and 15%. Additional data may be needed to determine if bundles exhibit an increase in volume at lower strain levels, mimicking the trend seen in fibers in the Meyer study. These results, taken together, seem to indicate that a negative Poisson's ratio value may be observed when testing excised muscle tissue.

Results from the current study raise the question as to what accounts for the discrepancy between the transverse isotropy observed in intact skeletal muscle and the directionally

independent relaxed modulus and permeability observed in excised muscle tissue. An examination of the optimized values for Poisson's ratio may offer some insight as to how the solid-fluid interaction creates the observed transverse isotropy in intact muscle while the directional dependent nature was not observed in excised muscle. Figure 5.6 shows the relative impact of Poisson's ratio on the load-relaxation response of skeletal muscle. In this plot, permeability and drained modulus are held constant, as are the loading conditions. The optimized values of Poisson's ratio from the study, -0.56 and -0.35 for LE and TE, respectively, are used. The reaction forces, normalized to the relaxed force are plotted versus time. The figure clearly shows a relative difference in the instantaneous reaction force between LE and TE, with the LE force being 40% greater than the TE. This difference mimics the transversely isotropic behavior observed in load-elongation experiments and is explained here by the change in Poisson's ratio between the longitudinal and transverse directions as the remaining variables have been held constant. The relaxed reaction forces are equivalent as was observed in the current experimental results. This result ties the transversely isotropic behavior witnessed in load-elongation<sup>149</sup> with the isotropic drained modulus under load-relaxation found in the current study.

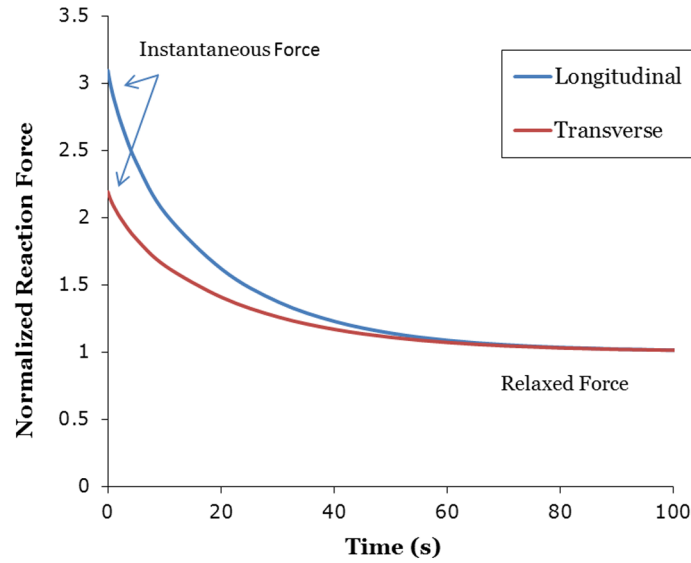


**Figure 5.6.** Change in reaction force with variation in Poisson's ratio. Reaction force is normalized to relaxed level. The longitudinal Poisson's ratio yields a 40% higher initial reaction force than the transverse reaction force, representative of the higher longitudinal modulus witnessed in load-elongation studies.

Additional work remains to build upon these results. An imaging study to validate the optimized Poisson's ratio values would add further confidence to the optimization. Further work examining the strain-level dependence<sup>172</sup> would help to understand the effect of cumulative deformations. Because the stress response of skeletal muscle has recently been described as being non-linear<sup>172</sup> (e.g., sensitive to the absolute strain level, not just the size of the imposed strain step), the calculated parameters should be evaluated at additional strain steps. Lastly, tests should be conducted at multiple strain rates to assess whether permeability and Poisson's ratio are also strain-rate dependent.

In conclusion, poroelastic material properties of skeletal muscle not previously reported were successfully determined from longitudinal and transverse load-relaxation tests. Interestingly, the LE and TE relaxed moduli and permeability did not differ, and unexpectedly, the Poisson's ratio values in both directions were negative. It was postulated that the Poisson's ratio provides the missing link that ties the transversely isotropic behavior witnessed in load-elongation<sup>149</sup> with the isotropic drained modulus under load-relaxation. While there is much work to be done to confirm and expand upon these results, modeling muscle as a poroelastic material offers a promising paradigm shift in explaining the time-dependent behaviors of muscle.



## **Chapter 6 – Intramuscular Pressure from a Poroelastic Model of Skeletal Muscle Tissue**

### **Abstract**

Advances in the development of pressure microsensors have brought the measurement of intramuscular pressure (IMP) closer to being a minimally-invasive clinical reality. Being able to measure IMP, as a mechanical correlate to muscle tension, would represent the first practical method developed for obtaining objective data on individual muscle performance. Computational modeling of skeletal muscle is important in helping to interpret IMP measurements. Despite being able to accurately predict the stress-strain response of skeletal muscle, a transversely isotropic, hyperelastic, and nearly incompressible constitutive model has been shown to yield inaccurate predictions of IMP. Being composed of approximately 77% water, and known to exhibit time-dependent behaviors, a poroelastic model of skeletal muscle was developed. This model, which was shown to be able to predict the reaction forces of muscle under load-relaxation, is evaluated in this current work for IMP prediction. A finite element analysis is used to predict IMP in simulations of load-relaxation experiments of excised rabbit tibialis anterior muscle specimens strained to 20%. IMP predictions were within 10 mmHg of experimental results, which compares very favorably when compared to the 200 mmHg errors in predictions made by the single-phase continuum model. The major discrepancy between the model and empirical pressures concerns the relaxed pressure level. While the poroelastic model predicts a complete relaxation of the IMP (i.e., pressure magnitude goes to 0 mmHg), there is a residual pressure observed in experimental measurements. A residual pressure, if added to the model, can make the predicted IMP exhibit a similar pattern as seen in the experimental recording. This residual pressure could be the result of restricted fluid flow through the muscle tissue. Further examination is required to add a biological rationale supporting inclusion of a pressure residual to the computational model. The agreement shown between empirical and model pressure from this poroelastic model mark the first time a 3D model of skeletal muscle was able to be used for deriving IMP.

## Introduction

Evaluation of the force of a single *in situ* muscle is difficult to implement in a clinical setting. Muscle force is typically assessed through either manual muscle testing, isokinetic/isometric dynamometry, or electromyography (EMG). Manual muscle testing is a subjective evaluation of a patient's ability to move voluntarily against gravity and to resist force applied by an examiner.<sup>6-8,178</sup> This is the most common method for assessing muscle strength, in large part because of the lack of instrumentation required and ease of implementation. Muscle testing using dynamometers adds accuracy by quantifying functional mechanical output of a limb. Additionally, dynamometry has been shown to be more sensitive to differences in muscle strength.<sup>17-20</sup> However, like manual muscle testing, dynamometry only provides estimates of joint moment. These methods fail to provide detailed information about individual muscle performance. EMG quantifies neuromuscular activation signals, and is used to infer muscle function. Despite the abundance of work performed to determine the degree to which EMG signals and muscle forces are related,<sup>45-51</sup> the basic problem remains that EMG cannot provide a quantitative measurement of muscle force.

Intramuscular pressure (IMP), the pressure applied by muscle fibers on interstitial fluid, has been considered as a correlate for muscle force.<sup>55</sup> Numerous studies in animal models<sup>55-58</sup> and humans<sup>62-72</sup> have shown that an approximately linear relationship exists between IMP and muscle force. A microsensor has recently been developed that is accurate<sup>83</sup>, biocompatible<sup>84</sup>, and, at  $<300\text{ }\mu\text{m}$ , appropriately sized for clinical use. While muscle force and pressure have been shown to be correlates, there remain questions about how the absolute magnitude of the pressure should be interpreted. There are reports indicating that IMP is non-uniform within the muscle.<sup>88,89</sup> Moreover, some investigators have reported that the absolute IMP depends on the depth of the recording catheter within the muscle, the shape of the muscle,<sup>71,90</sup> and the compliance of the surrounding tissue.<sup>91</sup> It would not be practicable to evaluate how the magnitude of IMP may be distributed within a muscle through empirical methods. Rather, computational modeling may provide the means to fully evaluate IMP generation in muscles of various shapes and operating conditions.

Since the introduction of the Hill muscle model,<sup>97</sup> there have been several types of computational models developed to describe the response of skeletal muscle to perturbation. The first attempts to enhance the complexity of the standard Hill model came in the development of 2D<sup>106</sup> and 3D<sup>130</sup> arrangements of 1D Hill elements. Over time, the emphasis has shifted to the generation of computational models based on continuum mechanics.<sup>103,105,132,148</sup> These have been developed, in part, to help account for behaviors influenced by complex 3D geometries through finite element modeling (FEM).<sup>103</sup> These continuum models were joined with other formulations<sup>107,108,131</sup> that used FEM to reproduce the length-tension behavior of skeletal muscle. As shown in Chapter 4, while a hyperelastic continuum-mechanics based formulation is fully capable of length-tension characterization, it fails at predicting the length-pressure relationship of skeletal muscle.

There has been one published report, albeit only in 2D, investigating the length-pressure relationship of skeletal muscle using computational modeling.<sup>105</sup> This study attempted to recognize the importance of separating the solid, muscle fiber portion of skeletal muscle from the fluid component. This was incorporated through the introduction of a penalty function for enforcing incompressibility that had solid phase and fluid phase components. It is unclear, however, how these parameters were characterized or what their precise biological manifestation represented. Use of a poroelastic model of skeletal muscle could help overcome these limitations. A poroelastic model of skeletal model was presented in Chapter 5. This model was characterized using optimization and inverse FEM of load-relaxation of muscle under tension. The goal of this study is to examine this poroelastic model for its ability to accurately predict IMP in skeletal muscle under tension.

## **Materials and Methods**

### *Load-Relaxation Tests*

Four tibialis anterior (TA) muscles from New Zealand White rabbits were obtained with institutional approval (IACUC A17308). Muscle harvest and testing was performed within two hours of

**Table 6.1**  
Mean (SD) of specimen dimensions.  
All measurements in mm (see Appendix A.6).

	length	width	thickness
mean	27.5	8.6	4.7
standard deviation	1.7	3.3	1.3

animal sacrifice to prevent confounding effects of rigor.<sup>136</sup> Test samples were excised from the TA muscle belly to provide specimen boundary conditions representative of the test conditions from the experiments used to characterize the model parameters (see Chapter 5). Specimens were mounted on an MTS 858 material test device (MTS, Eden Prairie, MN) using thin film clamps (Imada, Northbrook, IL). Gage specimen dimensions (see Table 6.1) were collected using digital calipers after application of a pre-stress corresponding to 1% ultimate stress.<sup>149</sup>

Specimens were subject to a single load-relaxation test to avoid issues with allowing proper relaxation between trials. Specimens were strained to 20%, safely within the range where the material would be free from plastic deformation and plastic deformation.<sup>172</sup> Deformations, determined from crosshead displacements, were imposed at a rate of 3.8 mm/sec, corresponding to 0.1 fiber-lengths/sec<sup>133</sup> corresponding with the deformation rate used in the characterizing experiments. Subsequent to the loading, specimens underwent a 300 second relaxation period. Strains were calculated using the Green strain formula,

$$e = \frac{1}{2}(\lambda^2 - 1) \quad (6.1)$$

where  $\lambda$  is the stretch ratio,

$$\lambda = \frac{l_i}{l_o} \quad (6.2)$$

where  $l_o$  is the original crosshead displacement and  $l_i$  is the current crosshead displacement. Stress was calculated as the second Piola-Kirchoff stress by dividing the measured force by the initial cross-sectional area. Force measurements were sampled using a 1000-gf load cell (Transducer Techniques, Temecula, CA).

IMP measurements were obtained using a 250- $\mu\text{m}$ -diameter fiber-optic pressure sensor (Luna Innovations, Blacksburg, VA). The pressure microsensor was inserted into the central portion of the specimen using a 20-gage hypodermic needle which was withdrawn after sensor placement. IMP and displacement data were collected at 20 Hz through the MTS controller.

### *Finite Element Model*

A finite element (FE) model was created in ABAQUS (Simulia Corp., Providence, RI) for each experimental muscle specimen using the gage measurements obtained during material testing (Table 6.1). A rectangular mesh with 1350 nodes was populated by 8-noded elements with linear displacements and pore pressure degrees of freedom (C3D8P). Pressure was assumed to be zero at the nodes on the unclamped surfaces. Likewise, there were no flow restrictions placed on these nodes. Clamped surface nodes were restricted to have zero fluid flow. Displacement boundary conditions were defined as encastre at the stationary cross-head and  $u_x=u_y=0$ ,  $u_z=d$  at the moving cross-head, where  $u_x$ ,  $u_y$ ,  $u_z$  represent displacement in the  $x$ ,  $y$ , and  $z$  directions, respectively, and  $d$  represents the imposed displacement. Model predicted pressure was reported as the pore pressure from a node located in the center of the model, representative of the sensor head location during experiments. Model predicted pressures were graphically compared to experimental pressure values.

The assumption of free surface fluid flow as an applied boundary condition on the external faces of the model was also evaluated. Surface fluid flow was initially assigned as free flow at all surface nodes. Flow was restricted on opposing surface pairs of the rectangular mesh after, allowing flow only through the larger surfaces or only through the smaller surfaces in turn. Fluid flow boundary conditions were evaluated by comparing the developed pressure for each of the flow conditions.

An additional simulation was run to evaluate whether the poroelastic model would be able to predict the load-elongation response of skeletal muscle detailed in Chapter 2. The FE mesh described earlier in this chapter was modified to match experimental specimen geometry. The model was strained at  $0.05\%\text{s}^{-1}$  to 20% strain, mimicking experimental conditions. Model stress (total reaction force/cross-sectional area) was compared to

experimental values reported in Chapter 2. Because pressure was not collected in those experiments, pressure data was taken from Davis (2003).

## Results

IMP levels dropped significantly at the onset of relaxation, falling to -14 mmHg in under 1.8 seconds (Fig. 6.1A). As the relaxation continues, the pressure rises and settles around -8 mmHg within 150 seconds. Results of the model simulations show a similar overall trend (Fig. 6.1B). The response overall was slower, with minimum pressures reached in over 2.5 seconds, and stabilization occurring later as well. The model differs from the experimental results as well in that the poroelastic model relaxes completely to zero mmHg.

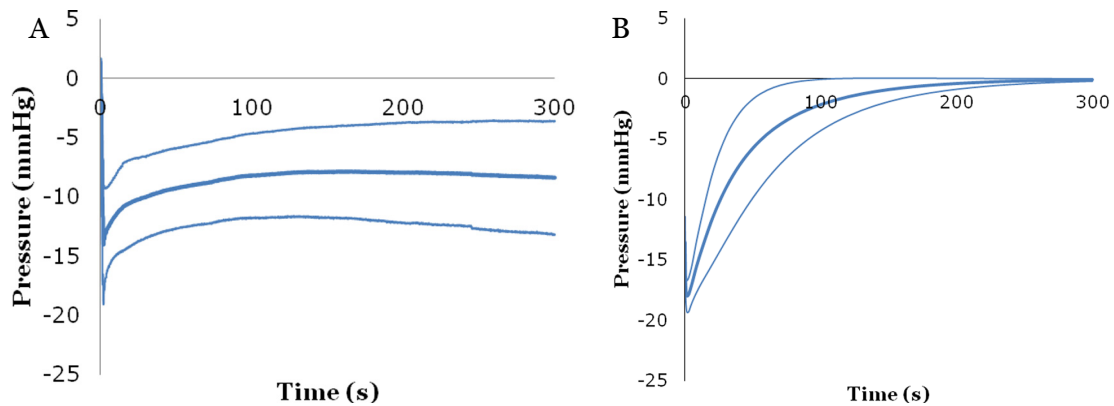


**Figure 6.1.** Mean (dark line)  $\pm$  one standard deviation (light lines) of relaxation phase of experimental IMP (A) and model predicted pressure (B). Both plots show immediate decrease in pressure immediately after the onset of relaxation followed by sudden reversal with pressure relaxing to stabilization.

Figure 6.2 shows an examination of the cross-section of the FE model showing pore pressure levels in the central portion of the specimen. Results are shown for both the minimum pressure level (Fig. 6.2A) and the point of pressure stabilization (Fig. 6.2B). As the figures show, the maximal pressure amplitude occurs in the central portion of the specimen with pressure amplitudes decreasing spatially with proximity to the surface.

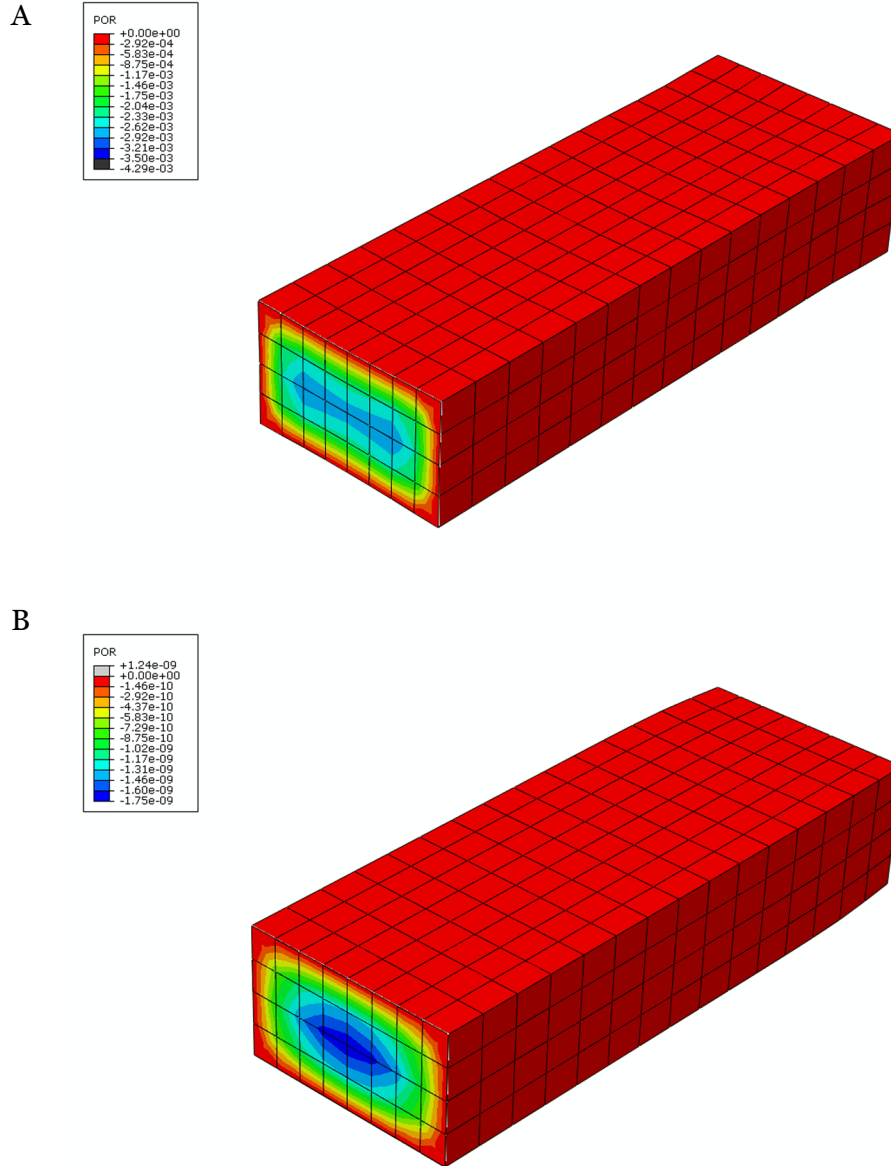


**Figure 6.2.** FEM output of specimen cross-section immediately after beginning relaxation phase of load-relaxation test (A) and 150 msec into relaxation phase (B). Pressure values in legend expressed in MPa. Pressure values are higher in specimen mid-section and reduce towards surface. It should be noted that the pressure values in (B) are much smaller in magnitude than in (A), indicating pressure stabilization within tissue. Also notable is a slight bulging of the tissue cross-section, an effect of the negative Poisson's ratio assigned to the material model as a result of material classification described in Chapter 5.

As demonstrated in Figure 6.3, the progressive reduction in surface areas for fluid flow from does incrementally alter the pattern of pressure relaxation over time. The initial

model had no restrictions on flow through any of the model surfaces. This condition is given as All Flow in Figure 6.3. Recalling the rectangular shape of the model cross-section (Fig. 6.2), the Large Flow curve refers to a restriction of fluid flow to only the surfaces with larger areas; likewise, Small Flow indicates where flow was restricted to only the smaller surface pair. As one would anticipate, when the flow is controlled, the rate of relaxation is slowed. This slowing is minimal between All Flow and Large Flow, where the available surface area for fluid flux is closest. The Small Flow condition, however, showed a qualitatively considerable slowing of pressure stabilization. This is not reflective, however, of the pattern of pressure change demonstrated experimentally (Fig. 6.1A), where a minimal pressure quickly transitions and stabilizes to a residual pressure level. The Small Flow condition does, in fact, still converge to zero mmHg, albeit after a longer relaxation time. These findings argue against a change in the fluid flow boundary condition as the cause of the residual pressure witnessed empirically.

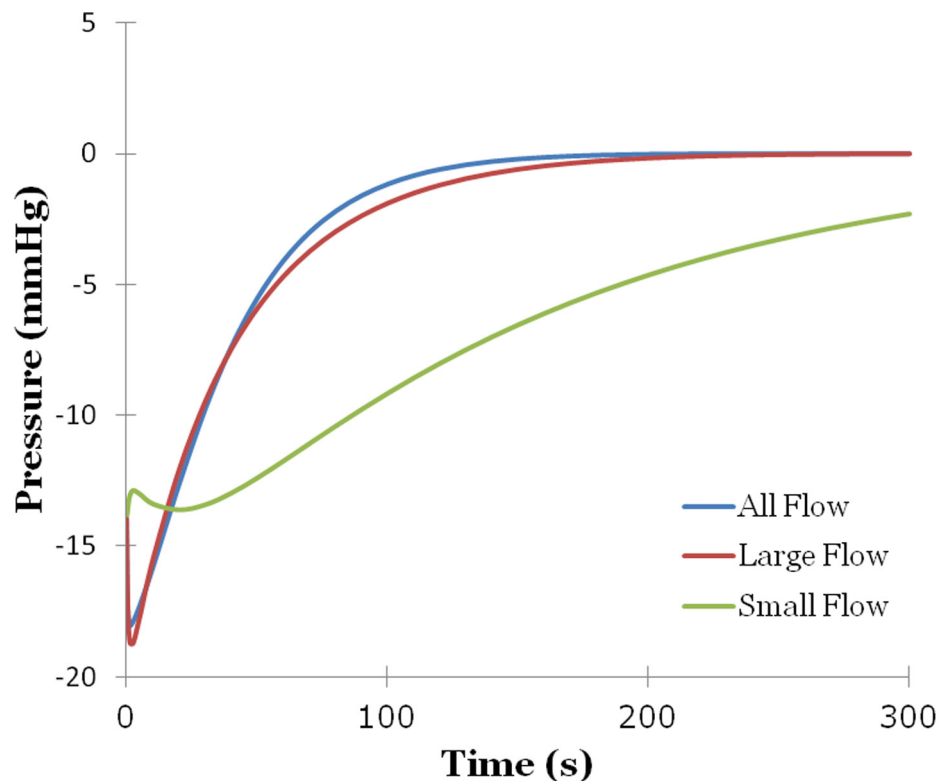


**Figure 6.3.** Changes in the surface area available for fluid flow affects pressure relaxation time. As the surface area through which fluid is allowed to flow is reduced, relaxation time increases. Given time, each case relaxes to zero mmHg.



If a non-zero residual pressure is incorporated into the model, the resulting pressure prediction can be made to behave very much like the experimental results. A simulation of one of the trials was run with an applied residual pressure of -1.2 kPa, corresponding to -9 mmHg. The results of the resulting pore pressure are plotted along with the corresponding experimental data in Figure 6.4. Indeed, there is good agreement between the computational and empirical values.

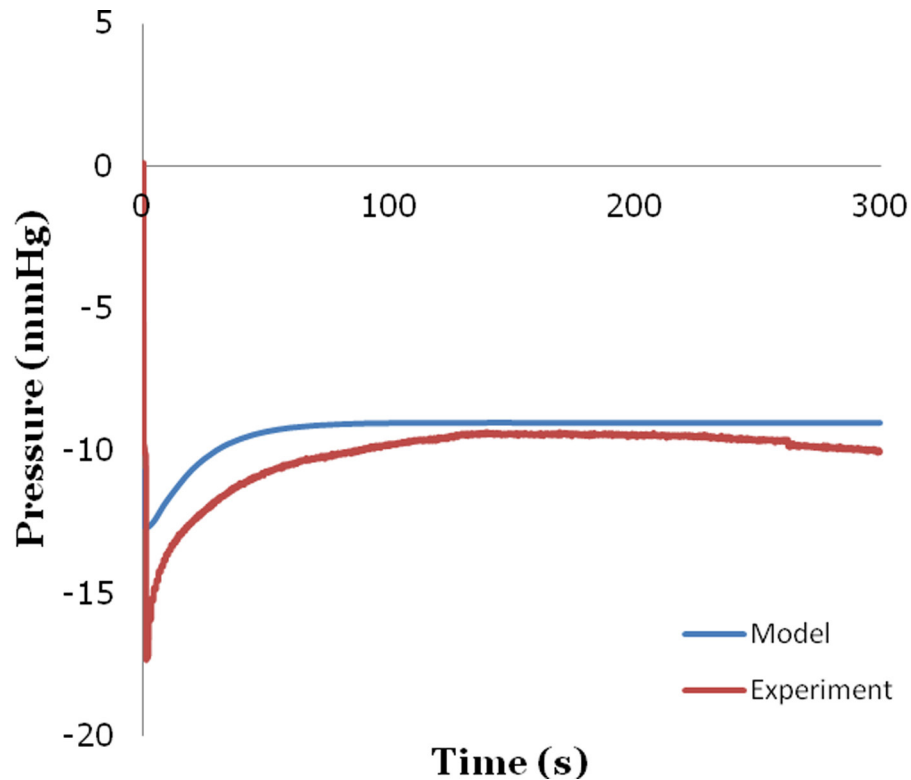


**Figure 6.4.** Pressure prediction vs empirical measurement for relaxation of muscle strained to 20% incorporating a residual pressure term. This causes the model to not stabilize to zero.

The poroelastic model does not predict the behavior of the intact muscle under load-elongation (Fig. 6.5). The stress is underpredicted by an order of magnitude (Fig. 6.5A). Pressure in the model is less predictive. Under elongation, experimental pressure values (Fig. 6.5B) increased exponentially with strain in the same manner as stress. In the model, a negative gage pressure develops, stabilizing at -2 mmHg.

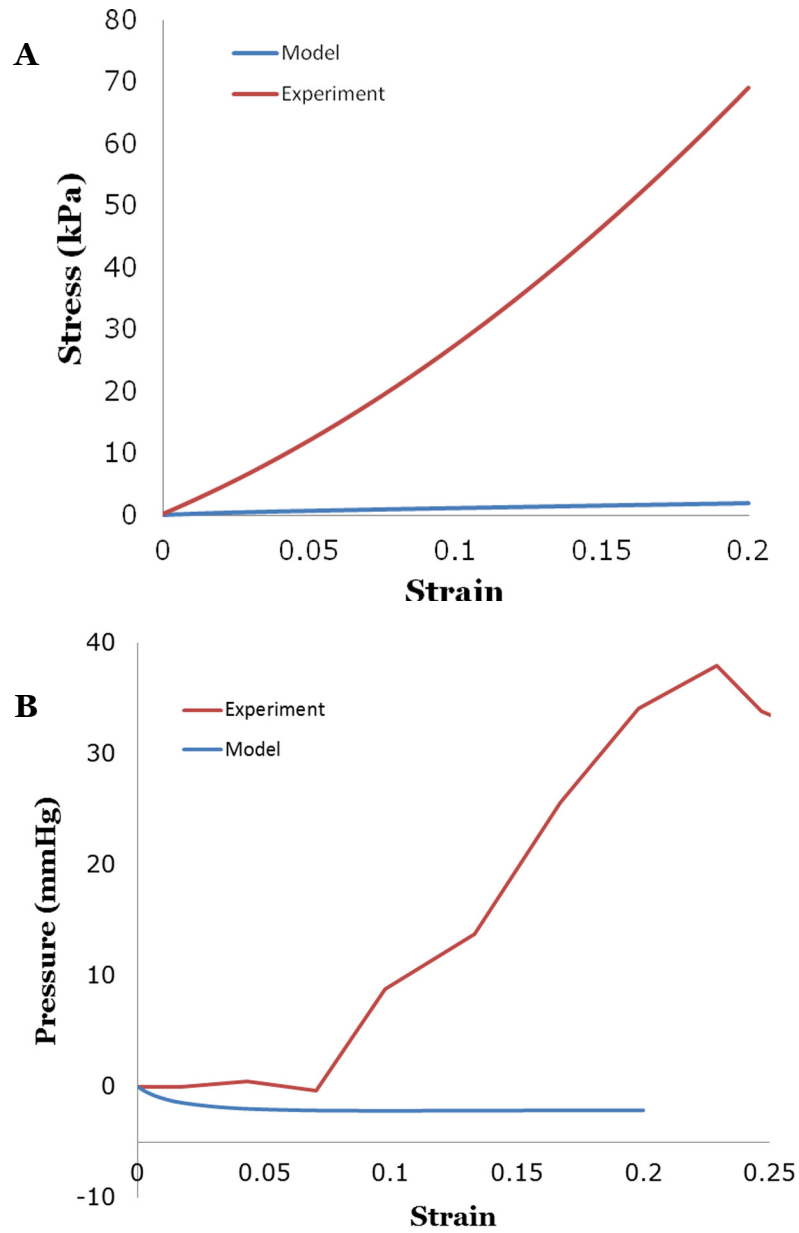


**Figure 6.5.** Comparison of (A) stress and (B) IMP from poroelastic model and experimental load-elongation data. The muscle underpredicts the experimental stress results by an order of magnitude. This is most likely because excised muscle tissue was used to characterize the poroelastic model and does not incorporate all connective tissues that contribute to material strength and, possibly, barriers to fluid flow. Likewise, pressure predictions are lower than the experimental data. The lack of connective tissue does not restrict the behavior characterized by the negative Poisson's ratio in the poroelastic model, allowing the pressure to take on negative values.

## Discussion

The poroelastic model represents the trend of the IMP observed during load relaxation in skeletal muscle. The timing of the minimum modeled pressure is within 1 second of the empirically-observed minimum. While the model magnitudes do not precisely match those of the empirical results, they fall within 10 mmHg. This is substantially closer than the 200 mmHg error seen in the hyperelastic model prediction at 20% strain (Fig. 4.4).

The largest discrepancy between the poroelastic model pressure response and the experimental data is the level of the stabilized pressure response. Regardless of the level of the instantaneous pressure, the model pressure stabilizes to 0 mmHg (Fig. 6.1). This should be expected as there were no constraining residual pressures imposed on the model. With the absence of a reason to check the flow, a poroelastic model will, given time, stabilize to a zero-pressure level. Zero-pressure stabilization was not witnessed empirically. A non-zero pressure was consistently observed in all experiments (Fig. 6.1A).

At this time, however, the only rationale that exists for incorporation of a residual pressure is the evidence from the experimental trials. Credence would be given to the computational model if a physiological understanding for the existence of the pressure residual could be provided. This would make the model more of a biological analog, and not merely the result of an academic curve-fitting exercise. A boundary, such as the perimysium (Fig. 1.2) may allow free movement of the fluid within the tissue it surrounds while confining the fluid within its boundaries. Additional studies of the exact nature of the movement of interstitial fluid are needed to precisely understand this phenomenon.

The poroelastic model, as characterized using results of load-relaxation tests, was unable to predict either the stress-strain or pressure-strain behavior of intact muscle under load-elongation. It is believed that this is because the intact muscle contains many more muscular architectural aspects than the excised muscle used to characterize the poroelastic model. These tissues would add to the material strength of the muscle, and possibly impede fluid movement, which would both contribute to increase the stress

response of the muscle under strain. This is further supported by examination of the comparison of model and experimental pressure measurements (Fig. 6.5B). While the experimental pressure response follows the expected pattern (a generally hyperelastic response with increasing strain), the model predicts a slight negative response. With the negative Poisson's ratio used in this model (see Chapter 5), this decrease in pressure is not surprising. It is hypothesized that the additional connective tissues in the intact muscle (e.g., perimysium, epimysium) will contribute to modify the Poisson's ratio and result in a pressure increase when the muscle tissue is subject to increasing strain.

In conclusion, it has been shown that a poroelastic model of skeletal muscle, characterized using the reaction force developed during load-relaxation testing, is capable of predicting the instantaneous intramuscular pressure response of skeletal muscle. A mechanism for implementing a residual pressure in the model exists, which would allow for complete prediction of the relaxation of pressure. Additional studies of interstitial fluid flow may provide a biological rationale to incorporate this observed phenomenon. This brings us close to realizing the goal of having a computational model of IMP in skeletal muscle.

## **Chapter 7 – Significance of Research**

### **Introduction**

Intramuscular pressure (IMP) has been put forward as a mechanism that can be used to quantify active and passive tension in skeletal muscle.<sup>55,62-72</sup> Practical interpretation of IMP requires a thorough understanding of how pressure is developed in muscle tissue. Since IMP has been shown to be heterogeneous within a muscle,<sup>71,88-90</sup> the variation of IMP needs to be understood for the measurement to be interpreted in a meaningful way. The goal of this research program was to develop a model of skeletal muscle tissue, aimed at enhancing the understanding of the application of IMP as a clinically useful measurement.

### **Skeletal Muscle Material Property Definition**

Load-elongation experiments were performed under longitudinal extension, transverse extension, and longitudinal shear to characterize a model of skeletal muscle as a transversely isotropic, hyperelastic, and nearly incompressible material (Chapter 2). These experiments mark the first time a set of data sufficient for characterization of a 3D, transversely isotropic material were performed in a single study. This model has been shown to be predictive of the length-tension relationship in muscle, as validated<sup>149</sup> through comparison against an independent set of experimental data.<sup>59</sup>

To incorporate the description of time-dependent aspects of muscle, longitudinal and transverse load-relaxation experiments were performed. Results of these experiments were used to characterize a poroelastic model using optimization and inverse finite element analysis (Chapter 5). While a viscoelastic model could be used to predict the force-length and force-velocity characteristics of muscle, analysis of a viscoelastic model would not contribute to an understanding of the underlying physical behaviors that result in the time-dependent behavior of the tissue in the way that a poroelastic model can.<sup>84</sup> By virtue of the separation of the solid and fluid components in the model, a poroelastic model allows for consideration of the interaction of the constitutive phases. Additionally, it was hypothesized in Chapter 6 that the residual pressures seen in muscle during empirical load-relaxation experiments may be caused by fluid that is prevented

from freely flowing throughout the muscle by connective tissue boundaries. These boundaries could be incorporated into a poroelastic model and evaluated for their effect on IMP.

Comparison of the longitudinal and transverse relaxed moduli indicates that the solid matrix of skeletal muscle may be modeled as isotropic. While previous investigations have indicated that the time-dependent behavior of muscle is more attributable to the fluid/solid interaction,<sup>84,165</sup> this marks the first known time a study has further attributed the observed transverse isotropy of skeletal muscle to such interactions.

Perhaps the most surprising revelation of this work came when samples of excised muscle tissue under tensile load-relaxation exhibited negative Poisson's ratio behavior. The volume expansion that occurs with applied tensile strains was responsible for the relatively large drop in pressure seen during load-relaxation tests. Since this phenomenon has not been described for intact muscle, it is hypothesized that this expansion of the tissue may be attributable to the testing of excised tissue. Further investigation of the strain response of skeletal muscle tissue at other scales (e.g., single fiber, bundle, and whole muscle) are warranted to determine how tissue constraints change with increasing organizational complexity.

While the Poisson's ratios were found to be negative under both longitudinal and transverse stress-relaxation, they were significantly different from each other, with the longitudinal Poisson's ratio being larger in magnitude. This is an important observation in helping to understand the differences seen in the instantaneous and relaxed responses of skeletal muscle under tensile loading. Recall that, while this study demonstrated that relaxed skeletal muscle can be modeled as isotropic, the instantaneous reaction of muscle has been consistently demonstrated to be isotropic. An analysis of the effect of the Poisson's ratio term in a poroelastic model revealed that this term was one responsible for bridging this difference in the model. For a given relaxed stress level, the more negative Poisson's ratio, the longitudinal Poisson's ratio in this study, resulted in a higher instantaneous stress; the less negative, transverse Poisson's ratio correlated with a lower instantaneous stress. The pattern of a higher instantaneous tensile modulus in the longitudinal direction than in the transverse direction is consistent with other reports of tensile load-elongation in skeletal muscle.

The poroelastic model was characterized using reaction force data from load-relaxation experiments performed low strain levels (i.e., 3.5% strain). The model showed to have a qualitatively high ability to predict the load-relaxation response of experimental data collected at 18% strain.

## **Fitting Experimental Data to Continuum Models**

Chapter 3 describes the method that was developed for assessing the best fit of empirical data to given constitutive models.<sup>148</sup> Use of the root mean squared error is combined with an analysis of the standardized residuals to form a quantitative approach at determining a best fit of model output to experimental data. In the case demonstrated in Chapter 3, this is shown for creating a best fit of reaction force data, but this process could be used for any data predicted by a computational model that is experimentally measured. The root mean squared error provides a relative estimate of how close a model fits the data as a whole. The additional assessment of the distribution of the standardized residuals enforces that the fit of the model has no local bias and the error is normally distributed over the data set.

Additionally, this investigation examined how to best use multiple sets of data to fit a constitutive formulation. The fitting of multi-dimensional data to a multivariate model is complex. It was previously unclear whether fitting constitutive model by either simultaneously fitting all available stress–strain data from multiple samples (the ALL method) or by fitting data curves from individual samples and averaging resultant model parameters (the EACH method). The current investigation, the first such study known to consider how to best handle fitting data from multiple data sets, shows that a better fit is obtained by fitting all data simultaneously. This was demonstrated best in the finding that there was a lower RMSE between experimental data and characterized models than that of the EACH method for every evaluated case, the use of the ALL method fits data better for every one of the 45 combinations of terms in the evaluated polynomial formulation.

## **Ability to Predict IMP using Finite Element Modeling**

Models of skeletal muscle with hyperelastic and poroelastic constitutive models were both shown to be able to predict the tension generated in skeletal muscle. In order to

have utility for understanding IMP, the models need to be evaluated for their ability to predict pressure as well. This work marks the first analysis of pressure in a 3D, continuum-mechanics based model. Not having an independent fluid component, the single-phase hyperelastic model reports pressure as the hydrostatic pressure. The assumptions imposed on this model (i.e., hyperelastic, transversely isotropic, and nearly incompressible) are similar to other single-phase continuum mechanics models currently used in other investigations. As the analysis in Chapter 4 revealed, the pressures predicted by this model is an order of magnitude higher than empirical measurements.

The poroelastic model, on the other hand, is able to calculate the pressure generated in the fluid phase of the analyzed volume. As demonstrated in Chapter 6, there is excellent agreement with the predicted instantaneous pressure level of the model and the experimental data. Errors for the pressure predicted by the poroelastic model, under load-relaxation at 20% strain, were <10 mmHg. This is a large improvement over the 200 mmHg errors seen in the hyperelastic model, making this the first 3D model of skeletal muscle tissue validated against empirical data.

## **Future Directions**

It has been shown that a time-sensitive model is needed to predict IMP in skeletal muscle. A poroelastic model is able to characterize the instantaneous pressure developed in skeletal muscle. The experimental data and model predictions diverge in their description of the pressure level in relaxed skeletal muscle. IMP measurements consistently showed pressure converging to a residual level. A poroelastic model, having no mechanism for maintaining a residual pressure, will, by definition, relax to a state of zero pressure. It was shown that a residual pressure could be applied to the model, creating good agreement throughout the entire time course of load-relaxation. Without having a rationale for implementing a residual pressure to a poroelastic model of skeletal muscle, however, such an effort may be viewed as a purely academic exercise in curve-fitting. Rather, it would add much more insight if a correlative biological mechanism was found. An understanding of this mechanism would add credence to the implementation of a residual pressure, and allow for a deeper understanding of the biological significance of pressure levels. Accordingly, an understanding of how interstitial fluid flows in



skeletal muscle is needed. Additional experimentation and analyses could reveal that strain level and/or strain-rate sensitivity must be accounted for.

It should be further noted that the poroelastic model presented here is of excised tissue. In order to have a clinically meaningful predictive tool, the model must be expanded to be representative of an intact muscle. This requires implementation of a finite element model of a whole muscle. The framework for this effort has already been well documented by the work of Blemker, et al.<sup>103,115,179</sup> Additionally, an understanding of how fluid flows in an intact muscle, bounded *in situ* by other biological tissues, is required.

During the data collection for this work, it became apparent that there is a dearth of information describing the experimental conditions necessary to produce accurate results for replication of *in vivo* skeletal muscle behavior. A detailed study of the changes in muscle tension and pressure response given changes in testing environment would add considerably to the accumulated knowledge of muscle testing. Results of the same, performed for muscle on various scales (i.e., fiber, bundle, intact muscle), would be invaluable.

In summary, this work has shown that a single-phase continuum mechanics-based model, while fully capable of predicting instantaneous stress-strain behavior in skeletal muscle, cannot predict IMP. Examination of skeletal muscle as a poroelastic model has yielded the first 3D model able to predict intramuscular pressure, validated against experimental load-relaxation data. Further, this analysis is the first to describe that the solid phase of muscle behaves as an isotropic material. This material model also showed excised muscle tissue to have a negative Poisson's ratio under both longitudinal and transverse load-relaxation; the difference in these values can be attributed to being reflective of the differences that cause muscle to have a transversely isotropic instantaneous response and an isotropic relaxed response. Taken together, these revelations add considerably to the understanding of how skeletal muscle works, as well as establishing a course for future investigations.

## References

1. Lazarides E. Intermediate filaments as mechanical integrators of cellular space. *Nature*. 1980;283(5744):249-256.
2. Podolsky RJ, Shoenberg M. Force generation and shortening in skeletal muscle. *Handbook of Physiology*. Baltimore, MD: American Physiological Society; 1983. p. 173-188.
3. Huxley AF, Niedergerke R. Structural changes in muscle during contraction; interference microscopy of living muscle fibres. *Nature*. 1954;173(4412):971-3.
4. Huxley H, Hanson J. Changes in the cross-striations of muscle during contraction and stretch and their structural interpretation. *Nature*. 1954;173(4412):973-6.
5. Huxley HE. The mechanism of muscular contraction. *Science*. 1969;164(886):1356-65.
6. Beasley WC. Quantitative muscle testing: principles and applications to research and clinical services. *Archives of Physical Medicine and Rehabilitation*. 1961;42:398-425.
7. Kendall EP, McCreary EK. *Muscles: Testing and Function*. Baltimore: Williams & Wilkins; 1983.
8. Wakim KG, Gersten JW, et al. Objective recording of muscle strength. *Archives of Physical Medicine and Rehabilitation*. 1950;31(2):90-100.
9. Frese E, Brown M, Norton BJ. Clinical reliability of manual muscle testing. Middle trapezius and gluteus medius muscles. *Physical Therapy*. 1987;67(7):1072-6.
10. Bohannon RW. Make tests and break tests of elbow flexor muscle strength. *Physical Therapy*. 1988;68(2):193-4.
11. Bohannon RW. Hand-held compared with isokinetic dynamometry for measurement of static knee extension torque (parallel reliability of dynamometers). *Clinical Physics and Physiological Measurement*. 1990;11(3):217-22.
12. Wikholm JB, Bohannon RW. Hand-held Dynamometer Measurements: Tester Strength Makes a Difference. *Journal of Orthopaedic & Sports Physical Therapy*. 1991;13(4):191-8.
13. Fowler WM, Jr., Gardner GW. Quantitative strength measurements in muscular dystrophy. *Archives of Physical Medicine and Rehabilitation*. 1967;48(12):629-44.

14. Sunderland A, Tinson D, Bradley L, Hewer RL. Arm function after stroke. An evaluation of grip strength as a measure of recovery and a prognostic indicator. *Journal of Neurology, Neurosurgery, and Psychiatry*. 1989;52(11):1267-72.
15. Armstrong LE, Winant DM, Swasey PR, et al. Using isokinetic dynamometry to test ambulatory patients with multiple sclerosis. *Physical Therapy*. 1983;63(8):1274-9.
16. Tripp EJ, Harris SR. Test-retest reliability of isokinetic knee extension and flexion torque measurements in persons with spastic hemiparesis. *Physical Therapy*. 1991;71(5):390-6.
17. Aitkens S, Lord J, Bernauer E, et al. Relationship of manual muscle testing to objective strength measurements. *Muscle & Nerve*. 1989;12(3):173-7.
18. Beasley WC. Instrumentation and equipment for quantitative clinical muscle testing. *Archives of Physical Medicine and Rehabilitation*. 1956;37(10):604-21.
19. Bohannon RW. Manual muscle test scores and dynamometer test scores of knee extension strength. *Archives of Physical Medicine and Rehabilitation*. 1986;67(6):390-2.
20. Schwartz S, Cohen ME, Herbison GJ, Shah A. Relationship between two measures of upper extremity strength: manual muscle test compared to hand-held myometry. *Archives of Physical Medicine and Rehabilitation*. 1992;73(11):1063-8.
21. Salmons S. Report on the 8th International Conference on Medical and Biological Engineering. *Biomedical Engineering*. 1969;4:467-474.
22. Abraham LD, Marks WB, Loeb GE. The distal hindlimb musculature of the cat. Cutaneous reflexes during locomotion. *Experimental Brain Research*. 1985;58(3):594-603.
23. Gregor RJ, Roy RR, Whiting WC, et al. Mechanical output of the cat soleus during treadmill locomotion: in vivo vs in situ characteristics. *Journal of Biomechanics*. 1988;21(9):721-32.
24. Herzog W, Leonard TR, Guimaraes AC. Forces in gastrocnemius, soleus, and plantaris tendons of the freely moving cat. *Journal of Biomechanics*. 1993;26(8):945-53.
25. Hodgson JA. The relationship between soleus and gastrocnemius muscle activity in conscious cats--a model for motor unit recruitment? *Journal of Physiology*. 1983;337:553-62.
26. Lovely RG, Gregor RJ, Roy RR, Edgerton VR. Weight-bearing hindlimb stepping in treadmill-exercised adult spinal cats. *Brain Research*. 1990;514(2):206-18.

27. Walmsley B, Hodgson JA, Burke RE. Forces produced by medial gastrocnemius and soleus muscles during locomotion in freely moving cats. *Journal of Neurophysiology*. 1978;41(5):1203-16.
28. Whiting WC, Gregor RJ, Roy RR, Edgerton VR. A technique for estimating mechanical work of individual muscles in the cat during treadmill locomotion. *Journal of Biomechanics*. 1984;17(9):685-94.
29. Cooney WP, An K-N, Chao EYS. Direct measurement of tendon forces in the hand. *Transaction of the 32nd Annual Meeting of the Orthopaedic Research Society*. 1986;11:53.
30. Fukashiro S, Komi PV, Jarvinen M, Miyashita M. In vivo Achilles tendon loading during jumping in humans. *European Journal of Applied Physiology and Occupational Physiology*. 1995;71(5):453-8.
31. Komi PV. Relevance of in vivo force measurements to human biomechanics. *Journal of Biomechanics*. 1990;23 Suppl 1:23-34.
32. Shaari CM, Sanders I. Quantifying how location and dose of botulinum toxin injections affect muscle paralysis. *Muscle & Nerve*. 1993;16(9):964-9.
33. Komi PV, Belli A, Huttunen V, et al. Optic Fibre as a Transducer of Tendonmuscular Forces. *European Journal of Applied Physiology and Occupational Physiology*. 1996;72:278-280.
34. Arndt AN, Komi PV, Bruggemann GP, Lukkariniemi J. Individual muscle contributions to the in vivo achilles tendon force. *Clinical Biomechanics*. 1998;13(7):532-541.
35. Finni T, Komi PV, Lepola V. In vivo human triceps surae and quadriceps femoris muscle function in a squat jump and counter movement jump. *European Journal of Applied Physiology*. 2000;83(4 -5):416-26.
36. Finni T, Komi PV, Lukkariniemi J. Achilles tendon loading during walking: application of a novel optic fiber technique. *European Journal of Applied Physiology and Occupational Physiology*. 1998;77(3):289-91.
37. Bogey RA, Barnes LA, Perry J. Computer algorithms to characterize individual subject EMG profiles during gait. *Archives of Physical Medicine and Rehabilitation*. 1992;73(9):835-41.
38. Bogey RA, Barnes LA, Perry J. A computer algorithm for defining the group electromyographic profile from individual gait profiles. *Archives of Physical Medicine and Rehabilitation*. 1993;74(3):286-91.
39. Close JR. *Functional Anatomy of the Extremities*. Springfield: C.C. Thomas; 1973.
40. Kamavuako EN, Farina D, Yoshida K, Jensen W. Relationship between grasping force and features of single-channel intramuscular EMG signals. *Journal of Neuroscience Methods*. 2009;185(1):143-50.

41. Onishi H, Yagi R, Akasaka K, et al. Relationship between EMG signals and force in human vastus lateralis muscle using multiple bipolar wire electrodes. *Journal of Electromyography and Kinesiology*. 2000;10(1):59-67.
42. Guimaraes AC, Herzog W, Allinger TL, Zhang YT. The EMG-force relationship of the cat soleus muscle and its association with contractile conditions during locomotion. *Journal of Experimental Biology*. 1995;198(Pt 4):975-87.
43. Solomonow M, Guzzi A, Baratta R, et al. EMG-force model of the elbows antagonistic muscle pair. The effect of joint position, gravity and recruitment. *American Journal of Physical Medicine*. 1986;65(5):223-44.
44. Alkner BA, Tesch PA, Berg HE. Quadriceps EMG/force relationship in knee extension and leg press. *Medicine & Science in Sports & Exercise*. 2000;32(2):459-63.
45. Bigland B, Lippold OC. The relation between force, velocity and integrated electrical activity in human muscles. *Journal of Physiology*. 1954;123(1):214-24.
46. Bouisset S. EMG and muscle force in normal muscle activities. In: Desmedt JE, editor. *New Development in EMG and Clinical Physiology*. Basel, Switzerland: Karger; 1973.
47. Hatze H. A general myocybernetic control model of skeletal muscle. *Biological Cybernetics*. 1978;28(3):143-57.
48. Hof AL, van den Berg J. Linearity between the weighted sum of the EMGs of the human triceps surae and the total torque. *Journal of Biomechanics*. 1977;10(9):529-39.
49. Inman VT, Ralston HJ, Saunders JB, et al. Relation of human electromyogram to muscular tension. *Electroencephalography and Clinical Neurophysiology*. 1952;4(2):187-94.
50. Komi PV. Measurement of the force-velocity relationship in human muscle under concentric and eccentric contractions. In: Karger, editor. *Medicine and Sport*. Volume 8. Basel, Switzerland 1973. p. 224-229.
51. Milner-Brown HS, Stein RB. The relation between the surface electromyogram and muscular force. *Journal of Physiology*. 1975;246(3):549-69.
52. Bilodeau M, Arsenault AB, Gravel D, Bourbonnais D. Influence of gender on the EMG power spectrum during an increasing force level. *Journal of Electromyography and Kinesiology*. 1992;2(3):121-9.
53. Zecca M, Micera S, Carrozza MC, Dario P. Control of multifunctional prosthetic hands by processing the electromyographic signal. *Critical Reviews in Biomedical Engineering*. 2002;30(4-6):459-85.
54. Patterson PE, Anderson M. The use of self organizing maps to evaluate myoelectric signals. *Biomed Sci Instrum*. 1999;35:147-52.

55. Hill AV. The pressure developed in muscle during contraction. *Journal of Physiology*. 1948;107:518-526.
56. Kirkebo A, Wisnes A. Regional tissue fluid pressure in rat calf muscle during sustained contraction or stretch. *Acta Physiologica Scandinavica*. 1982;114(4):551-6.
57. Mazella H. On the pressure developed by the contraction of striated muscle and its influence on muscular circulation. *Archives of International Physiology*. 1954;62:334-347.
58. Sutherland DH, Woo S-Y, Schoon J, et al. The potential application of a small solid state pressure transducer to measure muscle activity during gait. *Transactions of the Orthopaedic Research Society*. 1977;2:289.
59. Davis J, Kaufman KR, Lieber RL. Correlation between active and passive isometric force and intramuscular pressure in the isolated rabbit tibialis anterior muscle. *Journal of Biomechanics*. 2003;36(4):505-12.
60. Ward SR, Davis J, Kaufman KR, Lieber RL. Relationship between muscle stress and intramuscular pressure during dynamic muscle contractions. *Muscle & Nerve*. 2007;36(3):313-9.
61. Winters TM, Sepulveda GS, Cottler PS, et al. Correlation Between Isometric Force and Intramuscular Pressure in Rabbit Tibialis Anterior Muscle With an Intact Anterior Compartment. *Muscle & Nerve*. 2009;40(1):79-85.
62. Aratow M, Ballard RE, Crenshaw AG, et al. Intramuscular pressure and electromyography as indexes of force during isokinetic exercise. *Journal of Applied Physiology*. 1993;74(6):2634-40.
63. Hargens AR, Sejersted OM, Kardel KR, et al. Intramuscular fluid pressure: A function of contraction force and tissue depth. *Transactions of the Orthopaedic Research Society*. 1982;7:371.
64. Hussain SNA, Magder S. Diaphragmatic intramuscular pressure in relation to tension, shortening, and blood flow. *Journal of Applied Physiology*. 1991;71(1):159-167.
65. Järvholm U, Palmerud G, Herberts P, et al. Intramuscular pressure and electromyography in the supraspinatus muscle at shoulder abduction. *Clinical Orthopaedics & Related Research*. 1989;245:102-109.
66. Körner L, Parker P, Almström C, et al. Relationship on intramuscular pressure to the force output and myoelectric signal of skeletal muscle. *Journal of Orthopaedic Research*. 1984;2:289-296.
67. Mubarak SJ, Hargens AR, Owen CA, et al. The wick catheter technique for measurement of intramuscular pressure: A new research and clinical tool. *Journal of Bone and Joint Surgery. American Volume*. 1976;58A(7):1016-1020.

68. Owen CA, Garetto LP, Hargens AR, et al. Relationship of intramuscular pressure to strength and muscular contraction. *Transactions of the Orthopaedic Research Society*. 1977;2:246.
69. Parker PA, Korner L, Kadefors R. Estimation of muscle force from intramuscular total pressure. *Medical & Biological Engineering & Computing*. 1984;22(5):453-7.
70. Petrofsky JS, Hendershot DM. The interrelationship between blood pressure, intramuscular pressure, and isometric endurance in fast and slow twitch skeletal muscle in the cat. *European Journal of Applied Physiology & Occupational Physiology*. 1984;53(2):106-11.
71. Sejersted OM, Hargens AR, Kardel KR, et al. Intramuscular fluid pressure during isometric contraction of human skeletal muscle. *Journal of Applied Physiology*. 1984;56(2):287-95.
72. Sylvest O, Hvid N. Pressure measurements in human striated muscles during contraction. *Acta Rheumatologica Scandinavica*. 1959;5:216-22.
73. Sjogaard G, Jensen BR, Hargens AR, Sogaard K. Intramuscular pressure and EMG relate during static contractions but dissociate with movement and fatigue. *Journal of Applied Physiology*. 2004;96(4):1522-9; discussion.
74. Vedsted P, Blangsted AK, Sogaard K, et al. Muscle tissue oxygenation, pressure, electrical, and mechanical responses during dynamic and static voluntary contractions. *European Journal of Applied Physiology*. 2006;96(2):165-77.
75. Matsen FA, Mayo KA, Sheridan GW, Krugmire RB, Jr. Monitoring of intramuscular pressure. *Surgery*. 1976;79:702-709.
76. Rorabeck CH, Castle GSP, Hardie R, Logan J. Compartmental pressure measurements: An experimental investigation using the slit catheter. *Journal of Trauma*. 1981;21:446-449.
77. Styf JR. Evaluation of injection techniques in recording of intramuscular pressure. *Journal of Orthopaedic Research*. 1989;7:812-816.
78. Crenshaw AG, Styf JR, Mubarak SJ, Hargens AR. A new "transducer tipped" fiber optic catheter for measuring intramuscular pressures. *Journal of Orthopaedic Research*. 1990;8(4):464-468.
79. Willy C, Gerngross H, Sterk JC. Measurement of intracompartmental pressure with use of a new electronic transducer-tipped catheter system. *Journal of Bone and Joint Surgery. American Volume*. 1999;81A:158-168.
80. Baumann JU, Sutherland DH, Hanggi A. Intramuscular pressure during walking: an experimental study using the wick catheter technique. *Clinical Orthopaedics and Related Research*. 1979(145):292-9.

81. McDermott AGP, Marble AE, Yabsley RH, Phillips B. Monitoring dynamic anterior compartment pressure during exercise. *American Journal of Sports Medicine*. 1981;10:83-89.
82. Crenshaw AG, Styf JR, Hargens AR. Intramuscular pressures during exercise: An evaluation of a fiberoptic transducer-tipped catheter system. *European Journal of Applied Physiology*. 1992;65:178-182.
83. Cottler PS, Karpen WR, Morrow DA, Kaufman KR. Performance characteristics of a new generation pressure microsensor for physiologic applications. *Annals of Biomedical Engineering*. 2009;37(8):1638-45.
84. Yang C, Zhao C, Wold L, Kaufman KR. Biocompatibility of a physiological pressure sensor. *Biosensors and Bioelectronics*. 2003;19(1):51-8.
85. Kaufman KR, Wavering T, Morrow D, et al. Performance characteristics of a pressure microsensor. *Journal of Biomechanics*. 2003;36(2):283-7.
86. Wavering T, Meller S, Evans M, et al. Interferometric optical fiber microcantilever beam biosensor. *SPIE Biochemical and Biomolecular Sensing*. 2000;10:10.1117/12.411717.
87. Ward SR, Lieber RL. IMP and stress as a function of transducer placement within a muscle. *Muscle Physiology Laboratory, University of California, San Diego*. 2009.
88. Ameredes BT, Provenzano MA. Regional intramuscular pressure development and fatigue in the canine gastrocnemius muscle in situ. *Journal of Applied Physiology*. 1997;83(6):1867-76.
89. Crenshaw AG, Gerdle B, Heiden M, et al. Intramuscular pressure and electromyographic responses of the vastus lateralis muscle during repeated maximal isokinetic knee extensions. *Acta Physiologica Scandinavica*. 2000;170(2):119-26.
90. Jarvholm U, Palmerud G, Karlsson D, et al. Intramuscular pressure and electromyography in four shoulder muscles. *Journal of Orthopaedic Research*. 1991;9(4):609-19.
91. Garfin SR, Tipton CM, Mubarak SJ, et al. Role of fascia in maintenance of muscle tension and pressure. *Journal of Applied Physiology*. 1981;51(2):317-20.
92. Zajac FE. Muscle and tendon: properties, models, scaling, and application to biomechanics and motor control. *Critical Reviews in Biomedical Engineering*. 1989;17(4):359-411.
93. Cobb M. Timeline: Exorcizing the animal spirits, Jan Swammerdam on nerve function. *Nature Reviews Neuroscience*. 2002;3(5):395-400.
94. McMahan TA, editor. *Muscles, Reflexes, and Locomotion*. Princeton, NJ: Princeton University Press; 1984.



95. Bosboom EMH, Hesselink MKC, Oomens CWJ, et al. Passive transverse mechanical properties of skeletal muscle under in vivo compression. *Journal of Biomechanics*. 2001;34(10):1365-1368.
96. Blix M. Die Langrund dei Spannung des Muskels. *Acta Physiologica Scandinavia*. 1894;5:149-206.
97. Hill AV. The Heat of Shortening and the Dynamic Constants of Muscle. *Proceedings of the Royal Society of London, Series B*. 1938(126):136-195.
98. Delp SL, Loan JP. A graphics-based software system to develop and analyze models of musculoskeletal structures. *Computers in Biology and Medicine*. 1995;25(1):21-34.
99. Kaufman KR, An KN, Litchy WJ, Chao EY. Physiological prediction of muscle forces--II. Application to isokinetic exercise. *Neuroscience*. 1991;40(3):793-804.
100. Buchanan TS, Lloyd DG, Manal K, Besier TF. Estimation of muscle forces and joint moments using a forward-inverse dynamics model. *Medicine and Science in Sports and Exercise*. 2005;37(11):1911-1916.
101. Meyer GA, McCulloch AD, Ward SR, Lieber RL. Passive Viscoelastic Scaling in Desmin Knockout Muscles. *Workshop on Multi-Scale Muscle Mechanics*. 2009:36.
102. van der Linden BJ, Koopman HF, Grootenboer HJ, Huijing PA. Modelling functional effects of muscle geometry. *Journal of Electromyography and Kinesiology*. 1998;8(2):101-9.
103. Blemker SS, Pinsky PM, Delp SL. A 3D model of muscle reveals the causes of nonuniform strains in the biceps brachii. *Journal of Biomechanics*. 2005;38(4):657-665.
104. Huijing PA. Muscular force transmission necessitates a multilevel integrative approach to the analysis of function of skeletal muscle. *Exercise and Sports Science Reviews*. 2003;31(4):167-75.
105. Jenkyn TR, Koopman B, Huijing P, et al. Finite element model of intramuscular pressure during isometric contraction of skeletal muscle. *Physics in Medicine and Biology*. 2002;47(22):4043-61.
106. Yucesoy CA, Koopman BH, Huijing PA, Grootenboer HJ. Three-dimensional finite element modeling of skeletal muscle using a two-domain approach: linked fiber-matrix mesh model. *Journal of Biomechanics*. 2002;35(9):1253-62.
107. Gielen AWJ, Oomens CWJ, Bovendeerd PHM, et al. A Finite Element Approach for Skeletal Muscle using a Distributed Moment Model of Contraction. *Computer Methods in Biomechanics & Biomedical Engineering*. 2000;3:231-144.
108. Johansson T, Meier P, Blickhan R. A finite-element model for the mechanical analysis of skeletal muscles. *Journal of Theoretical Biology*. 2000;206(1):131-149.

109. Martins JAC, Pires EB, Salvado R, Dinis PB. A numerical model of passive and active behavior of skeletal muscles. *Computer Methods in Applied Mechanics and Engineering*. 1998;151(3-4):419-433.
110. Criscione JC, Douglas AS, Hunter WC. Physically based strain invariant set for materials exhibiting transversely isotropic behavior. *Journal of the Mechanics and Physics of Solids*. 2001;49(4):871-897.
111. Humphrey JD, Strumpf RK, Yin FC. Determination of a constitutive relation for passive myocardium: II. Parameter estimation. *Journal of Biomechanical Engineering*. 1990;112(3):340-6.
112. Weiss JA, Maker BN, Govindjee S. Finite element implementation of incompressible, transversely isotropic hyperelasticity. *Computer Methods in Applied Mechanics and Engineering*. 1996;135(1-2):107-128.
113. Van Loocke M, Lyons CG, Simms CK. A validated model of passive muscle in compression. *Journal of Biomechanics*. 2006;39(16):2999-3009.
114. Van Loocke M, Lyons CG, Simms CK. Viscoelastic properties of passive skeletal muscle in compression: Stress-relaxation behaviour and constitutive modelling. *Journal of Biomechanics*. 2008;41(7):1555-1566.
115. Blemker SS, Delp SL. Three-dimensional representation of complex muscle architectures and geometries. *Annals of Biomedical Engineering*. 2005;33(5):661-73.
116. Anderson J, Joumaa V, Stevens L, et al. Passive stiffness changes in soleus muscles from desmin knockout mice are not due to titin modifications. *Pflügers Archiv-European Journal of Physiology*. 2002;444(6):771-776.
117. Anderson J, Li ZL, Goubel F. Passive stiffness is increased in soleus muscle of desmin knockout mouse. *Muscle & Nerve*. 2001;24(8):1090-1092.
118. Boriek AM, Capetanaki Y, Hwang W, et al. Desmin integrates the three-dimensional mechanical properties of muscles. *American Journal of Physiology-Cell Physiology*. 2001;280(1):C46-C52.
119. Gosselin LE, Adams C, Cotter TA, et al. Effect of exercise training on passive stiffness in locomotor skeletal muscle: role of extracellular matrix. *Journal of Applied Physiology*. 1998;85(3):1011-1016.
120. Hete B, Shung KK. A Study of the Relationship between Mechanical and Ultrasonic Properties of Dystrophic and Normal Skeletal-Muscle. *Ultrasound in Medicine and Biology*. 1995;21(3):343-352.
121. Lin RM, Chang GL, Chang LT. Biomechanical properties of muscle-tendon unit under high-speed passive stretch. *Clinical Biomechanics*. 1999;14(6):412-417.

122. Linder-Ganz E, Gefen A. Mechanical compression-induced pressure sores in rat hindlimb: muscle stiffness, histology, and computational models. *Journal of Applied Physiology*. 2004;96(6):2034-2049.
123. Gareis H, Solomonow M, Baratta R, et al. The isometric length-force models of nine different skeletal muscles. *Journal of Biomechanics*. 1992;25(8):903-16.
124. Hawkins D, Bey M. Muscle and tendon force-length properties and their interactions in vivo. *Journal of Biomechanics*. 1997;30(1):63-70.
125. Muhl ZF. Active length-tension relation and the effect of muscle pinnation on fiber lengthening. *Journal of Morphology*. 1982;173(3):285-92.
126. Aïmedieu P, Mitton D, Faure JP, et al. Dynamic stiffness and damping of porcine muscle specimens. *Med Eng Phys*. 2003;25(9):795-799.
127. Mathur AB, Collinsworth AM, Reichert WM, et al. Endothelial, cardiac muscle and skeletal muscle exhibit different viscous and elastic properties as determined by atomic force microscopy. *Journal of Biomechanics*. 2001;34(12):1545-53.
128. Gao Y, Kostrominova TY, Faulkner JA, Wineman AS. Age-related changes in the mechanical properties of the epimysium in skeletal muscles of rats. *Journal of Biomechanics*. 2008;41(2):465-9.
129. Yucesoy CA, Koopman BH, Baan GC, et al. Effects of inter- and extramuscular myofascial force transmission on adjacent synergistic muscles: assessment by experiments and finite-element modeling. *Journal of Biomechanics*. 2003;36(12):1797-811.
130. Lemos RR, Epstein M, Herzog W, Wyvill B. A framework for structured modeling of skeletal muscle. *Computer Methods in Biomechanics & Biomedical Engineering*. 2004;7(6):305-17.
131. Oomens CW, Maenhout M, van Oijen CH, et al. Finite element modelling of contracting skeletal muscle. *Philosophical Transactions of the Royal Society of London B: Biological Sciences*. 2003;358(1437):1453-60.
132. Odegard GM, Haut Donahue TL, Morrow DA, Kaufman KR. Constitutive Modeling of Skeletal Muscle Tissue with an Explicit Strain-Energy Function. *Journal of Biomechanical Engineering*. 2008;130(6):61017.
133. Lieber RL, Blevins FT. Skeletal muscle architecture of the rabbit hindlimb: functional implications of muscle design. *Journal of Morphology*. 1989;199(1):93-101.
134. Haut Donahue TL, Gregersen C, Hull ML, Howell SM. Comparison of viscoelastic, structural, and material properties of double-looped anterior cruciate ligament grafts made from bovine digital extensor and human hamstring tendons (vol 123, pg 162, 2001). *Journal of Biomechanical Engineering*. 2001;123(5):523-523.

135. Morrow DA, Haut Donahue TL, Odegard GM, Kaufman KR. Tensile Material Properties of Skeletal Muscle Tissue in Longitudinal and Transverse Directions. Proceedings of the ASME 2008 Summer Bioengineering Conference. 2008:SBC2009-206211.
136. Van Ee CA, Chasse AL, Myers BS. Quantifying skeletal muscle properties in cadaveric test specimens: Effects of mechanical loading, postmortem time, and freezer storage. *Journal of Biomechanical Engineering*. 2000;122(1):9-14.
137. Timoshenko S, Goodier JN. *Theory of Elasticity*. New York: McGraw-Hill; 1951.
138. Ciarletta P, Dario P, Micera S. Pseudo-hyperelastic model of tendon hysteresis from adaptive recruitment of collagen type I fibrils. *Biomaterials*. 2008;29(6):764-70.
139. Yin L, Elliott DM. A biphasic and transversely isotropic mechanical model for tendon: application to mouse tail fascicles in uniaxial tension. *Journal of Biomechanics*. 2004;37(6):907-16.
140. Cheng T, Gan RZ. Mechanical properties of anterior malleolar ligament from experimental measurement and material modeling analysis. *Biomechanics and Modeling in Mechanobiology*. 2008;7(5):387-94.
141. Weiss JA, Gardiner JC, Bonifasi-Lista C. Ligament material behavior is nonlinear, viscoelastic and rate-independent under shear loading. *Journal of Biomechanics*. 2002;35(7):943-50.
142. Sweigart MA, Zhu CF, Burt DM, et al. Intraspecies and interspecies comparison of the compressive properties of the medial meniscus. *Annals of Biomedical Engineering*. 2004;32(11):1569-79.
143. Villegas DF, Maes JA, Magee SD, Donahue TL. Failure properties and strain distribution analysis of meniscal attachments. *Journal of Biomechanics*. 2007;40(12):2655-62.
144. Malvern LE. *Introduction to the Mechanics of a Continuous Medium*. Upper Saddle River, NJ: Prentice Hall; 1969.
145. Holzapfel GA. *Nonlinear Solid Mechanics: A Continuum Approach For Engineering*. New York: John Wiley & Sons, Ltd; 2000.
146. Bensamoun SF, Ringleb SI, Chen Q, et al. Thigh muscle stiffness assessed with magnetic resonance elastography in hyperthyroid patients before and after medical treatment. *Journal of Magnetic Resonance Imaging*. 2007;26(3):708-13.
147. Nakhostine M, Styf JR, van Leuven S, et al. Intramuscular pressure varies with depth. The tibialis anterior muscle studied in 12 volunteers. *Acta Orthopaedica Scandinavica*. 1993;64(3):377-81.
148. Morrow DA, Haut Donahue TL, Odegard GM, Kaufman KR. A Method for Assessing the Fit of a Constitutive Material Model to Experimental Stress-Strain

- Data. Computer Methods in Biomechanics & Biomedical Engineering. 2010;13(2).
149. Morrow DA, Haut Donahue TL, Odegard GM, Kaufman KR. Transversely isotropic tensile material properties of skeletal muscle tissue. *Journal of the Mechanical Behavior of Biomedical Materials*. 2010;3:124-129.
  150. Morrow DA, Haut Donahue TL, Odegard GM, Kaufman KR. Validation of a Finite Element Model of Passive Force and Pressure in Skeletal Muscle. *ASME 2009 Summer Bioengineering Conference*. 2009:SBC2009-206211.
  151. Morrow DA, Haut Donahue TL, Odegard GM, Kaufman KR. A Validated Finite Element Model of Force in Active and Passive Skeletal Muscle. *ASME 2010 Summer Bioengineering Conference*. 2010:SBC2010-19385.
  152. Smith LR, Gerace-Fowler L, Lieber RL. Muscle extracellular matrix applies a transverse stress on fibers with axial strain. *Journal of Biomechanics*. 2011;44(8):1618-20.
  153. Fung YC, Fronek K, Patitucci P. Pseudoelasticity of arteries and the choice of its mathematical expression. *The American Journal of Physiology*. 1979;237(5):H620-31.
  154. Holzapfel GA, Gasser TC, Odgen RW. A New Constitutive Framework for Arterial Wall Mechanics and a Comparative Study of Material Models. *Journal of Elasticity*. 2000;61(1-3):1-48.
  155. Itskov M, Ehret AE, Mavrilas D. A polyconvex anisotropic strain-energy function for soft collagenous tissues. *Biomechanics and Modeling in Mechanobiology*. 2006;5(1):17-26.
  156. MEEM 6990 - Nonlinear Solid Mechanics Course Materials Odegard GM. Houghton, MI: Michigan Technological University; 2006.
  157. Verification Manual. Providence, RI: Dassault Systemes; 2010. 2.2.1-20 p.
  158. Elliott GF, Lowy J, Worthington CR. An X-ray and light-diffraction study of the filament lattice of striated muscle in the living state and in rigor. *Journal of Molecular Biology*. 1963;6(4):295-IN9.
  159. Rehorn MR, Blemker SS. Passive Properties of Muscle Fibers are Velocity Dependent. 34th Annual Meeting of the American Society of Biomechanics. 2010.
  160. Wang K, McCarter R, Wright J, et al. Viscoelasticity of the sarcomere matrix of skeletal muscles. The titin-myosin composite filament is a dual-stage molecular spring. *Biophysical Journal*. 1993;64(4):1161-77.
  161. Yang M, Taber LA. The possible role of poroelasticity in the apparent viscoelastic behavior of passive cardiac muscle. *Journal of Biomechanics*. 1991;24(7):587-97.

162. Huyghe JM, van Campen DH, Arts T, Heethaar RM. The constitutive behaviour of passive heart muscle tissue: a quasi-linear viscoelastic formulation. *Journal of Biomechanics*. 1991;24(9):841-9.
163. McGowan CP, Neptune RR, Herzog W. A phenomenological model and validation of shortening-induced force depression during muscle contractions. *Journal of Biomechanics*. 2010;43(3):449-54.
164. Sabra KG, Archer A. Tomographic elastography of contracting skeletal muscles from their natural vibrations. *Applied Physics Letters*. 2009;95(20):-.
165. Tsaturyan AK, Izacov VJ, Zhelamsky SV, Bykov BL. Extracellular fluid filtration as the reason for the viscoelastic behaviour of the passive myocardium. *Journal of Biomechanics*. 1984;17(10):749-55.
166. Ward SR, Lieber RL. Density and hydration of fresh and fixed human skeletal muscle. *Journal of Biomechanics*. 2005;38(11):2317-20.
167. Sjogaard G, Saltin B. Extra- and intracellular water spaces in muscles of man at rest and with dynamic exercise. *The American Journal of Physiology*. 1982;243(3):R271-80.
168. Hargens AR, Tipton CM, Gollnick PD, et al. Fluid shifts and muscle function in humans during acute simulated weightlessness. *Journal of Applied Physiology*. 1983;54(4):1003-9.
169. Sjogaard G, Adams RP, Saltin B. Water and ion shifts in skeletal muscle of humans with intense dynamic knee extension. *The American Journal of Physiology*. 1985;248(2 Pt 2):R190-6.
170. LeRoux MA, Setton LA. Experimental and biphasic FEM determinations of the material properties and hydraulic permeability of the meniscus in tension. *Journal of Biomechanical Engineering*. 2002;124(3):315-21.
171. Lei F, Szeri AZ. Inverse analysis of constitutive models: biological soft tissues. *Journal of Biomechanics*. 2007;40(4):936-40.
172. Meyer GA, McCulloch AD, Lieber RL. A Nonlinear Model of Passive Muscle Viscosity. *Journal of Biomechanical Engineering*. 2011;133(9):091007-9.
173. Kleinbaum DG, Kupper LL. Applied regression analysis and other multivariable methods. North Scituate, Mass.: Duxbury Press; 1978. 556 p.
174. Kellermayer MSZ, Smith SB, Bustamante C, Granzier HL. Mechanical fatigue in repetitively stretched single molecules of titin. *Biophysical Journal*. 2001;80(2):852-863.
175. Lieber RL, Runesson E, Einarsson F, Friden J. Inferior mechanical properties of spastic muscle bundles due to hypertrophic but compromised extracellular matrix material. *Muscle & Nerve*. 2003;28(4):464-471.

- 176. van Turnhout M, Peters G, Stekelenburg A, Oomens C. Passive transverse mechanical properties as a function of temperature of rat skeletal muscle in vitro. *Biorheology*. 2005;42(3):193-207.
- 177. Shah SB, Davis J, Weisleder N, et al. Structural and functional roles of desmin in mouse skeletal muscle during passive deformation. *Biophysical Journal*. 2004;86(5):2993-3008.
- 178. Daniels L, Worthingham C. Muscle testing technique of manual examination. Philadelphia: W.B. Saunders; 1980.
- 179. Blemker SS, Delp SL. Rectus femoris and vastus intermedius fiber excursions predicted by three-dimensional muscle models. *Journal of Biomechanics*. 2006;39(8):1383-91.

## **Appendix A**

### **Table Data**



## Appendix A.1

**Table A.1**  
Data for Table 2.1

<b>Specimen</b>	<b>Linear Modulus (kPa)</b>	<b>Ultimate Stress (kPa)</b>	<b>Failure Strain</b>
LE01	577.18	177.00	0.41
LE02	310.87	65.20	0.35
LE03	348.57	105.00	0.39
LE04	559.50	137.00	0.33
LE05	483.25	228.00	0.66
LE06	390.38	266.00	0.89
TE01	6.00	16.70	3.36
TE02	17.11	26.80	1.80
TE03	29.15	25.50	1.11
TE04	15.94	24.91	1.80
TE05	18.34	24.70	1.73
TE06	48.38	43.60	1.10
LS01	0.34	-	-
LS02	1.53	-	-
LS04	3.48	-	-
LS05	1.40	-	-
LS06	8.71	-	-

Note: LS tests not run to failure, therefore no ultimate stress or failure strain values exist for these tests. LS03 test failed, no results reported.

## Appendix A.2

**Table A.2**  
Data for Table 3.1

<b>Method</b>	<b>I1 Terms</b>	<b>I2 Terms</b>	<b>I4 Terms</b>	<b>RMSE LE (kPa)</b>	<b>RMSE TE (kPa)</b>	<b>RMSE LS (kPa)</b>
ALL	1	1	1	12.91	2.94	1.71
ALL	1	1	2	7.79	2.72	0.85
ALL	1	2	1	11.72	2.93	0.70
ALL	2	1	1	11.95	2.86	0.42
ALL	1	2	2	7.75	2.10	0.44
ALL	2	1	2	7.76	1.96	0.35
ALL	1	1	3	7.79	2.73	0.82
ALL	1	3	1	11.62	3.07	0.68
ALL	2	2	1	11.75	2.93	0.67
ALL	3	1	1	11.63	3.14	0.35
ALL	3	1	2	7.79	1.89	0.35
ALL	1	2	3	7.77	2.11	0.44
ALL	2	1	3	7.78	1.96	0.35
ALL	1	3	2	7.78	1.91	0.47
ALL	2	2	2	7.78	1.95	0.38
ALL	1	1	4	7.81	2.73	0.83
ALL	2	3	1	11.59	3.13	0.39
ALL	3	2	1	11.66	3.10	0.41
ALL	3	1	3	7.80	1.89	0.35
ALL	2	3	2	7.80	1.92	0.34
ALL	2	1	4	7.78	1.97	0.35

Table A.2 (continued)

<b>Method</b>	<b>I1 Terms</b>	<b>I2 Terms</b>	<b>I4 Terms</b>	<b>RMSE LE (kPa)</b>	<b>RMSE TE (kPa)</b>	<b>RMSE LS (kPa)</b>
ALL	3	2	2	7.80	1.88	0.36
ALL	1	2	4	7.76	2.11	0.45
ALL	1	3	3	7.80	1.90	0.47
ALL	2	2	3	7.80	1.95	0.39
ALL	1	1	5	7.62	2.74	0.77
ALL	3	3	1	11.64	3.00	0.59
ALL	1	2	5	7.63	2.11	0.44
ALL	2	3	3	7.82	1.91	0.34
ALL	3	1	4	7.81	1.90	0.35
ALL	2	2	4	7.80	1.96	0.37
ALL	3	2	3	7.82	1.88	0.36
ALL	3	3	2	7.81	1.86	0.38
ALL	2	1	5	7.63	1.97	0.35
ALL	1	3	4	7.80	1.91	0.47
ALL	3	1	5	7.65	1.89	0.35
ALL	2	3	4	7.82	1.92	0.34
ALL	1	3	5	7.65	1.91	0.46
ALL	3	3	3	7.83	1.87	0.38
ALL	3	2	4	7.82	1.88	0.37
ALL	2	2	5	7.65	1.95	0.41
ALL	2	3	5	7.67	1.92	0.34
ALL	3	2	5	7.66	1.88	0.35

Table A.2 (continued)

<b>Method</b>	<b>I1 Terms</b>	<b>I2 Terms</b>	<b>I4 Terms</b>	<b>RMSE LE (kPa)</b>	<b>RMSE TE (kPa)</b>	<b>RMSE LS (kPa)</b>
ALL	3	3	4	7.83	1.87	0.39
ALL	3	3	5	7.68	1.87	0.36
EACH	2	2	1	13.02	2.54	0.52
EACH	1	1	1	14.23	2.84	1.36
EACH	1	1	5	25.18	2.73	0.83
EACH	1	1	4	21.52	2.73	0.83
EACH	1	1	2	9.09	2.72	0.91
EACH	1	1	3	16.92	2.73	0.83
EACH	2	3	4	8.22	2.04	0.41
EACH	1	2	1	12.90	2.61	0.67
EACH	3	2	3	13.02	2.20	0.37
EACH	3	3	1	12.93	3.03	0.89
EACH	2	3	5	8.30	2.03	0.42
EACH	2	1	2	8.45	2.08	0.36
EACH	2	3	3	12.79	2.05	0.42
EACH	1	3	1	12.86	4.29	0.53
EACH	3	2	4	8.48	2.16	0.37
EACH	1	3	2	8.32	2.54	0.38
EACH	3	1	3	12.91	2.18	0.36
EACH	2	1	3	13.17	2.02	0.36
EACH	2	3	1	12.86	4.10	0.67
EACH	2	2	3	13.26	2.00	0.36

Table A.2 (continued)

<b>Method</b>	<b>I1 Terms</b>	<b>I2 Terms</b>	<b>I4 Terms</b>	<b>RMSE LE (kPa)</b>	<b>RMSE TE (kPa)</b>	<b>RMSE LS (kPa)</b>
EACH	1	2	2	8.31	2.11	0.47
EACH	2	2	2	8.47	2.02	0.35
EACH	1	3	3	12.35	2.19	0.39
EACH	3	3	5	8.51	2.06	0.49
EACH	1	3	5	18.12	2.17	0.39
EACH	2	3	2	8.37	2.38	0.45
EACH	1	3	4	8.07	2.17	0.39
EACH	3	3	3	12.69	2.09	0.50
EACH	3	3	4	8.15	2.06	0.49
EACH	3	1	4	8.38	2.14	0.36
EACH	1	2	5	25.73	2.11	0.44
EACH	3	2	1	12.76	7.10	0.36
EACH	3	2	2	8.42	2.83	0.37
EACH	2	2	5	23.54	2.00	0.37
EACH	3	1	5	21.82	2.13	0.36
EACH	2	1	5	8.55	2.02	0.36
EACH	3	1	2	8.38	2.91	0.36
EACH	2	2	4	8.98	2.00	0.36
EACH	2	1	4	8.92	2.02	0.36
EACH	3	1	1	12.72	7.21	0.36
EACH	3	2	5	22.03	2.15	0.37
EACH	3	3	2	8.39	2.40	0.62

Table A.2 (*continued*)

<b>Method</b>	<b>I1 Terms</b>	<b>I2 Terms</b>	<b>I4 Terms</b>	<b>RMSE LE (kPa)</b>	<b>RMSE TE (kPa)</b>	<b>RMSE LS (kPa)</b>
EACH	1	2	4	8.07	2.11	0.44
EACH	2	1	1	12.99	2.98	0.39
EACH	1	2	3	12.20	2.11	0.44

## Appendix A.3

**Table A.3**  
Data for Table 5.1

<b>Specimen</b>	<b>Strain</b>	<b>Stress (MPa)</b>	<b>Ln Stress (Ln MPa)</b>
LE02	0.028	0.1147	-2.165435
LE02	0.058	0.2524	-1.37674
LE02	0.088	0.4934	-0.706435
LE02	0.118	0.8893	-0.117321
LE02	0.150	1.405	0.3400373
LE03	0.036	0.05786	-2.849729
LE03	0.072	0.2683	-1.31565
LE03	0.111	0.5945	-0.520035
LE03	0.150	1.115	0.1088544
LE03	0.190	2.104	0.7438403
LE04	0.032	0.3	-1.203973
LE04	0.066	0.9259	-0.076989
LE04	0.100	1.84	0.6097656
LE04	0.135	3.365	1.213428
LE04	0.172	5.736	1.7467621
LE05	0.036	0.2633	-1.334461
LE05	0.072	0.9458	-0.055724
LE05	0.111	1.989	0.687632
LE05	0.150	3.812	1.338154
LE05	0.190	6.952	1.9390294
LE06	0.028	0.3578	-1.027781
LE06	0.058	0.9976	-0.002403
LE06	0.088	2.233	0.803346
LE06	0.118	4.717	1.551173

Table A.3 (continued)

<b>Specimen</b>	<b>Strain</b>	<b>Stress (MPa)</b>	<b>Ln Stress (Ln MPa)</b>
LE06	0.150	9.097	2.2079447
LE07	0.031	0.1501	-1.896454
LE07	0.063	0.5605	-0.578926
LE07	0.095	1.257	0.2287279
LE07	0.129	2.936	1.0770481
LE07	0.164	6.182	1.8216419
LE08	0.072	0.5694	-0.563172
LE08	0.111	1.483	0.3940671
LE08	0.150	2.976	1.0905801
LE08	0.190	5.619	1.7261537
LE09	0.030	0.07008	-2.658118
LE09	0.091	0.6044	-0.503519
LE09	0.123	1.034	0.0334348
LE09	0.156	1.673	0.5146184
LE10	0.055	0.5387	-0.618596
LE10	0.113	1.669	0.5122247
LE10	0.175	3.762	1.3249507
LE10	0.239	7.949	2.0730462
LE10	0.305	16.56	2.8069902
LE11	0.025	0.1911	-1.654958
LE11	0.051	0.5386	-0.618782
LE11	0.078	1.216	0.1955668
LE11	0.105	2.354	0.856116
LE11	0.133	4.743	1.5566699
TE01	0.026	0.1122	-2.187472
TE01	0.054	0.2644	-1.330292



Table A.3 (continued)

<b>Specimen</b>	<b>Strain</b>	<b>Stress (MPa)</b>	<b>Ln Stress (Ln MPa)</b>
TE01	0.081	0.5048	-0.683593
TE01	0.110	0.9135	-0.090472
TE01	0.139	1.562	0.4459671
TE02	0.025	0.2305	-1.467504
TE02	0.051	0.6147	-0.486621
TE02	0.078	1.135	0.1266327
TE02	0.105	1.929	0.6570017
TE02	0.133	3.065	1.1200476
TE03	0.028	0.1261	-2.07068
TE03	0.056	0.3414	-1.0747
TE03	0.085	0.6233	-0.472727
TE03	0.115	1.313	0.2723146
TE03	0.146	2.478	0.9074518
TE04	0.020	0.1851	-1.686859
TE04	0.041	0.6293	-0.463147
TE04	0.062	1.456	0.375693
TE04	0.083	2.295	0.8307329
TE04	0.105	3.653	1.2955488
TE05	0.038	0.09131	-2.393462
TE05	0.078	0.2674	-1.31901
TE05	0.119	0.5479	-0.601662
TE05	0.161	1.057	0.0554347
TE05	0.205	1.878	0.6302074
TE06	0.030	0.1116	-2.192834
TE06	0.062	0.2828	-1.263015
TE06	0.094	0.6029	-0.506004

Table A.3 (continued)

<b>Specimen</b>	<b>Strain</b>	<b>Stress (MPa)</b>	<b>Ln Stress (Ln MPa)</b>
TE06	0.127	1.392	0.3307416
TE06	0.161	2.672	0.9828273
TE07	0.023	0.1648	-1.803023
TE07	0.047	0.4307	-0.842343
TE07	0.072	1.096	0.0916672
TE07	0.097	2.887	1.0602179
TE07	0.122	4.014	1.3897883
TE08	0.034	0.2474	-1.396749
TE08	0.069	0.6096	-0.494952
TE08	0.105	1.484	0.3947411
TE08	0.142	3.313	1.1978541
TE08	0.181	6.21	1.8261609
TE09	0.030	0.1283	-2.053384
TE09	0.062	0.3925	-0.935219
TE09	0.094	0.619	-0.47965
TE09	0.127	1.334	0.288182
TE09	0.161	2.129	0.7556524
TE10	0.030	0.151	-1.890475
TE10	0.062	0.3776	-0.97392
TE10	0.094	0.7447	-0.294774
TE10	0.127	1.261	0.2319051
TE10	0.161	2.477	0.9070482

## Appendix A.4

**Table A.4**  
Data for Table 5.2

Specimen	length (mm)	width (mm)	thickness (mm)	area (mm <sup>2</sup> )
LE02	25.0	7.01	4.09	28.67
LE03	20.0	7.34	4.26	31.27
LE04	22.0	4.84	3.01	14.57
LE05	20.0	4.89	3.45	16.87
LE06	25.0	4.41	3.44	15.17
LE07	23.0	5.48	3.20	17.54
LE08	20.0	4.74	3.23	15.31
LE09	24.0	4.89	3.84	18.78
LE10	13.0	5.43	3.43	18.62
LE11	28.0	5.09	3.72	18.93
TE01	11.5	4.73	4.34	20.53
TE02	12.0	4.89	3.94	19.27
TE03	11.0	5.57	3.98	22.17
TE04	15.0	4.30	3.10	13.33
TE05	10.0	6.50	3.40	22.10
TE06	13.0	4.76	3.53	16.80
TE07	8.0	7.76	3.25	25.22
TE09	9.0	4.90	3.80	18.62
TE11	10.0	6.81	3.20	21.79
TE12	10.0	6.60	3.30	21.78

## Appendix A.5

**Table A.5**  
Data for Table 5.3

<b>Specimen</b>	<b>Permeability (mm/s)</b>	<b>Poisson's Ratio</b>	<b>Modulus (kPa)</b>
LE02	9.12E-05	-0.68	3.40
LE03	2.10E-04	-0.55	3.90
LE04	3.15E-05	-0.47	13.65
LE05	5.74E-05	-0.54	7.60
LE06	1.24E-04	-0.44	14.10
LE07	8.83E-05	-0.60	5.95
LE08	1.74E-04	-0.71	4.40
LE09	1.19E-04	-0.56	4.83
LE10	2.88E-05	-0.44	10.77
LE11	5.98E-05	-0.63	11.38
TE01	6.68E-05	-0.50	4.55
TE02	8.50E-05	-0.16	11.04
TE03	8.97E-05	-0.56	6.13
TE04	2.50E-05	-0.30	12.62
TE05	3.58E-04	-0.13	4.68
TE06	1.14E-04	-0.47	5.84
TE07	3.12E-04	-0.38	2.85
TE09*	3.84E-04	0.18	6.57
TE11**	1.15E-03	-0.34	3.37
TE12	5.28E-05	-0.30	5.23

Notes: \* TE09 not included in summary statistics because Poisson's Ratio value fell outside of two standard deviations. \*\* TE11 not included in summary statistics with permeability outside of two standard deviations.

## Appendix A.6

**Table A.6**  
Data for Table 6.1

<b>Specimen</b>	<b>length (mm)</b>	<b>width (mm)</b>	<b>thickness (mm)</b>	<b>area (mm<sup>2</sup>)</b>
IMP05	26.0	5.7	3.7	21.1
IMP06	27.0	11.5	5.8	66.2
IMP08	27.0	11.5	5.8	66.2
IMP09	30.0	5.8	3.4	19.8

## **Appendix B**

### **Copyright Permissions**

## Appendix B.1

Letter for Chapter 1 and Figure 1.6

**From:** Beth Darchi [mailto:DarchiB@asme.org]

**Sent:** Tuesday, June 07, 2011 9:05 AM

**To:** Morrow, Duane A.

**Subject:** FW: ASME PUBLICATIONS PERMISSION REQUEST FORM SUBMISSION

Dear Mr. Morrow:

It is our pleasure to grant you permission to use **Excerpt 1, 2** from " Constitutive Modeling of Skeletal Muscle Tissue With an Explicit Strain-Energy Function," by Odegard, Haut Donahue, Morrow, and Kaufman, Journal of Biomechanical Engineering, Vol. 130, 2008, cited in your letter for inclusion in a publication entitled DEVELOPMENT OF A CONTINUUM MECHANICS MODEL OF PASSIVE SKELETAL MUSCLE to be published by ProQuest/UMI.

As is customary, we ask that you ensure full acknowledgment of this material, the author(s), source and ASME as original publisher on all printed copies being distributed.

Many thanks for your interest in ASME publications.

Sincerely,

Beth Darchi

Permissions & Copyrights

ASME, 3 Park Avenue

New York, NY 10016

T: 212-591-7700

F: 212-591-7841

E: [darchib@asme.org](mailto:darchib@asme.org)

-----Original Message-----

From: webmaster@asme.org [mailto:webmaster@asme.org]

Sent: Wednesday, June 01, 2011 11:19 PM

To: permissions@asme.org

Cc: morrow.duane@mayo.edu

Subject: ASME PUBLICATIONS PERMISSION REQUEST FORM SUBMISSION

ASME PUBLICATIONS PERMISSION REQUEST FORM HAS BEEN SUBMITTED:

ASME Publication Title: Journal of Biomechanical Engineering

Complete List of Authors: Odegard, Haut Donahue, Morrow, and Kaufman

Paper Title (Conference/Journal): Constitutive Modeling of Skeletal Muscle Tissue With an Explicit Strain-Energy Function

Paper Number (Conference):

Volume Number (Journal): 130

Page(s) in the publication of

the permission request: 061017-1 through 061017-9

Year of Publication: 2008

I would like to... Republish in a Doctoral Thesis

Portion to be used: Excerpt

List Figure Numbers: 1, 2

List Table Numbers: 0

Number of Copies: 10

Usage: Both

Title of outside publication: DEVELOPMENT OF A CONTINUUM MECHANICS MODEL OF PASSIVE SKELETAL MUSCLE

Publisher: ProQuest/UMI

Comments: I am an author of this work and would like to include portions of it in a chapter in my PhD Dissertation.

First Name: Duane

Last Name: Morrow

Address Line 1: 817 17th Ave NE

Address Line 2:

City: Rochester

State: MN

Zip: 55906

Phone: 507-951-9473

Fax:

Email: [morrow.duane@mayo.edu](mailto:morrow.duane@mayo.edu)



## Appendix B.2

### Letter for Chapter 1 and Figures 1.7 and 1.8

Rightslink Printable License

Page 1 of 3

#### SPRINGER LICENSE TERMS AND CONDITIONS

Sep 30, 2011

This is a License Agreement between Duane A Morrow ("You") and Springer ("Springer") provided by Copyright Clearance Center ("CCC"). The license consists of your order details, the terms and conditions provided by Springer, and the payment terms and conditions.

**All payments must be made in full to CCC. For payment instructions, please see information listed at the bottom of this form.**

License Number	2758890097821
License date	Sep 30, 2011
Licensed content publisher	Springer
Licensed content publication	Annals of Biomedical Engineering
Licensed content title	Performance Characteristics of a New Generation Pressure Microsensor for Physiologic Applications
Licensed content author	Patrick S. Cottler
Licensed content date	Jan 1, 2009
Volume number	37
Issue number	8
Type of Use	Thesis/Dissertation
Portion	Excerpts
Author of this Springer article	Yes and you are the sole author of the new work
Order reference number	
Title of your thesis / dissertation	DEVELOPMENT OF A CONTINUUM MECHANICS MODEL OF PASSIVE SKELETAL MUSCLE
Expected completion date	Dec 2011
Estimated size(pages)	200
Total	0.00 USD

#### Terms and Conditions

##### Introduction

The publisher for this copyrighted material is Springer Science + Business Media. By clicking "accept" in connection with completing this licensing transaction, you agree that the following terms and conditions apply to this transaction (along with the Billing and Payment terms and conditions established by Copyright Clearance Center, Inc. ("CCC"), at the time that you opened your Rightslink account and that are available at any time at <http://myaccount.copyright.com>).

##### Limited License

With reference to your request to reprint in your thesis material on which Springer Science and Business Media control the copyright, permission is granted, free of charge, for the use

indicated in your enquiry. Licenses are for one-time use only with a maximum distribution equal to the number that you identified in the licensing process.

This License includes use in an electronic form, provided it is password protected or on the university's intranet, destined to microfilming by UMI and University repository. For any other electronic use, please contact Springer at (permissions.dordrecht@springer.com or permissions.heidelberg@springer.com)

The material can only be used for the purpose of defending your thesis, and with a maximum of 100 extra copies in paper.

Although Springer holds copyright to the material and is entitled to negotiate on rights, this license is only valid, provided permission is also obtained from the (co) author (address is given with the article/chapter) and provided it concerns original material which does not carry references to other sources (if material in question appears with credit to another source, authorization from that source is required as well). Permission free of charge on this occasion does not prejudice any rights we might have to charge for reproduction of our copyrighted material in the future.

#### Altering/Modifying Material: Not Permitted

However figures and illustrations may be altered minimally to serve your work. Any other abbreviations, additions, deletions and/or any other alterations shall be made only with prior written authorization of the author(s) and/or Springer Science + Business Media. (Please contact Springer at permissions.dordrecht@springer.com or permissions.heidelberg@springer.com)

#### Reservation of Rights

Springer Science + Business Media reserves all rights not specifically granted in the combination of (i) the license details provided by you and accepted in the course of this licensing transaction, (ii) these terms and conditions and (iii) CCC's Billing and Payment terms and conditions.

#### Copyright Notice:

Please include the following copyright citation referencing the publication in which the material was originally published. Where wording is within brackets, please include verbatim.

"With kind permission from Springer Science+Business Media: <book/journal title, chapter/article title, volume, year of publication, page, name(s) of author(s), figure number (s), and any original (first) copyright notice displayed with material>."

**Warranties:** Springer Science + Business Media makes no representations or warranties with respect to the licensed material.

#### Indemnity

You hereby indemnify and agree to hold harmless Springer Science + Business Media and CCC, and their respective officers, directors, employees and agents, from and against any and all claims arising out of your use of the licensed material other than as specifically authorized pursuant to this license.

#### No Transfer of License

This license is personal to you and may not be sublicensed, assigned, or transferred by you to any other person without Springer Science + Business Media's written permission.

**No Amendment Except in Writing**

This license may not be amended except in a writing signed by both parties (or, in the case of Springer Science + Business Media, by CCC on Springer Science + Business Media's behalf).

**Objection to Contrary Terms**

Springer Science + Business Media hereby objects to any terms contained in any purchase order, acknowledgment, check endorsement or other writing prepared by you, which terms are inconsistent with these terms and conditions or CCC's Billing and Payment terms and conditions. These terms and conditions, together with CCC's Billing and Payment terms and conditions (which are incorporated herein), comprise the entire agreement between you and Springer Science + Business Media (and CCC) concerning this licensing transaction. In the event of any conflict between your obligations established by these terms and conditions and those established by CCC's Billing and Payment terms and conditions, these terms and conditions shall control.

**Jurisdiction**

All disputes that may arise in connection with this present License, or the breach thereof, shall be settled exclusively by the country's law in which the work was originally published.

Other terms and conditions:

v1.2

**If you would like to pay for this license now, please remit this license along with your payment made payable to "COPYRIGHT CLEARANCE CENTER" otherwise you will be invoiced within 48 hours of the license date. Payment should be in the form of a check or money order referencing your account number and this invoice number RLNK500637850.**

**Once you receive your invoice for this order, you may pay your invoice by credit card. Please follow instructions provided at that time.**

**Make Payment To:**

**Copyright Clearance Center  
Dept 001  
P.O. Box 843006  
Boston, MA 02284-3006**

**For suggestions or comments regarding this order, contact RightsLink Customer Support: [customercare@copyright.com](mailto:customercare@copyright.com) or +1-877-622-5543 (toll free in the US) or +1-978-646-2777.**

**Gratis licenses (referencing \$0 in the Total field) are free. Please retain this printable license for your reference. No payment is required.**

---

## Appendix B.3

Letter for Figures 1.1 and 1.6



ELSEVIER

### LICENSING AGREEMENT

---

**Licensee:**

Duane Morrow  
Mayo Clinic  
817 17<sup>th</sup> Avenue, NE  
Rochester, MN 55906  
Phone: 507-951-9473  
[morrow.duane@mayo.edu](mailto:morrow.duane@mayo.edu)

---

**Description of Content:** (2) Netter images – Labeled, Low-resolution

ID: 8725      Organization of Skeletal Muscle  
ID: 8159      Muscle Length – Muscle Tension Relationships

- 
- This license grants permission to licensee for use of the above listed Netter images in the licensee's Ph.D. dissertation entitled "*Development of a Continuum Mechanics Model of Passive Skeletal Muscle.*"
  - The license is effective starting June 14, 2011 and is valid for this project only.
  - The licensee agrees to pay a licensing fee of **\$198.00** USD for use of the above listed images in this manner.
  - No additional use or reproduction of the images is allowed without further permission. Elsevier maintains complete copyright for the above listed images under US Copyright Law.
  - No editorial changes can be made to the images during the development or production of this project.
  - The following copyright line must appear with the images: *Netter illustration from [www.netterimages.com](http://www.netterimages.com). © Elsevier Inc. All rights reserved.*
  - The license may be cancelled at any time should licensee be found to be in breach of these terms and breach is not cured within 5 days.
  - If no payment is received as outlined above, the license will be cancelled immediately and no use of the images is allowed. Any such use without payment of the outlined fees constitutes copyright violation.

\_\_\_\_\_  
Elsevier, Inc.  
Director of Licensing  
1600 John F. Kennedy Blvd., Suite 1800  
Philadelphia, PA 19103-2899

6/14/11  
Date

## Appendix B.4

### Letter for Figures 1.2 and 1.5



## HUMAN KINETICS

1607 North Market Street • P.O. Box 5076 • Champaign IL 61825-5076 • (217) 351-5076 • Fax (217) 351-2674 • [www.HumanKinetics.com](http://www.HumanKinetics.com)

June 2, 2011

Duane A. Morrow  
817 17<sup>th</sup> Avenue NE  
Rochester, MN 55906

RE: Request to reprint figures 1.4 (part A only) and 1.13, and the associated caption text, on pages 8 and 17, respectively, of *Skeletal Muscle: Form and Function, Second Edition*, by B.R. MacIntosh, P.F. Gardiner, and A.J. McComas, in your PhD dissertation study [ID #3265]

Dear Mr. Morrow:

Thank you for your interest in material published by Human Kinetics.

We are pleased to approve your permission request for this one-time use of figures 1.4 (part A only) and 1.13, and the associated caption text, on pages 8 and 17, respectively, of *Skeletal Muscle: Form and Function*, by B.R. MacIntosh, P.F. Gardiner, and A.J. McComas in your dissertation study. This is your confirmation that we are granting nonexclusive print rights in all languages throughout the world, contingent upon your use of the following credit line adjacent to the reprinted material.

**CREDIT LINE:**

Reprinted, with permission, from B.R. MacIntosh, P.F. Gardiner, and A.J. McComas, 2006, *Skeletal muscle: Form and function*, 2<sup>nd</sup> ed. (Champaign, IL: Human Kinetics), 8 [or 17].

**FEE: WAIVED**

In the future, should you wish to formally publish this material please request permission again.

Unfortunately, we cannot grant permission for your use of figure 1.4 part B, because we do not control the rights to that photo. It was provided courtesy of Dr. John Maguire. I have not been able to locate any contact information for Dr. Maguire.

Sincerely,

Martha Gullo  
Rights Manager  
Ph: 217-351-5076 ext. 2223  
Email: [marthag@hkusa.com](mailto:marthag@hkusa.com)

Health, Physical Education, Recreation & Dance Division    Scientific, Technical & Medical Division    Trade Book Division  
Active Living Partners    American Sport Education Program    Distance Education Division    Journal Division    YMCA Education Center

## Appendix B.5

### Letter for Figures 1.3 and 1.4

August 3, 2011

Hello Mr. Morrow,

Permission is granted per the specific details of your request below. No other rights may be assumed.

Best regards,  
Lawrence

Lawrence Guerra  
Manager of Reprints and Licensing  
W. H. Freeman and Company/Worth Publishers  
41 Madison Avenue  
New York, NY 10010  
PH: 212-561-8214  
FX: 212-561-8269

**From:** Morrow, Duane A.  
**Sent:** Sunday, June 12, 2011 7:23 PM  
**To:** [permissionsdept@whfreeman.com](mailto:permissionsdept@whfreeman.com)  
**Subject:** Permissions Request for PhD Dissertation

Dear Permissions Department,

I am writing to request use of two figures from the book Molecular Cell Biology, 4th edition, by Lodish, Berk, Zipursky et al (New York, W. H. Freeman, 2000). I would like to use Figure 18-30 and 19-57 in my PhD dissertation entitled, "Development of a Continuum Mechanics Model of Passive Skeletal Muscle." This dissertation will be submitted in partial fulfillment of my degree in Mechanical Engineering - Engineering Mechanics at the Michigan Technological University to be published through ProQuest/UMI.

If you have any questions or concerns, please feel free to contact me, and thank you for your time and consideration.

Duane Morrow  
817 17th Ave NE  
Rochester, MN 55906  
507-951-9473  
[morrow.duane@mayo.edu](mailto:morrow.duane@mayo.edu)

## Appendix B.6

### Letter for Figure 1.9

Rightslink Printable License

Page 1 of 6

#### ELSEVIER LICENSE TERMS AND CONDITIONS

Oct 06, 2011

This is a License Agreement between Duane A Morrow ("You") and Elsevier ("Elsevier") provided by Copyright Clearance Center ("CCC"). The license consists of your order details, the terms and conditions provided by Elsevier, and the payment terms and conditions.

**All payments must be made in full to CCC. For payment instructions, please see information listed at the bottom of this form.**

Supplier	Elsevier Limited The Boulevard, Langford Lane Kidlington, Oxford, OX5 1GB, UK
Registered Company Number	1982084
Customer name	Duane A Morrow
Customer address	817 17th Ave NE Rochester, MN 55906
License number	2763131269843
License date	Oct 06, 2011
Licensed content publisher	Elsevier
Licensed content publication	Journal of Biomechanics
Licensed content title	Correlation between active and passive isometric force and intramuscular pressure in the isolated rabbit tibialis anterior muscle
Licensed content author	Jennifer Davis, Kenton R Kaufman, Richard L Lieber
Licensed content date	April 2003
Licensed content volume number	36
Licensed content issue number	4
Number of pages	8
Start Page	505
End Page	512
Type of Use	reuse in a thesis/dissertation
Intended publisher of new work	other
Portion	figures/tables/illustrations
Number of figures/tables/illustrations	1
Format	both print and electronic
Are you the author of this Elsevier article?	No

<https://s100.copyright.com/App/PrintableLicenseFrame.jsp?publisherID=70&licenseID=2...> 10/6/2011

Will you be translating?	No
Order reference number	
Title of your thesis/dissertation	DEVELOPMENT OF A CONTINUUM MECHANICS MODEL OF PASSIVE SKELETAL MUSCLE
Expected completion date	Dec 2011
Estimated size (number of pages)	200
Elsevier VAT number	GB 494 6272 12
Permissions price	0.00 USD
VAT/Local Sales Tax	0.0 USD / 0.0 GBP
Total	0.00 USD
Terms and Conditions	

### INTRODUCTION

1. The publisher for this copyrighted material is Elsevier. By clicking "accept" in connection with completing this licensing transaction, you agree that the following terms and conditions apply to this transaction (along with the Billing and Payment terms and conditions established by Copyright Clearance Center, Inc. ("CCC"), at the time that you opened your Rightslink account and that are available at any time at <http://myaccount.copyright.com>).

### GENERAL TERMS

2. Elsevier hereby grants you permission to reproduce the aforementioned material subject to the terms and conditions indicated.

3. Acknowledgement: If any part of the material to be used (for example, figures) has appeared in our publication with credit or acknowledgement to another source, permission must also be sought from that source. If such permission is not obtained then that material may not be included in your publication/copies. Suitable acknowledgement to the source must be made, either as a footnote or in a reference list at the end of your publication, as follows:

“Reprinted from Publication title, Vol /edition number, Author(s), Title of article / title of chapter, Pages No., Copyright (Year), with permission from Elsevier [OR APPLICABLE SOCIETY COPYRIGHT OWNER].” Also Lancet special credit - “Reprinted from The Lancet, Vol. number, Author(s), Title of article, Pages No., Copyright (Year), with permission from Elsevier.”

4. Reproduction of this material is confined to the purpose and/or media for which permission is hereby given.

5. Altering/Modifying Material: Not Permitted. However figures and illustrations may be altered/adapted minimally to serve your work. Any other abbreviations, additions, deletions and/or any other alterations shall be made only with prior written authorization of Elsevier Ltd. (Please contact Elsevier at [permissions@elsevier.com](mailto:permissions@elsevier.com))



6. If the permission fee for the requested use of our material is waived in this instance, please be advised that your future requests for Elsevier materials may attract a fee.

7. **Reservation of Rights:** Publisher reserves all rights not specifically granted in the combination of (i) the license details provided by you and accepted in the course of this licensing transaction, (ii) these terms and conditions and (iii) CCC's Billing and Payment terms and conditions.

8. **License Contingent Upon Payment:** While you may exercise the rights licensed immediately upon issuance of the license at the end of the licensing process for the transaction, provided that you have disclosed complete and accurate details of your proposed use, no license is finally effective unless and until full payment is received from you (either by publisher or by CCC) as provided in CCC's Billing and Payment terms and conditions. If full payment is not received on a timely basis, then any license preliminarily granted shall be deemed automatically revoked and shall be void as if never granted. Further, in the event that you breach any of these terms and conditions or any of CCC's Billing and Payment terms and conditions, the license is automatically revoked and shall be void as if never granted. Use of materials as described in a revoked license, as well as any use of the materials beyond the scope of an unrevoked license, may constitute copyright infringement and publisher reserves the right to take any and all action to protect its copyright in the materials.

9. **Warranties:** Publisher makes no representations or warranties with respect to the licensed material.

10. **Indemnity:** You hereby indemnify and agree to hold harmless publisher and CCC, and their respective officers, directors, employees and agents, from and against any and all claims arising out of your use of the licensed material other than as specifically authorized pursuant to this license.

11. **No Transfer of License:** This license is personal to you and may not be sublicensed, assigned, or transferred by you to any other person without publisher's written permission.

12. **No Amendment Except in Writing:** This license may not be amended except in a writing signed by both parties (or, in the case of publisher, by CCC on publisher's behalf).

13. **Objection to Contrary Terms:** Publisher hereby objects to any terms contained in any purchase order, acknowledgment, check endorsement or other writing prepared by you, which terms are inconsistent with these terms and conditions or CCC's Billing and Payment terms and conditions. These terms and conditions, together with CCC's Billing and Payment terms and conditions (which are incorporated herein), comprise the entire agreement between you and publisher (and CCC) concerning this licensing transaction. In the event of any conflict between your obligations established by these terms and conditions and those established by CCC's Billing and Payment terms and conditions, these terms and conditions shall control.

14. **Revocation:** Elsevier or Copyright Clearance Center may deny the permissions described in this License at their sole discretion, for any reason or no reason, with a full refund payable to you. Notice of such denial will be made using the contact information provided by you. Failure to receive such notice will not alter or invalidate the denial. In no event will Elsevier

or Copyright Clearance Center be responsible or liable for any costs, expenses or damage incurred by you as a result of a denial of your permission request, other than a refund of the amount(s) paid by you to Elsevier and/or Copyright Clearance Center for denied permissions.

### LIMITED LICENSE

The following terms and conditions apply only to specific license types:

15. **Translation:** This permission is granted for non-exclusive world **English** rights only unless your license was granted for translation rights. If you licensed translation rights you may only translate this content into the languages you requested. A professional translator must perform all translations and reproduce the content word for word preserving the integrity of the article. If this license is to re-use 1 or 2 figures then permission is granted for non-exclusive world rights in all languages.

16. **Website:** The following terms and conditions apply to electronic reserve and author websites:

**Electronic reserve:** If licensed material is to be posted to website, the web site is to be password-protected and made available only to bona fide students registered on a relevant course if:

This license was made in connection with a course,

This permission is granted for 1 year only. You may obtain a license for future website posting,

All content posted to the web site must maintain the copyright information line on the bottom of each image,

A hyper-text must be included to the Homepage of the journal from which you are licensing at <http://www.sciencedirect.com/science/journal/xxxxx> or the Elsevier homepage for books at <http://www.elsevier.com> , and

Central Storage: This license does not include permission for a scanned version of the material to be stored in a central repository such as that provided by Heron/XanEdu.

17. **Author website** for journals with the following additional clauses:

All content posted to the web site must maintain the copyright information line on the bottom of each image, and

the permission granted is limited to the personal version of your paper. You are not allowed to download and post the published electronic version of your article (whether PDF or HTML, proof or final version), nor may you scan the printed edition to create an electronic version,

A hyper-text must be included to the Homepage of the journal from which you are licensing at <http://www.sciencedirect.com/science/journal/xxxxx> , As part of our normal production process, you will receive an e-mail notice when your article appears on Elsevier's online service ScienceDirect ([www.sciencedirect.com](http://www.sciencedirect.com)). That e-mail will include the article's Digital Object Identifier (DOI). This number provides the electronic link to the published article and should be included in the posting of your personal version. We ask that you wait until you receive this e-mail and have the DOI to do any posting.

Central Storage: This license does not include permission for a scanned version of the material to be stored in a central repository such as that provided by Heron/XanEdu.

18. **Author website** for books with the following additional clauses:

Authors are permitted to place a brief summary of their work online only.

A hyper-text must be included to the Elsevier homepage at <http://www.elsevier.com>

All content posted to the web site must maintain the copyright information line on the bottom of each image

You are not allowed to download and post the published electronic version of your chapter, nor may you scan the printed edition to create an electronic version.

Central Storage: This license does not include permission for a scanned version of the material to be stored in a central repository such as that provided by Heron/XanEdu.

19. **Website** (regular and for author): A hyper-text must be included to the Homepage of the journal from which you are licensing at

<http://www.sciencedirect.com/science/journal/xxxxx>, or for books to the Elsevier homepage at <http://www.elsevier.com>

20. **Thesis/Dissertation**: If your license is for use in a thesis/dissertation your thesis may be submitted to your institution in either print or electronic form. Should your thesis be published commercially, please reapply for permission. These requirements include permission for the Library and Archives of Canada to supply single copies, on demand, of the complete thesis and include permission for UMI to supply single copies, on demand, of the complete thesis. Should your thesis be published commercially, please reapply for permission.

21. **Other Conditions**:

v1.6

**If you would like to pay for this license now, please remit this license along with your payment made payable to "COPYRIGHT CLEARANCE CENTER" otherwise you will be invoiced within 48 hours of the license date. Payment should be in the form of a check or money order referencing your account number and this invoice number RLNK500641077.**

**Once you receive your invoice for this order, you may pay your invoice by credit card. Please follow instructions provided at that time.**

**Make Payment To:**  
**Copyright Clearance Center**  
**Dept 001**  
**P.O. Box 843006**  
**Boston, MA 02284-3006**

**For suggestions or comments regarding this order, contact RightsLink Customer Support: [customercare@copyright.com](mailto:customercare@copyright.com) or +1-877-622-5543 (toll free in the US) or +1-978-646-2777.**

**Gratis licenses (referencing \$0 in the Total field) are free. Please retain this printable license for your reference. No payment is required.**



## Appendix B.7

### Letter for Figure 1.10

11/29/11

Copyright Clearance Center



**Confirmation Number: 10557954**  
**Order Date: 10/05/2011**

#### Customer Information

**Customer:** Duane Morrow  
**Account Number:** 3000403827  
**Organization:** Duane Morrow  
**Email:** morrow.duane@mayo.edu  
**Phone:** +1 (507)9519473  
**Payment Method:** Invoice

#### Order Details

##### Muscle & nerve

Billing Status:  
**N/A**

**Order detail ID:** 57294303

**Permission Status:** **Granted**

**Article Title:** Correlation between isometric force and intramuscular pressure in rabbit tibialis anterior muscle with an intact anterior compartment

**Permission type:** Republish or display content  
**Type of use:** reuse in a dissertation/thesis

**Order License Id:** 2762811084859

**Author(s):** Winters, Taylor M.  
**DOI:** 10.1002/MUS.21298  
**Date:** Jul 01, 2009  
**ISSN:** 1097-4598  
**Publication Type:** e-Journal

**Start page:** 79  
**End page:** 85  
**Requestor type:** University/Academic  
**Format:** Print and electronic  
**Portion:** Figure/table

**Volume:** 40  
**Issue:** 1  
**Start page:** 79  
**Publisher:** JOHN WILEY & SONS, INC.  
**Author/Editor:** Wiley InterScience (Online service)

**Number of figures/tables:** 1  
**Original Wiley figure/table number(s):** Figure 4

**Will you be translating?** No

**Order reference number**

**Note:** This item was invoiced separately through our **RightsLink service**. [More info](#)

**\$ 0.00**

**Total order items: 1**

**Order Total: \$0.00**

[Get Permission](#) | [License Your Content](#) | [Products & Solutions](#) | [Partners](#) | [Education](#) | [About CCC](#)  
[Privacy Policy](#) | [Terms & Conditions](#)

Copyright 2011 Copyright Clearance Center

<https://www.copyright.com/printOrder.do?id=10557954>

1/1

## Appendix B.8

### Letter for Chapter 2

#### ELSEVIER LICENSE TERMS AND CONDITIONS

Jun 14, 2011

---

---

This is a License Agreement between Duane A Morrow ("You") and Elsevier ("Elsevier") provided by Copyright Clearance Center ("CCC"). The license consists of your order details, the terms and conditions provided by Elsevier, and the payment terms and conditions.

**All payments must be made in full to CCC. For payment instructions, please see information listed at the bottom of this form.**

Supplier	Elsevier Limited The Boulevard, Langford Lane Kidlington, Oxford, OX5 1GB, UK
Registered Company Number	1982084
Customer name	Duane A Morrow
Customer address	817 17th Ave NE Rochester, MN 55906
License number	2679701432823
License date	May 31, 2011
Licensed content publisher	Elsevier
Licensed content publication	Journal of the Mechanical Behavior of Biomedical Materials
Licensed content title	Transversely isotropic tensile material properties of skeletal muscle tissue
Licensed content author	Duane A. Morrow, Tammy L. Haut Donahue, Gregory M. Odegard, Kenton R. Kaufman
Licensed content date	January 2010
Licensed content volume number	3

Licensed content issue number	1
Number of pages	6
Start Page	124
End Page	129
Type of Use	reuse in a thesis/dissertation
Portion	full article
Format	both print and electronic
Are you the author of this Elsevier article?	Yes
Will you be translating?	No
Order reference number	1
Title of your thesis/dissertation	Development of a Continuum Mechanics Model of Passive Skeletal Muscle
Expected completion date	Aug 2011
Estimated size (number of pages)	200
Elsevier VAT number	GB 494 6272 12
Permissions price	0.00 USD
VAT/Local Sales Tax	0.0 USD / 0.0 GBP
<b>Total</b>	0.00 USD
Terms and Conditions	

### INTRODUCTION

1. The publisher for this copyrighted material is Elsevier. By clicking "accept" in connection with completing this licensing transaction, you agree that the following terms and conditions apply to this transaction (along with the Billing and Payment terms and conditions established by Copyright Clearance Center, Inc. ("CCC"), at the time that you opened your Rightslink account and that are available at any time at <http://myaccount.copyright.com>).

### GENERAL TERMS

2. Elsevier hereby grants you permission to reproduce the aforementioned material subject to the terms and conditions indicated.

3. Acknowledgement: If any part of the material to be used (for example, figures) has appeared in our publication with credit or acknowledgement to another source, permission must also be sought from that source. If such permission is not obtained then that material may not be included in your publication/copies. Suitable acknowledgement to the source must

be made, either as a footnote or in a reference list at the end of your publication, as follows:

“Reprinted from Publication title, Vol /edition number, Author(s), Title of article / title of chapter, Pages No., Copyright (Year), with permission from Elsevier [OR APPLICABLE SOCIETY COPYRIGHT OWNER].” Also Lancet special credit - “Reprinted from The Lancet, Vol. number, Author(s), Title of article, Pages No., Copyright (Year), with permission from Elsevier.”

4. Reproduction of this material is confined to the purpose and/or media for which permission is hereby given.

5. Altering/Modifying Material: Not Permitted. However figures and illustrations may be altered/adapted minimally to serve your work. Any other abbreviations, additions, deletions and/or any other alterations shall be made only with prior written authorization of Elsevier Ltd. (Please contact Elsevier at [permissions@elsevier.com](mailto:permissions@elsevier.com))

6. If the permission fee for the requested use of our material is waived in this instance, please be advised that your future requests for Elsevier materials may attract a fee.

7. Reservation of Rights: Publisher reserves all rights not specifically granted in the combination of (i) the license details provided by you and accepted in the course of this licensing transaction, (ii) these terms and conditions and (iii) CCC's Billing and Payment terms and conditions.

8. License Contingent Upon Payment: While you may exercise the rights licensed immediately upon issuance of the license at the end of the licensing process for the transaction, provided that you have disclosed complete and accurate details of your proposed use, no license is finally effective unless and until full payment is received from you (either by publisher or by CCC) as provided in CCC's Billing and Payment terms and conditions. If full payment is not received on a timely basis, then any license preliminarily granted shall be deemed automatically revoked and shall be void as if never granted. Further, in the event that you breach any of these terms and conditions or any of CCC's Billing and Payment terms and conditions, the license is automatically revoked and shall be void as if never granted. Use of materials as described in a revoked license, as well as any use of the materials beyond the scope of an unrevoked license, may constitute copyright infringement and publisher reserves the right to take any and all action to protect its copyright in the materials.

9. Warranties: Publisher makes no representations or warranties with respect to the licensed material.

10. Indemnity: You hereby indemnify and agree to hold harmless publisher and CCC, and their respective officers, directors, employees and agents, from and against any and all claims



arising out of your use of the licensed material other than as specifically authorized pursuant to this license.

11. **No Transfer of License:** This license is personal to you and may not be sublicensed, assigned, or transferred by you to any other person without publisher's written permission.

12. **No Amendment Except in Writing:** This license may not be amended except in a writing signed by both parties (or, in the case of publisher, by CCC on publisher's behalf).

13. **Objection to Contrary Terms:** Publisher hereby objects to any terms contained in any purchase order, acknowledgment, check endorsement or other writing prepared by you, which terms are inconsistent with these terms and conditions or CCC's Billing and Payment terms and conditions. These terms and conditions, together with CCC's Billing and Payment terms and conditions (which are incorporated herein), comprise the entire agreement between you and publisher (and CCC) concerning this licensing transaction. In the event of any conflict between your obligations established by these terms and conditions and those established by CCC's Billing and Payment terms and conditions, these terms and conditions shall control.

14. **Revocation:** Elsevier or Copyright Clearance Center may deny the permissions described in this License at their sole discretion, for any reason or no reason, with a full refund payable to you. Notice of such denial will be made using the contact information provided by you. Failure to receive such notice will not alter or invalidate the denial. In no event will Elsevier or Copyright Clearance Center be responsible or liable for any costs, expenses or damage incurred by you as a result of a denial of your permission request, other than a refund of the amount(s) paid by you to Elsevier and/or Copyright Clearance Center for denied permissions.

### **LIMITED LICENSE**

The following terms and conditions apply only to specific license types:

15. **Translation:** This permission is granted for non-exclusive world **English** rights only unless your license was granted for translation rights. If you licensed translation rights you may only translate this content into the languages you requested. A professional translator must perform all translations and reproduce the content word for word preserving the integrity of the article. If this license is to re-use 1 or 2 figures then permission is granted for non-exclusive world rights in all languages.

16. **Website:** The following terms and conditions apply to electronic reserve and author websites:

**Electronic reserve:** If licensed material is to be posted to website, the web site is to be password-protected and made available only to bona fide students registered on a relevant

course if:

This license was made in connection with a course,

This permission is granted for 1 year only. You may obtain a license for future website posting,

All content posted to the web site must maintain the copyright information line on the bottom of each image,

A hyper-text must be included to the Homepage of the journal from which you are licensing at <http://www.sciencedirect.com/science/journal/xxxxx> or the Elsevier homepage for books at <http://www.elsevier.com> , and

Central Storage: This license does not include permission for a scanned version of the material to be stored in a central repository such as that provided by Heron/XanEdu.

**17. Author website** for journals with the following additional clauses:

All content posted to the web site must maintain the copyright information line on the bottom of each image, and

the permission granted is limited to the personal version of your paper. You are not allowed to download and post the published electronic version of your article (whether PDF or HTML, proof or final version), nor may you scan the printed edition to create an electronic version,

A hyper-text must be included to the Homepage of the journal from which you are licensing at <http://www.sciencedirect.com/science/journal/xxxxx> , As part of our normal production process, you will receive an e-mail notice when your article appears on Elsevier's online service ScienceDirect ([www.sciencedirect.com](http://www.sciencedirect.com)). That e-mail will include the article's Digital Object Identifier (DOI). This number provides the electronic link to the published article and should be included in the posting of your personal version. We ask that you wait until you receive this e-mail and have the DOI to do any posting.

Central Storage: This license does not include permission for a scanned version of the material to be stored in a central repository such as that provided by Heron/XanEdu.

**18. Author website** for books with the following additional clauses:

Authors are permitted to place a brief summary of their work online only.

A hyper-text must be included to the Elsevier homepage at <http://www.elsevier.com>

All content posted to the web site must maintain the copyright information line on the bottom of each image

You are not allowed to download and post the published electronic version of your chapter, nor may you scan the printed edition to create an electronic version.

Central Storage: This license does not include permission for a scanned version of the material to be stored in a central repository such as that provided by Heron/XanEdu.

19. **Website** (regular and for author): A hyper-text must be included to the Homepage of the journal from which you are licensing at <http://www.sciencedirect.com/science/journal/xxxxx>. or for books to the Elsevier homepage at <http://www.elsevier.com>

20. **Thesis/Dissertation**: If your license is for use in a thesis/dissertation your thesis may be submitted to your institution in either print or electronic form. Should your thesis be published commercially, please reapply for permission. These requirements include permission for the Library and Archives of Canada to supply single copies, on demand, of the complete thesis and include permission for UMI to supply single copies, on demand, of the complete thesis. Should your thesis be published commercially, please reapply for permission.

21. **Other Conditions**:

v1.6

**Gratis licenses (referencing \$0 in the Total field) are free. Please retain this printable license for your reference. No payment is required.**

**If you would like to pay for this license now, please remit this license along with your payment made payable to "COPYRIGHT CLEARANCE CENTER" otherwise you will be invoiced within 48 hours of the license date. Payment should be in the form of a check or money order referencing your account number and this invoice number RLNK0.**

**Once you receive your invoice for this order, you may pay your invoice by credit card. Please follow instructions provided at that time.**

**Make Payment To:**

**Copyright Clearance Center**

**Dept 001**

**P.O. Box 843006**

**Boston, MA 02284-3006**

**For suggestions or comments regarding this order, contact Rightslink Customer Support: [customercare@copyright.com](mailto:customercare@copyright.com) or +1-877-622-5543 (toll free in the US) or +1-978-646-2777.**

## Appendix B.9

Letter for Chapter 3



RightsLink®



**Taylor & Francis**  
Taylor & Francis Group

**Title:** A method for assessing the fit of a constitutive material model to experimental stress-strain data

**Author:** Duane A. Morrow, Tammy Haut Donahue, Gregory M. Odegard et al.

**Publication:** Computer Methods in Biomechanics & Bio Engineering

**Publisher:** Taylor & Francis

**Date:** Apr 1, 2010

Copyright © 2010 Taylor & Francis

### Thesis/Dissertation Reuse Request

Taylor & Francis is pleased to offer reuses of its content for a thesis or dissertation free of charge contingent on resubmission of permission request if work is published.